Finite volume simulation of the Gatenby-Gawlinski model for acid-mediated tumor invasion with heterogeneous diffusion and homogenization

Elisa Scanu, Corrado Mascia, Chiara Simeoni

Research Report : finite volume simulation of the Gatenby-Gawlinski model for acid-mediated tumor invasion with heterogeneous diffusion and homogenization

Elisa Scanu, Corrado Mascia

Dipartimento di Matematica G. Castelnuovo, Sapienza Università di Roma
piazzale Aldo Moro 2 - 00185 Roma (Italy)

e.scanu@qmul.ac.uk – corrado.mascia@uniroma1.it

Chiara Simeoni

Laboratoire de Mathématiques J.A. Dieudonné CNRS UMR 7351
Université Côte D'Azur, Parc Valrose - 06108 Nice Cedex 2 (France)

chiara.simeoni@univ-cotedazur.fr

September 30th, 2020

Contents

Introduction

Nowadays, cancer research is one of the most active and interdisciplinary investigation fields [30, 31], and it allows for useful application of several mathematical results. A lot of effort is made in order to improve the actual strategies: in the past few years, the role of mathematics has been crucial to support experimental studies [2, 12, 10, 21, 28], although such models have often several limitations, so that they are becoming indispensable for designing new therapies and preventive measures.

We focus on the so-called *Warburg effect* and its mathematical modelling by means of the *acid-mediated invasion* hypothesis, namely the typical strategy of acidity increasing against the environment operated by tumours to regulate their growth, which has already been translated into a system of reaction-diffusion equations [7, 10, 11, 21]. Starting from the seminal work by Gatenby-Gawlinsky [10, 11, 12], the main theoretical issues are the existence of travelling wave solutions and the numerical simulation of experimental results.

Before starting the investigation, it is worth framing the biomedical context behind the model, by illustrating characteristics of the Warburg effect [28, 29]. This phenomenon concerns the metabolism of cancer cells, essentially providing their glucose uptake rates: indeed, it has been firstly observed by Otto Warburg in the 1920s, and afterwards confirmed through many experiments, that tumour cells tend to rely on glycolytic metabolism even in presence of huge oxygen amounts. From a strictly biomedical point of view, it is important noticing that normal cells undergo glucose metabolism by employing oxidative phosphorylation pathways, which is the most effective process in terms of adenosine triphosphate production (ATP) and requires oxygen as

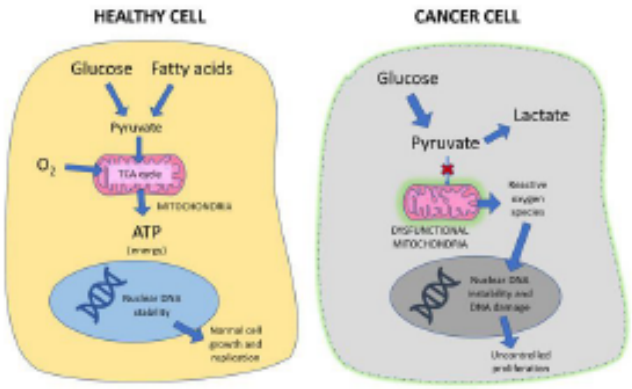

Figure 1: Pathaways of healthy and cancer cells metabolism

main resource. Tumour cells behaviour seems to forbear the conventional pathway and appeals instead to glycolysis, thus inducing lactic acid fermentation, a product generally released in hypoxia regimes (see Figure 1).

Although the Warburg effect has been intensely studied during the past twenty years, how this phenomenon happens and affects cancer proliferation is partly an open problem. For example, the passage from normal to glycolytic metabolism done by cancer cells is still object of researches [23, 26]. Moreover, by exploiting a combination of modelling and in vitro experiments, it has been shown how cancer metabolic changes are able to define a micro-environment where the better adapted malignant cells overwhelm the others and spatial structures are created [1, 23].

In this work, we suppose that carcinogenesis has already happened. The early growth stages of a primary tumour are a consequence of successive divisions of their initial cells. Then, when a critical size (of about 10^4 cells) is reached, a further growth requires aggressive action on the surrounding healthy tissue. This is done in different ways, one of which consists in coopting blood vessels to provide oxygen and nutrients to the expanding colony [4] and another strategy consists in releasing products, such as the lactic acid, which favour the death of healthy cells.

As regards the mathematical analysis, we make a crucial assumption, namely that acidification caused by lactic acid production is advantageous for the spread of cancer cells, whilst it destroys healthy cells. Hence, the original modelling based on reaction-diffusion equations developed by Gatenby and Gawlinski [10, 11, 12] is suitable to perform numerical investigation and to analyse travelling wave solutions, because it takes into account all the previously explained behaviours of healthy and cancer cells in an acid environment.

The manuscript is organised as follows.
In the first chapter, we present analytical results for the Gatenby-Gawlinsky model, including its non-dimensionalized version and the analysis of travelling wave solutions, and we illustrate the passages leading to an approximation for various biological regimes. In the second chapter, which constitutes the original part of the manuscript, we introduce the numerical algorithm, together with its consistency and convergence analysis, and we simulate many different cases depending on the biological context. Finally, we make considerations on a possible homogenisation in the long run of travelling front solutions and we provide a comparison between analytical and numerical approximations.

Acknowledgements

This research project has been partially supported by the French government, managed by the National Research Agency (ANR) under the UCA JEDI Investments for the Future project — reference no. ANR-15-IDEX-01

Chapter 1

Modelling and analysis

The model, firstly proposed by Gatenby and Gawlinski [10, 11, 12], is developed in order to reproduce cancer cells invasion within a healthy tissue, starting from a stage in which the carcinogenesis has already happened and, then, it is not further taken into account. The attention is on the interaction between malignant and healthy cells occurring at the tumour-host interface, where a significant role is played by the lactic acid production and spreading, because of glycolytic metabolism exploited by the tumour cells.

From a mathematical point of view, we analyse the following system:

$$\begin{cases} U_t = \rho_1 U\big(1 - \frac{U}{\kappa_1}\big) - \delta_1 UW \\ V_t = \rho_2 V\big(1 - \frac{V}{\kappa_2}\big) + D_2\big[\big(1 - \frac{U}{\kappa_1}\big)V_x\big]_x \\ W_t = \rho_3 V - \delta_3 W + \big(D_3 W_x\big)_x \end{cases} \tag{1.1}$$

where $D_3 = D_3(x)$ is a heterogeneous positive diffusion function. From a biological point of view, the function D_3 accounts for the different physical composition of tissues (see Figure 1.1), which typically are not homogeneous structurally diversified according to their function and position [16].

The boundary and initial conditions for the system (1.1) will be specified later on.

1.1 Nondimensionalised system and the Fisher-KPP equation

The system (1.1) is a mathematical model for the growth, diffusion and chemical action of tumour cells against the surrounding environment. We adopt a non-dimensionalisation technique starting from (1.1), where U and V are the healthy and tumour tissue concentrations with carrying capacities κ_1 and κ_2, respectively, and W is the excess of H^+ ions concentration induced by the tumour cells metabolism [28, 29].

A logistic-type growth is assumed in the first and second equation with steady states $U = 0$ and $V = 0$ which are unstable so that small perturbations drive the concentrations towards the stable states $U = \kappa_1$ and $V = \kappa_2$, with growth rates ρ_1 and ρ_2, respectively. The diffusion rate for lactic acid depends on the heterogeneous function D_3 it has been experimentally found that the diffusion rate for tumours typically depends on the concentration of healthy cells in the surrounding environment [28], which is translated into the nonlinear (possibly degenerate) diffusion term in the second equation of system (1.1).

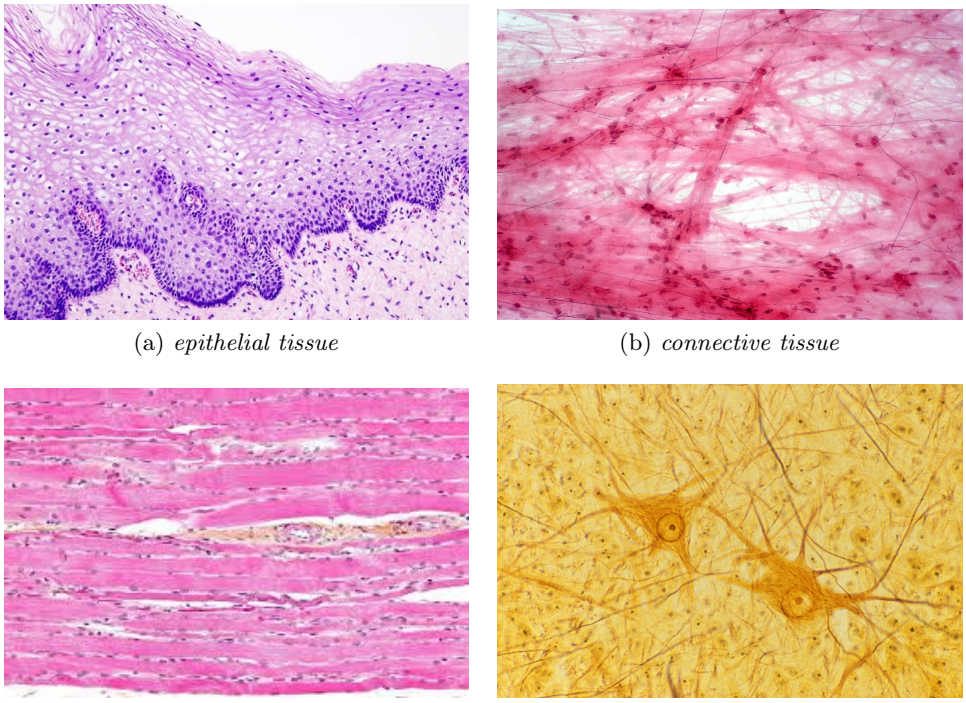

(a) *epithelial tissue* (b) *connective tissue*

(c) *muscular tissue* (d) *nervous tissue*

Figure 1.1: Microscope images of different types of biological tissues. Source: [33, 34, 35, 36]

The destructive effects of acidity on the healthy tissue are described by the reaction term in the first equation, while the (linear) production of lactic acid constant rate ρ_3, and its loss due to deactivation kinetics, with constant rate δ_3 are included into the third equation.
We consider the nondimensionalised system, where u, v and w correspond to nondimensionalised rescaled concentrations of healthy tissue, tumour cells and excess H^+ ions, respectively, which satisfy $0 \leq u, v, w \leq 1$. We introduce the following rescaled variables and parameters:

$$u = \frac{U}{\kappa_1}, \quad v = \frac{V}{\kappa_2}, \quad w = \frac{\delta_3}{\rho_3 \kappa_2} W,$$
$$d = \frac{\delta_1 \rho_3 \kappa_2}{\delta_3 \rho_1}, \quad r = \frac{\rho_2}{\rho_1}, \quad c = \frac{\delta_3}{\rho_1}.$$

In our case, we have taken D_3 as a inhomogeneous diffusion function, hence we adimensionalise with respect to $\max D_3$ and we introduce the normalised diffusion function A. Thus, the other variables for the system are

$$t \longmapsto \rho_1 t, \quad x \longmapsto \sqrt{\frac{\rho_1}{\max D_3}}\, x,$$
$$D = \frac{D_2}{\max D_3}, \quad A = \frac{D_3}{\max D_3}$$

Although in the case of constant diffusion the adimensionalisation would lead to a known value of $A = 1$, we prefer to explicitly indicating A in the system for future applications in the inhomo-

geneous case. Thus, we obtain the non-dimensionalised system

$$\begin{cases} u_t = u(1-u) - duw \\ v_t = rv(1-v) + D[(1-u)v_x]_x \\ w_t = c(v-w) + (Aw_x)_x \end{cases} \tag{1.2}$$

which is used for the analysis performed in the following sections.

Focusing on the biological interpretation of the model (1.2), the parameter r denotes the reproduction rate of tumour tissue and c the production of H^+ ions. The variation of the tumour cells concentration is a consequence of its internal population dynamics and the diffusion term of the second equation.
It is worthwhile noticing that if $u \equiv 0$, namely to the absence of healthy tissue, then the second equation becomes a reaction-diffusion *Fisher-KPP equation*

$$v_t = rv(1-v) + Dv_{xx} \tag{1.3}$$

which exhibits front-type solutions connecting the equilibrium states given by $f(v) = 0$ with $f = rv(1-v)$. The model (1.3) typically occurs in *phase transition problems*; in particular, Ronald Fisher proposed this equation in 1937 [9] in the context of population dynamics to describe the spatial spread of an advantageous allele and explored its travelling wave solutions. Indeed, it can be proven that for every wave speed $\theta \geq 2\sqrt{rD}$ there exists a propagating front which switches from the equilibrium state $v(+\infty) = v_+ = 0$ to the equilibrium state $v(-\infty) = v_- = 1$ (decreasing profile). On the other hand, no monotone invasion front exist for $\theta < 2\sqrt{rD}$. Moreover, each travelling wave solution has a unique shape profile and it is stable against near-field perturbations [13, 25].
For the parameters of the system (1.2), we assume $0 < D \ll 1$, because its form derives from the ratio $\frac{D_2}{D_3}$ between the diffusivity of malignant cells and that of the H^+ ions. Then it is reasonable to take D_3 much larger than D_2. Finally, d measures the destructiveness of the lactic acid on the healthy tissue, which can be interpreted as the tumour aggressiveness.

In this section, we focus on the analysis of *travelling waves solutions* for the Gatenby-Gawlinski model (1.1), which are special solutions of the form:

$$\phi(x,t) = \Phi(x - \theta t) \tag{1.4}$$

where θ is a constant *wave speed* and the profile Φ propagates along the real line (usually normalised according to the problem context). If Φ is required to satisfy boundary conditions of the form

$$\Phi(-\infty) = \phi_- \quad \text{and} \quad \Phi(+\infty) = \phi_+$$

then the solution is also called *propagating front*.
We point out that propagating fronts are a particular case of travelling wave solutions, which are especially interesting for our work.

In order to analyse the front-type solutions, we use the change of variables $z = x - \theta t$ where θ is the wave speed and we make a slight abuse of notation by assuming that

$$u(x,t) = u(z) \quad v(x,t) = v(z) \quad w(x,t) = w(z)$$

By substitution to the system (1.2) and by taking A homogeneous we obtain

$$\begin{cases} \theta u' + u(1-u) - duw = 0 \\ D[(1-u)v']' + \theta v' + rv(1-v) = 0 \\ Aw'' + \theta w' + c(v-w) = 0 \end{cases} \tag{1.5}$$

where the derivatives are referred to the variable z.
We point out that we have taken an homogeneous diffusion term for the lactic acid in order to avoid an analytical problem in (1.5). Indeed, it is not easy to calculate the z-derivative for A in the heterogeneous case, as the system is not autonomous, because the dependence of A on the spatial variable makes the wave lose their invariance by translations.

In order to be consistent with the biological model, we consider $\theta > 0$ and the following asymptotic conditions:

$$(u,v,w)(-\infty) = (0,1,1), \;\; (u,v,w)(+\infty) = (1,0,0) \quad \text{for } d \geq 1 \tag{1.6}$$

or

$$(u,v,w)(-\infty) = (1-d,1,1), \;\; (u,v,w)(+\infty) = (1,0,0) \quad \text{for } 0 < d < 1 \tag{1.7}$$

together with the asymptotic conditions $(u',v',w')(\pm\infty) = 0$ which correspond to the steady states of the underlining dynamical system (1.5). In particular, if $d \geq 1$, then the solutions (1.7) behind the tumour front, due to the strong acidity effects, describe a process, called *homogeneous invasion*, where the healthy tissue is completely destroyed, whilst if $0 < d < 1$, then the solutions (1.6) describe a situation, called *heterogeneous invasion*, with a residual concentration of healthy tissue given by the value $1 - d$.
Moreover, the profiles u, v, w are assumed to be monotonic, increasing in the case of u and decreasing in the case of v and w.
It is important to point out that no rigorous proof of the existence of front-type solutions for the system (1.2) is presently available, and this issue remains an open problem.

1.2 Preliminary results

Following the approach by Fasano et al. [7], in this section, we introduce some technical lemmas which are used for the analysis of travelling wave solutions to system (1.2).
We remark that, although the results in [7] apply to the case of homogeneous (constant) diffusion D_3, we decide to trace the rescaled value A of this coefficient for some prospective comments (refer to Chapter 2).

Lemma 1.2.1. *Let A, θ, $c > 0$ and f a bounded continuous function. Then the equation:*

$$AW'' + \theta W' - cW = f \tag{1.8}$$

admits the solution:

$$W(z) = \frac{1}{r_2 - r_1}[I_1(z) + I_2(z)] \tag{1.9}$$

where

$$\begin{aligned} r_1 &= \frac{-\theta + \sqrt{\theta^2 + 4Ac}}{2A} > 0, \\ r_2 &= \frac{-\theta - \sqrt{\theta^2 + 4Ac}}{2A} < 0 \end{aligned} \tag{1.10}$$

and

$$I_1(z) = \frac{1}{A}\int_z^{+\infty} e^{-r_1(s-z)} f(s)\,ds, \quad I_2(z) = \frac{1}{A}\int_{-\infty}^{z} e^{-r_2(s-z)} f(s)\,ds. \tag{1.11}$$

Moreover, if $\lim_{z\to\pm\infty} f(z) = f(\pm\infty) = f_\pm$ *both exist, then*

$$I_1(+\infty) = \frac{f(+\infty)}{Ar_1}, \tag{1.12}$$

together with

$$I_1(-\infty) = \begin{cases} 0 & \text{if } \int_{-\infty}^{+\infty} e^{-r_1 s} f(s)\,ds \text{ is finite} \\ \frac{f(-\infty)}{Ar_1} & \text{if } \int_{-\infty}^{+\infty} e^{-r_1 s} f(s)\,ds \text{ is not finite} \end{cases} \tag{1.13}$$

$$I_2(-\infty) = \frac{f(-\infty)}{Ar_2}, \tag{1.14}$$

and together with

$$I_2(+\infty) = \begin{cases} 0 & \text{if } \int_{-\infty}^{+\infty} e^{-r_2 s} f(s)\,ds \text{ is finite} \\ -\frac{f(+\infty)}{Ar_2} & \text{if } \int_{-\infty}^{+\infty} e^{-r_2 s} f(s)\,ds \text{ is not finite} \end{cases} \tag{1.15}$$

Proof. The outcome is achieving by using the standard formula of variation of constants for the equation (1.8), which provides

$$\begin{aligned} W(z) = {} & \frac{e^{r_1 z}}{A}\left[c_1 - \frac{1}{r_2 - r_1}\int_0^z e^{-r_1 s} f(s)\,ds\right] \\ & + \frac{e^{r_2 z}}{A}\left[c_2 + \frac{1}{r_2 - r_1}\int_0^z e^{-r_2 s} f(s)\,ds\right] \end{aligned}$$

where r_1 and r_2 are given in (1.10), while c_1 and c_2 are arbitrary constants. Therefore, we choose

$$c_1 = \frac{1}{r_2 - r_1}\int_0^{+\infty} e^{-r_1 s}\frac{f(s)}{A}\,ds, \quad c_2 = \frac{1}{r_2 - r_1}\int_{-\infty}^{0} e^{-r_2 s}\frac{f(s)}{A}\,ds,$$

since f is bounded and both these integrals converge. Hence we obtain (1.9)-(1.11).
A direct calculation also gives:

$$I_1(+\infty) = \lim_{z\to+\infty} \frac{\int_z^{+\infty} e^{-r_1 s} f(s)\,ds}{Ae^{-r_1 z}} = \lim_{z\to+\infty} \frac{e^{-r_1 z} f(z)}{-r_1 Ae^{-r_1 z}}$$

and we obtain (1.12). If $\int_{-\infty}^{+\infty} e^{-r_1 s} f(s)\,ds$ is finite, then $I_1(-\infty) = 0$. On the other hand, if $\int_{-\infty}^{+\infty} e^{-r_1 s} f(s)\,ds$ is not finite, then

$$I_1(-\infty) = \lim_{z\to-\infty} \frac{\int_z^{+\infty} e^{-r_1 s} f(s)\,ds}{Ae^{-r_1 z}} = \lim_{z\to-\infty} \frac{-e^{-r_1 z} f(z)}{-r_1 Ae^{-r_1 z}}$$

and hence (1.13) holds. The case for I_2 is similar, so the proof of (1.14)-(1.15) is omitted. □

Lemma 1.2.2. *Let* $\phi(z) = e^{-\int_0^z g(s)\,ds}$*, for a continuous function* g *with bounded limits at infinity, namely* $\lim_{z\to\pm\infty} g(z) = g(\pm\infty) = g_\pm$ *both exist. Assuming* $l > 0$ *it holds that*

1. *if* $g(+\infty) = l$, *then* $\phi(+\infty) = 0$
2. *if* $g(+\infty) = -l$, *then* $\phi(+\infty) = +\infty$
3. *if* $g(-\infty) = l$, *then* $\phi(-\infty) = +\infty$
4. *if* $g(-\infty) = -l$, *then* $\phi(-\infty) = 0$

Proof. Only the case 1. is given, because the others are similar.
If $g(+\infty) = l > 0$, then there exists $M > 0$ such that $|g(s) - l| < l/2$ for all $s > M$. Hence, for all $z > M$ we have that

$$0 \leq \phi(z) = e^{-\int_0^M g(s)\,ds} e^{-\int_M^z g(s)\,ds} \leq e^{-\int_0^M g(s)\,ds} e^{-l(z-M)/2}$$

which finally implies $\phi(z) \to 0$ as $z \to +\infty$. □

We make use of the previous results to deduce an equivalent system corresponding to (1.5) with asymptotic conditions (1.6)-(1.7). We start by recalling the second equation of system (1.5) as following

$$\begin{aligned} 0 &= D[(1-u)v'' - u'v'] + \theta v' + rv(1-v) \\ v(-\infty; D) &= 1, \;\; v(+\infty; D) = 0. \end{aligned} \tag{1.16}$$

Then, we apply Lemma 1.2.1 to the third equation, with $f(s) = -cv(s; D)$, and we obtain

$$w(z; D) = \frac{c}{A(r_1 - r_2)} \left[e^{r_1 z} \int_z^{+\infty} e^{-r_1 s} v(s; D)\, ds + e^{r_2 z} \int_{-\infty}^{z} e^{-r_2 s} v(s; D)\, ds \right] \tag{1.17}$$

and r_1 and r_2 as defined in (1.14).
Moreover, since $f(+\infty) = -cv(+\infty; D) = 0$, we have $I_1(+\infty) = I_2(+\infty) = 0$, and hence $w(+\infty; D) = 0$. On the other hand, since

$$-c \int_{-\infty}^{+\infty} e^{-r_1 s} v(s; D)\, ds = -\infty$$

we deduce from (1.13) and (1.14) that

$$\begin{aligned} w(-\infty; D) = \frac{c}{A(r_1 - r_2)} \big[& e^{r_1(-\infty)} \int_{-\infty}^{+\infty} e^{-r_1 s} v(s; D)\, ds \\ & + e^{r_2(-\infty)} \int_{-\infty}^{-\infty} e^{-r_2 s} v(s; D)\, ds \big] = 1 \end{aligned}$$

The first equation of system (1.5) is a *Bernoulli equation*, and it can be solved explicitly to obtain

$$\begin{aligned} u(z; D) &= \frac{\theta\, \phi(z; D)}{\int_z^{+\infty} \phi(s; D)\, ds}, \\ \phi(z; D) &= e^{-\int_0^z [1 - dw(s;D)]/\theta\, ds} \end{aligned} \tag{1.18}$$

Let $g(s) = [1 - dw(s; D)]/\theta$. then $g(+\infty) = 1/\theta > 0$ and $\phi(+\infty; D) = 0$ by using Lemma 1.2.2. It follows that

$$u(+\infty; D) = \theta \lim_{z \to +\infty} \frac{\phi(z; D)}{\int_z^{+\infty} \phi(s; D)\, ds} = \theta \lim_{z \to +\infty} \frac{-\phi(z; D) g(z)}{-\phi(z; D)} = \theta g(+\infty) = 1$$

for all $d > 0$. Furthermore, $g(-\infty) = (1-d)/\theta$. If $0 < d < 1$, then $\phi(-\infty; D) = \infty$ from Lemma 1.2.2, $\int_{-\infty}^{\infty} \phi(s; D)\, ds = +\infty$ and

$$u(-\infty; D) = \theta \lim_{z \to -\infty} \frac{\phi(z; D)}{\int_{-\infty}^{z} \phi(s; D)\, ds} = \theta \lim_{z \to -\infty} \frac{-\phi(z; D) g(z)}{-\phi(z; D)} = 1 - d.$$

If $d > 1$, then $\phi(-\infty; D) = 0$ from Lemma 1.2.2, together with

$$0 < \int_{-\infty}^{+\infty} \phi(s; D)\, ds \leq +\infty$$

and

$$u(-\infty; D) = \frac{\theta \phi(-\infty; D)}{\int_{-\infty}^{\infty} \phi(s; D)\, ds} = 0.$$

Finally, in $d = 1$, then g is a non-negative monotone increasing function satisfying $g(-\infty) = 0$. Although we can not apply Lemma 1.2.2, we notice that $0 < \phi(-\infty; D) \leq \infty$ and therefore $\int_{-\infty}^{+\infty} \phi(s; D)\, ds = +\infty$, so that it is straightforward to show that $u(-\infty; D) = 0$. Thus, we have proven the equivalence of the travelling waves model (1.5) with (1.6)-(1.7) with (1.16)-(1.18).

We conclude this section by enunciating two results (without proof) which are useful for analysing the asymptotic behaviour of the travelling wave solutions later on.

Lemma 1.2.3. *Let ϕ be a continuous function and α, s_L, $s_R \in \mathbb{R}$, with $\alpha > 0$. We consider $I(D) = \int_{s_L}^{s_R} e^{\phi(s)/D^\alpha}\, ds$ as $D \to 0^+$.*
Then the following statements hold:

1. *if $\phi'(s) < 0$ for all $s_L \leq s < s_R$, then*

$$I(D) \simeq -\frac{D^\alpha e^{\phi(s_L)/D^\alpha}}{\phi'(s_L)}$$

where the symbol $\simeq$ denotes the approximation approximation neglecting higher orders of D;

2. *if $\phi'(s) > 0$ for all $s_L < s \leq s_R$, then*

$$I(D) \simeq \frac{D^\alpha e^{\phi(s_R)/D^\alpha}}{\phi'(s_R)};$$

3. *if ϕ has a unique maximum at some point $s_L < s^* < s_R$ (thus $\phi'(s^*) = 0$ and $\phi''(s^*) < 0$), then*

$$I(D) \simeq \frac{\sqrt{2\pi} D^{\alpha/2} e^{\phi} s^*/D^\alpha}{\sqrt{-\phi''(s^*)}};$$

The proof follows from a standard application of Laplace's method to approximate integrals containing a large parameter [3].

Lemma 1.2.4. *Let d, c, A, $\theta_0 > 0$ and let us define*

$$\phi_-(z) = \frac{1}{\theta_0}\big[(d-1)z + \frac{d}{2\sqrt{c/A}}(1 - e^{\sqrt{c/A}z})\big],$$

$$\phi_+(z) = \frac{1}{\theta_0}\big[\frac{d}{2\sqrt{c/A}}(1 - e^{-\sqrt{c/A}z}) - z\big].$$

Then the following properties hold:

1. $\phi_-(0) = \phi_+(0) = 0$.

2. *the first and second order satisfy*

$$\phi'_-(z) = \frac{1}{\theta_0}\big(d - 1 - \frac{d}{2}e^{\sqrt{c/A}z}\big),\ \ \phi''_-(z) = -\frac{d\sqrt{c/A}}{2\theta_0}e^{\sqrt{c/A}z},$$

$$\phi'_+(z) = \frac{1}{\theta_0}\big(\frac{d}{2}e^{\sqrt{c/A}z} - 1\big),\ \ \phi''_-(z) = -\frac{d\sqrt{c/A}}{2\theta_0}e^{-\sqrt{c/A}z},$$

3. *if*

$$z_- = \frac{1}{\sqrt{c/A}}\log\frac{2(d-1)}{d} < 0 \ \textit{for}\ 1 < d < 2$$

then $\phi_-(z_-) > 0$, $\phi'_-(z_-) = 0$ *and* $\phi''_-(z_-) < 0$.

4. *if*

$$z_+ = \frac{1}{\sqrt{c/A}}\log\frac{d}{2} > 0 \ \textit{for}\ d > 2$$

then $\phi_+(z_+) > 0$, $\phi'_+(z_+) = 0$ *and* $\phi''_+(z_+) < 0$

1.3 Analysis of slow waves

Following the definition by Fasano et al. [7], a *slow travelling wave* is a solution (u, v, w) to the system (1.1) whose components are positive and such that $\theta = \theta_0 D^\alpha$ with $\theta_0,\ \alpha > 0$ and $\theta_0 = O(1)$ as $D \to 0^+$, in contrast to *fast travelling waves* for which $\theta = O(1)$.

We focus our attention on the analysis of slow waves solutions for (1.5). Indeed, since the choice of initial data designed to reproduce *in vitro* experiments is such that the data for the tumour is compactly supported on the right, then the existence of fast waves is not expected. However, from a biological and diagnostic point of view, fast waves are equally critical, therefore in future works it will be important to analyse them. Our forthcoming analysis makes use of *matched asymptotic expansions* method [3, 15].

We assume that the wave profiles possess two different regions: an *outer region*, corresponding to $|z| \gg 1$, where the solution and its derivatives do not exhibit large variations; an *inner region*, corresponding to a neighborhood of $z = 0$, where the derivatives undergo considerable changes. Furthermore, the branches of solution in inner and outer regions are matched in a sufficient smooth way.

We deal with the auxiliary system (1.16)-(1.18), which has been proven to be equivalent to (1.5).
Let us define:

$$u(z; D) = U(\xi; D),\ v(z; D) = V(\xi; D),\ w(z; D) = W(\xi; D),$$

where $\xi = z/D^\alpha$ denotes a rescaled variable suitable for the analysis inside the inner region. Substituting to (1.16)-(1.18) and taking the derivative with respect to ξ, we obtain

$$0 = D^{1-2\alpha}[(1 - U)\ddot{V} - \dot{U}\dot{V}] + \theta_0\dot{V} + rV(1 - V), \tag{1.19}$$

$$U(\xi;D)=\frac{\theta_0 D^\alpha\phi(D^\alpha\xi;D)}{\int_{D^\alpha\xi}^{+\infty}\phi(s;D)\,ds}, \tag{1.20}$$

$$\begin{aligned}W(\xi;D)=\frac{c}{A(r_1-r_2)}\Big[&e^{r_1D^\alpha\xi}\int_{D^\alpha\xi}^{+\infty}e^{-r_1s}V\big(\frac{s}{D^\alpha};D\big)\,ds\\&+e^{r_2D^\alpha\xi}\int_{-\infty}^{D^\alpha\xi}e^{-r_2s}V\big(\frac{s}{D^\alpha};D\big)\,ds,\Big]\end{aligned} \tag{1.21}$$

where the derivatives are taken with respect to ξ together with the following boundary conditions

$$U(\pm\infty;D)=u(0_\pm;D),\ V(\pm\infty;D)=v(0_\pm;D),\ W(\pm\infty;D)=w(0_\pm;D).$$

which are deduced from the matching requirement between inner and outer regions.

1.3.1 Uniform approximation for w

We define the outer solution as

$$u_{out}(z)=u(z;0),\ \ v_{out}(z)=v(z;0),\ \ w_{out}(z)=w(z;0),$$

while inner solution is given by

$$U_{in}(\xi)=U(\xi;0),\ \ V_{in}(\xi)=V(\xi;0),\ \ W_{in}(\xi)=W(\xi;0).$$

Looking at the equation for v in (1.16), we remark that the choice $D=0$ leads to

$$v_{out}(z)=\begin{cases}1 & \text{if } z<0\\ 0 & \text{if } z>0\end{cases}$$

Therefore, we can write the outer solution corresponding to the H^+ ions concentration as follows

$$w_{out}(z)=\frac{\sqrt{c}}{2\sqrt{A}}\Big[e^{\sqrt{c/A}z}\int_z^\infty e^{-\sqrt{c/A}s}v_{out}(s)\,ds+e^{-\sqrt{c/A}z}\int_{-\infty}^z e^{\sqrt{c/A}s}v_{out}(s)\,ds\Big],$$

and hence

$$w_{out}(z)=\begin{cases}1-\frac{1}{2}e^{\sqrt{c/A}z} & \text{if } z<0\\ \frac{1}{2}e^{-\sqrt{c/A}z} & \text{if } z>0\end{cases}$$

For the inner solution, putting $D=0$ in equation (1.21) and using the fact that $V_{in}(+\infty)=v_{out}(0_+)=0$ and $V_{in}(-\infty)=v_{out}(0_-)=1$, we obtain

$$W_{in}(\xi)=\frac{\sqrt{c}}{2\sqrt{A}}\Big[\int_0^\infty e^{-\sqrt{c/A}s}V_{in}(\infty)\,ds+\int_{-\infty}^0 e^{\sqrt{c/A}s}V_{in}(-\infty)\,ds\Big]=\frac{1}{2}$$

for any $\xi\in\mathbb{R}$.
We also consider the overlapping region where the value of w is the same for the inner and outer solution which is give by $w_c=W_{in}(\pm\infty)=w_{out}(0_\pm)=\frac{1}{2}$. In order to construct a uniform approximation for w, we add the inner and outer branches and then subtract the value in the overlapping region and we conclude that

$$w(z;D)\simeq w_{out}(z)+W_{in}\big(\frac{z}{D^\alpha}\big)-w_c=\begin{cases}1-\frac{1}{2}e^{\sqrt{c/A}z} & \text{if } z<0\\ \frac{1}{2}e^{-\sqrt{c/A}z} & \text{if } z>0\end{cases} \tag{1.22}$$

1.3.2 Uniform approximation for u as function of the parameter d

By substituting the uniform approximation (1.22) into the equation (1.18) we get

$$\phi(z;D) \simeq \begin{cases} e^{\phi_-(z)/D^\alpha} & \text{if } z<0 \\ e^{\phi_+(z)/D^\alpha} & \text{if } z>0 \end{cases}$$

and consequently, we deduce that

$$u(z;D) \simeq \begin{cases} \frac{\theta_0 D^\alpha e^{\phi_-(z)/D^\alpha}}{\int_z^0 e^{\phi_-(s)/D^\alpha}\,ds + \int_0^\infty e^{\phi_+(s)/D^\alpha}\,ds} & \text{if } z<0, \\ \frac{\theta_0 D^\alpha e^{\phi_+(z)/D^\alpha}}{\int_z^\infty e^{\phi_+(s)/D^\alpha}\,ds} & \text{if } z<0, \end{cases} \tag{1.23}$$

where ϕ_+ and ϕ_- are defined as in Lemma (1.2.4).
Now, we analyse three different cases, according to the value of the parameter d.

Case $0<d<1$

Suppose that $z>0$. Then for any $z \le s < \infty$ we have

$$\phi'_+(s) = \frac{1}{\theta_0}\left(\frac{d}{2}e^{-\sqrt{c/A}s} - 1\right) < \frac{1}{\theta_0}\left(\frac{d}{2} - 1\right) < 0.$$

Using Lemma (1.2.3) 1. we obtain the approximation

$$\int_z^\infty e^{\phi_+(s)/D^\alpha}\,ds \simeq -\frac{D^\alpha e^{\phi_+(z)/D^\alpha}}{\phi'_+(z)}$$

and by substituting in to (1.23), for $z>0$ we get

$$u(z;D) \simeq -\theta_0\phi'_+(z) = 1 - \frac{d}{2}e^{-\sqrt{c/A}z}. \tag{1.24}$$

Suppose that $z<0$. Then for any $0 \le s < \infty$ we have

$$\phi'_+(s) = \frac{1}{\theta_0}\big(\frac{d}{2}e^{-\sqrt{c/A}s} - 1\big) \le \frac{1}{\theta_0}\big(\frac{d}{2} - 1\big) < 0.$$

Using Lemma (1.2.3) 1. we obtain the approximation

$$\int_0^\infty e^{\phi_+(s)/D^\alpha}\,ds \simeq -\frac{D^\alpha e^{\phi_+(0)/D^\alpha}}{\phi'_+(0)} = \frac{2\theta_0 D^\alpha}{2-d}.$$

Moreover, for any $z \le s < 0$ we have

$$\phi'_-(s) = \frac{1}{\theta_0}\big(d - 1 - \frac{d}{2}e^{\sqrt{c/A}s}\big) < \frac{d-1}{\theta_0} < 0.$$

and using Lemma (1.2.3) 1. we obtain the approximation

$$\int_z^0 e^{\phi_-(s)/D^\alpha}\,ds \simeq -\frac{D^\alpha e^{\phi_-(z)/D^\alpha}}{\phi'_-(z)}.$$

Adding the two approximations and recalling that $\phi_-(z) > 0$ for $z < 0$ and $0 < d < 1$, we get for all $z < 0$

$$\int_z^0 e^{\phi_-(s)/D^\alpha}\, ds + \int_0^{+\infty} e^{\phi_+(s)/D^\alpha}\, ds \simeq -\frac{D^\alpha e^{\phi_-(z)/D^\alpha}}{\phi_-'(z)}.$$

Finally, by substituting this formula to (1.23) we conclude for $z < 0$ that

$$u(z; D) \simeq -\theta_0 \phi_-'(z) = 1 - d + \frac{d}{2} e^{\sqrt{c/A} z} \tag{1.25}$$

We notice that the value of u in the inner region is

$$U(\xi; D) = u(D^\alpha \xi; D) \simeq \begin{cases} 1 - d + \frac{d}{2} e^{\sqrt{c/A} D^\alpha \xi} & \text{if } \xi < 0 \\ 1 - \frac{d}{2} e^{-\sqrt{c/A} D^\alpha \xi} & \text{if } \xi > 0 \end{cases}$$

Hence, setting $D = 0$, we have $U_{in}(\xi) = 1 - \frac{d}{2}$ for $\xi \in \mathbb{R}$.

Case $1 < d < 2$

We skip the details of the analysis for the case $z > 0$ because it is the same as for $0 < d < 1$, hence we conclude that

$$u(z; D) \simeq 1 - \frac{d}{2} e^{-\sqrt{c/A} z}$$

together with

$$\int_0^{\infty} e^{\phi_+(s)/D^\alpha}\, ds \simeq \frac{2\theta_0 D^\alpha}{2 - d}.$$

Suppose $z < 0$ and take z_- as defined in Lemma (1.2.4). Then, we distinguish two sub-cases. Let $z_- < z < 0$. For any $z \le s < 0$, then $s > z_-$ and

$$\phi_-'(s) = \frac{1}{\theta_0}\left(d - 1 - \frac{d}{2} e^{\sqrt{c/A} s}\right) < \frac{1}{\theta_0}\left(d - 1 - \frac{d}{2} e^{\sqrt{c/A} z}\right) = 0.$$

Using Lemma (1.2.3) 1. we obtain the approximation

$$\int_z^0 e^{\phi_-(s)/D^\alpha}\, ds \simeq -\frac{D^\alpha e^{\phi_-(z)/D^\alpha}}{\phi_-'(z)}$$

and hence, using the fact that $\phi_-(z) < z$ for all $z_- < z < 0$, we get

$$\int_z^0 e^{\phi_-(s)/D^\alpha}\, ds + \int_0^{\infty} e^{\phi_+(s)/D^\alpha}\, ds \simeq -\frac{D^\alpha e^{\phi_-(z)/D^\alpha}}{\phi_-'(z)}.$$

Therefore, from (1.23) we obtain for $z_- < z < 0$ that

$$u(z; D) \simeq -\theta_0 \phi_-'(z) = 1 - d + \frac{d}{2} e^{\sqrt{c/A} z}. \tag{1.26}$$

Let $z < z_-$. Using Lemma (1.2.3) 3. and Lemma (1.2.4) 3., we have that $\phi_-(z_-) > 0$ and thus we obtain

$$\int_z^0 e^{\phi_-(s)/D^\alpha}\, ds \simeq \frac{\sqrt{2\pi} D^{\alpha/2} e^{\phi_-(z_-)/D^\alpha}}{\sqrt{-\phi_-''(z_-)}} = \sqrt{\frac{2\pi\theta_0}{\sqrt{c/A}(d-1)}} D^{\alpha/2} e^{\phi_-(z_-)/D^\alpha}$$

so that

$$\int_z^0 e^{\phi_-(s)/D^\alpha}\,ds + \int_0^\infty e^{\phi_+(s)/D^\alpha}\,ds \simeq \sqrt{\frac{2\pi\theta_0}{\sqrt{c/A}(d-1)}}D^{\alpha/2}e^{\phi_-(z_-)/D^\alpha}.$$

Therefore, for $z < z_-$ we conclude that

$$u(z;D) \simeq \sqrt{\frac{\sqrt{c/A}(d-1)\theta_0}{2\pi}}D^{\alpha/2}e^{[\phi_-(z)-\phi_-(z_-)]/D^\alpha} \tag{1.27}$$

We notice that the value of u in the inner region is

$$U(\xi;D) = u(D^\alpha\xi;D) \simeq \begin{cases} 1-d+\frac{d}{2}e^{\sqrt{c/A}D^\alpha\xi} & \text{if } \xi < 0 \\ 1-\frac{d}{2}e^{-\sqrt{c/A}D^\alpha\xi} & \text{if } \xi > 0 \end{cases}$$

Hence, setting $D = 0$, we have $U_{in}(\xi) = 1 - \frac{d}{2}$ for $\xi \in \mathbb{R}$.

Case $d > 2$

Suppose $z > 0$ and take z_+ as defined in Lemma (1.2.4). Then, we distinguish two sub-cases. Let $z > z_+$. For any $z \le s < \infty$, then $s > z_+$ and

$$\phi'_+(s) = \frac{1}{\theta_0}\left(\frac{d}{2}e^{-\sqrt{c/A}s} - 1\right) < \frac{1}{\theta_0}\left(\frac{d}{2}e^{-\sqrt{c/A}z} - 1\right) = 0.$$

Using Lemma (1.2.3) 1. we obtain the approximation

$$\int_z^\infty e^{\phi_+(s)/D^\alpha}\,ds \simeq -\frac{D^\alpha e^{\phi_+(z)/D^\alpha}}{\phi'_+(z)}$$

and hence, for all $z > z_+$, we get

$$u(z;D) \simeq -\theta_0\phi'_+(z) = 1 - \frac{d}{2}e^{-\sqrt{c/A}z}. \tag{1.28}$$

Let $0 < z < z_+$. Using Lemma (1.2.3) 3. and Lemma (1.2.4) 4., we obtain

$$\int_z^\infty e^{\phi_+(s)/D^\alpha}\,ds \simeq \frac{\sqrt{2\pi}D^{\alpha/2}e^{\phi_+(z_+)/D^\alpha}}{\sqrt{-\phi''_+(z_+)}} = \sqrt{\frac{2\pi\theta_0}{\sqrt{c/A}}}D^{\alpha/2}e^{\phi_+(z_+)/D^\alpha}$$

Thus, for $0 < z < z_+$ we conclude that

$$u(z;D) \simeq \sqrt{\frac{\sqrt{c/A}\theta_0}{2\pi}}D^{\alpha/2}e^{[\phi_+(z)-\phi_+(z_+)]/D^\alpha}$$

Now, suppose $z < 0$. Using Lemma (1.2.3) 3. and Lemma (1.2.4) 4. we have that

$$\int_0^\infty e^{\phi_+(s)/D^\alpha}\,ds \simeq \frac{\sqrt{2\pi}D^{\alpha/2}e^{\phi_+(z_+)/D^\alpha}}{\sqrt{-\phi''_+(z_+)}} = \sqrt{\frac{2\pi\theta_0}{\sqrt{c/A}}}D^{\alpha/2}e^{\phi_+(z_+)/D^\alpha}$$

and also for any $z < s \leq 0$,

$$\phi'_-(s) = \frac{1}{\theta_0}\big(d - 1 - \frac{d}{2}e^{\sqrt{c/A}s}\big) \geq \frac{1}{\theta_0}\big(d - 1 - \frac{d}{2}\big) = \frac{d-2}{2\theta_0} > 0$$

Using Lemma (1.2.3) 2. we obtain

$$\int_z^0 e^{\phi_-(s)/D^\alpha}\, ds \simeq \frac{D^\alpha e^{\phi_-(0)/D^\alpha}}{\phi'_-(0)} = \frac{2\theta_0 D^\alpha}{d-2}$$

and using the fact that $\phi_+(z_+) > 0$ from Lemma (1.2.4) 4. we have that

$$\int_z^0 e^{\phi_-(s)/D^\alpha}\, ds + \int_0^\infty e^{\phi_+(s)/D^\alpha}\, ds \simeq \sqrt{\frac{2\pi\theta_0}{\sqrt{c/A}}} D^{\alpha/2} e^{\phi_+(z_+)/D^\alpha}$$

Thus, for $z < 0$ we conclude that

$$u(z;D) \simeq \sqrt{\frac{\sqrt{c/A}\theta_0}{2\pi}} D^{\alpha/2} e^{[\phi_-(z)-\phi_+(z_+)]/D^\alpha} \tag{1.29}$$

We notice that the value of u in the inner region is

$$U(\xi;D) = u(D^\alpha\xi;D) \simeq \begin{cases} \sqrt{\frac{\sqrt{c/A}\theta_0}{2\pi}} D^{\alpha/2} e^{[\phi_-(D^\alpha\xi)-\phi_+(z_+)]/D^\alpha} & \text{if } \xi < 0 \\ \sqrt{\frac{\sqrt{c/A}\theta_0}{2\pi}} D^{\alpha/2} e^{[\phi_+(D^\alpha\xi)-\phi_+(z_+)]/D^\alpha} & \text{if } \xi > 0 \end{cases}$$

In order to prove that $U_{in}(\xi) = U(\xi;0) = 0$ for all $\xi \in \mathbb{R}$, we compute

$$\begin{aligned} \frac{\phi_-(D^\alpha\xi)}{D^\alpha} &= \frac{1}{\theta_0}\left[(d-1)\xi + \frac{d}{2\sqrt{c/A}}.\frac{1 - e^{\sqrt{c/A}D^\alpha\xi}}{D^\alpha}\right] \\ &= \frac{1}{\theta_0}\left[(d-1)\xi + \frac{d}{2\sqrt{c/A}}.\frac{-\sqrt{c/A}\xi D^\alpha - (\sqrt{c/A}\xi)^2 D^{2\alpha}/2! + O(D^{2\alpha})}{D^\alpha}\right] \\ &= \frac{(d-2)\xi}{2\theta_0} + O(D^\alpha). \end{aligned}$$

Then for $\xi < 0$ we have

$$\lim_{D\to 0^+} \frac{\phi_-(D^\alpha\xi)}{D^\alpha} = \frac{(d-2)\xi}{2\theta_0}$$

and hence $U_{in}(\xi) = 0$ for $\xi < 0$ since $\phi_+(z_+) > 0$ from Lemma 1.2.4 4.
We can use a similar approach to claim that

$$\lim_{D\to 0^+} \frac{\phi_+(D^\alpha\xi)}{D^\alpha} = \frac{(d-2)\xi}{2\theta_0}$$

and hence $U_{in}(\xi) = 0$ for $\xi > 0$ and $U_{in}(0) = 0$.

Limit cases $d = 1$ and $d = 2$

We deal with these two limit cases by taking the lateral limits of the previous cases.
If we take the limit as $d \to 1^-$ in (1.25) we obtain

$$u(z;D) \simeq \begin{cases} \frac{1}{2}e^{\sqrt{c/A}z} & \text{if } z < 0 \\ 1 - \frac{1}{2}e^{-\sqrt{c/A}z} & \text{if } z > 0. \end{cases}$$

and we obtain the same approximation if we take the limit as $d \to 1^+$ which implies $z_- \to -\infty$ in (1.27).
In the inner region we get

$$U(\xi;D) = u(D^\alpha \xi; D) \simeq \begin{cases} \frac{1}{2}e^{\sqrt{c/A}D^\alpha \xi} & \text{if } \xi < 0 \\ 1 - \frac{1}{2}e^{-\sqrt{c/A}D^\alpha \xi} & \text{if } \xi > 0 \end{cases}$$

and putting $D = 0$ we conclude that $U_{in}(\xi) = \frac{1}{2}$ for all $\xi \in \mathbb{R}$.
If we take the limit as $d \to 2^-$ which implies $z_- \to 0$ in (1.27) we obtain

$$u(z;D) \simeq \begin{cases} \sqrt{\frac{\sqrt{c/A}\theta_0}{2\pi}} D^{\alpha/2} e^{\phi_-(z)/D^\alpha} & \text{if } z < 0 \\ 1 - e^{-\sqrt{c/A}z} & \text{if } z > 0 \end{cases}$$

and we obtain the same approximation if we take the limit as $d \to 2^+$ which implies $z_+ \to 0$ in (1.29) we get the same approximation.
In the inner region we get

$$U(\xi;D) = u(D^\alpha \xi; D) \simeq \begin{cases} \sqrt{\frac{\sqrt{c/A}\theta_0}{2\pi}} D^{\alpha/2} e^{\phi_-(D^\alpha \xi)/D^\alpha} & \text{if } \xi < 0 \\ 1 - e^{-\sqrt{c/A}D^\alpha \xi} & \text{if } \xi > 0 \end{cases}$$

and putting $D = 0$ we conclude that $U_{in}(\xi) = 0$ for all $\xi \in \mathbb{R}$.
As a matter of fact, the value U_{in} is constant for all $d > 0$.

1.3.3 Uniform approximation for v

Finally, we consider the equation for the tumour cells concentration v. Putting $D = 0$ in (1.16), we can distinguish two cases.
If $\alpha > 1/2$, then $\ddot{V}_{in} = 0$, because the first order derivatives and the growth term are asymptotically null, therefore the second derivative has also to be null when $1 - 2\alpha < 0$, This means that $V_{in}(\xi)$ is a linear function, and hence the conditions $V_{in}(-\infty) = v_{out}(0_-) = 1$ and $V_{in}(+\infty) = v_{out}(0_+) = 0$ can not be satisfied simultaneously.
If $\alpha < 1/2$, then V_{in} satisfies the following Bernoulli equation

$$\theta_0 \dot{V}_{in} + r V_{in}(1 - V_{in}) = 0$$

with boundary conditions:

$$V_{in}(-\infty) = 1, \quad V_{in}(+\infty) = 0,$$

hence the solution is

$$V_{in}(\xi) = \frac{1}{1 + e^{r\xi/\theta_0}}.$$

If $\alpha = 1/2$, then V_{in} satisfies the following Fisher-KPP equation

$$K\ddot{V}_{in} + \theta_0\dot{V}_{in} + rV_{in}(1 - V_{in}) = 0$$

with boundary conditions

$$V_{in}(-\infty) = 1, \quad V_{in}(+\infty) = 0.$$

where $K = d/2$ if $0 < d \leq 2$ and $K = 1$ if $d > 2$. Therefore, there exists a solution of the form $V_{in}(\xi) = \phi_F(\xi; \theta_0)$ for all $\theta_0 \geq 2\sqrt{rK}$ [9].
We also consider the overlapping region where the value of v is the same for the inner and outer solution which is given by $v_c = V_{in}(+\infty) = v_{out}(0_+) = 0$ for $z > 0$ and $v_c = V_{in}(-\infty) = v_{out}(0_-) = 0$ for $z < 0$. We construct a uniform approximation for v by adding the inner and outer approximations and then we subtract the value in the overlapping region and hence we conclude that

$$\begin{aligned} v(z; D) &\simeq v_{out}(z) + V_{in}\left(\frac{z}{D^\alpha}\right) - v_c \\ &= \begin{cases} \frac{1}{1+e^{rz/(\theta_0 D^\alpha)}} & \text{if } \alpha < 1/2 \\ \phi_F(\frac{z}{\sqrt{D}}; \theta_0) & \text{if } \alpha = 1/2. \end{cases} \end{aligned} \tag{1.30}$$

We notice that we do not have valid solutions for $\alpha > 1/2$, as illustrated at the beginning of this section.

1.3.4 An estimate of the width of the interstitial gap

From a mathematical point of view, an *interstitial gap* for the system (1.5) is an interval I such that, for all $z \in I$ it holds

$$u(z; D) + v(z; D) \ll 1.$$

For the case $d > 2$, from the results in Section 1.3 it is clear that $I \simeq (0, z_+)$ and hence the width of the gap is estimated by the value

$$z_+ = \frac{1}{\sqrt{c/A}} \log \frac{d}{2}, \tag{1.31}$$

whilst for $0 < d \leq 2$ this gap does not exist. Indeed, when $0 < z < z_+$, we have

$$v(z; D) \simeq v_{out}(z) = 0$$

and

$$u(z; D) \simeq \sqrt{\frac{\theta_0\sqrt{c/A}}{2\pi}} D^{\alpha/2} e^{[\phi_+(z) - \phi_+(z_+)]/D^\alpha} = O(D^{\alpha/2} e^{-C/D^\alpha})$$

for some $C = C(z) > 0$ (using the fact that $\phi'_+(z) > 0$ for $0 < z < z_+$).

Nevertheless, for the case $a < d < 2$ we can also give an interpretation of the value z_-. Indeed, $v(z; D) \simeq v_{out}(z) = 1$ for $z < 0$. For $z < z_-$, u is almost zero because

$$u(z; D) \simeq \sqrt{\frac{\sqrt{c/A}(d-1)\theta_0}{2\pi}} D^{\alpha/2} e^{[\phi_-(z) - \phi_-(z_-)]/D^\alpha} = O(D^{\alpha/2} e^{-C/D^\alpha})$$

where $C = C(z) > 0$ since $\phi_-(z) > 0$ for $z < z_-$. For $z_- < z < 0$ we have that $u(z; D) = O(1)$ and it leaves $z = 0$ with a positive derivative.
Therefore, the interval $(z_-, 0)$ can be considered as an overlapping region where healthy and cancer tissues can be simultaneously found for $1 < d < 2$ and hence the width of this region is z_-.

Remark 1.3.1. We compare the estimate (1.31) for the width of the interstitial gap with the value proposed in [21] which is given for A homogeneous and $a \gg 1$ by the approximation

$$z_+ \simeq \frac{1}{\sqrt{c}} \log \frac{d}{2} + \sqrt{\frac{\theta}{\sqrt{c}}} \tag{1.32}$$

Despite no details are provided on the derivation of the above formula in [21], it is remarkable that estimate (1.31) is in excellent agreement with (1.32) not only for $a \gg 1$, but also for smaller values $a > 2$.

Chapter 2

Numerical approximation

For the numerical investigation we consider the non-dimensionalized system:

$$\begin{cases} u_t = u(1-u) - duw \\ v_t = rv(1-v) + D[(1-u)v_x]_x \\ w_t = c(v-w) + (Aw_x)_x \end{cases} \tag{2.1}$$

and the experimental domain is assumed to be the one-dimensional interval $[-L, L]$, with $L > 0$. This resultant version allows to operate with fewer (positive) parameters d, r, D and c , thus reducing their original range and coping with scaled functions u, v, w and A. For the numerical simulation, we consider the homogeneous Neumann boundary conditions.

The numerical results we will show are consistent with those illustrated in [7], together with an application of the analytical approach to the model.

Remark 2.0.1. We observe that the diffusion term in the third equation of (2.1) can be rewritten as

$$(Aw_x)_x = A_x w_x + Aw_{xx}$$

however, this alternative is not useful for the numerical simulation, as we will discuss later in Section 2.1.

2.1 The numerical algorithm

We adopt a numerical strategy based on the *finite volume method*, which guarantees consistency and stability in terms of closeness to the physics of the model [32]. The algorithm is semi-implicit in time and employs a non-uniform discretization mesh in space.

Let $C_i = [x_{i-\frac{1}{2}}, x_{i+\frac{1}{2}})$ be the (one-dimensional) finite volume centred in $x_i = \frac{x_{i-\frac{1}{2}} + x_{i+\frac{1}{2}}}{2}$, for $i = 1, 2, \ldots, N$, where N is the number of vertices, which is fixed. Let $\Delta x_i = |x_{i+\frac{1}{2}} - x_{i-\frac{1}{2}}|$ be the variable cells' size, hence $|x_i - x_{i-1}| = \frac{\Delta x_{i-1}}{2} + \frac{\Delta x_i}{2}$ is the length of an interfacial interval (see Figure 2.1).

We build a piecewise constant approximation of the function $A(x)$ by means of its *integral cell-averages*, namely

$$A_i = \frac{1}{\Delta x_i} \int_{C_i} A(x)\, dx\,.$$

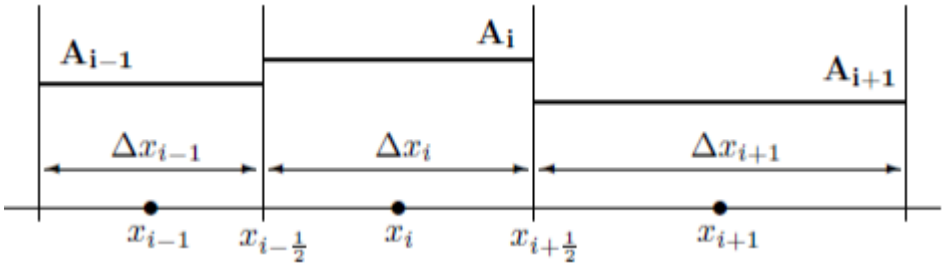

Figure 2.1: Piecewise constant reconstruction on non-uniform mesh

and we perform the same projection also for the solution to the system (2.1) by defining

$$u_i(t) = \frac{1}{\Delta x_i} \int_{C_i} u(x,t)\, dx\,,$$

for example.

Firstly, we consider the equation for the healthy tissue concentration u and its finite volume integral version given by

$$\frac{1}{\Delta x_i} \int_{C_i} u_t\, dx \;= \frac{1}{\Delta x_i} \int_{C_i} u(1-u)\, dx \;- \frac{d}{\Delta x_i} \int_{C_i} uw\, dx,$$

so that we obtain the following approximation

$$u_i' = u_i(1-u_i) - du_i w_i \tag{2.2}$$

where the time dependence on t is dropped for shortness (with an abused of notation for the symbols of the numerical variables).
Then, we consider the equation for the malignant tissue concentration v and its finite volume integral version given by

$$\frac{1}{\Delta x_i} \int_{C_i} v_t\, dx \;= \frac{r}{\Delta x_i} \int_{C_i} v(1-v)\, dx \;+ \frac{D}{\Delta x_i} \int_{C_i} \big[(1-u)v_x\big]_x\, dx$$

Hence, we need a specific approach for the discretization of the nonlinear diffusion term. We proceed by evaluating the differential term at the mesh interfaces, as suggested by the *theorem of the divergence* (which is actually the *fundamental theorem of integral calculus* in one dimension), and we make use of interfacial differences to approximate the derivatives as follows

$$\begin{aligned} \frac{D}{\Delta x_i} \Bigg[& \frac{(1-u_i)\Delta x_i + (1-u_{i+1})\Delta x_{i+1}}{\Delta x_i + \Delta x_{i+1}} \cdot \frac{v_{i+1} - v_i}{\frac{\Delta x_i}{2} + \frac{\Delta x_{i+1}}{2}} \\ & - \frac{(1-u_{i-1})\Delta x_{i-1} + (1-u_i)\Delta x_i}{\Delta x_{i-1} + \Delta x_i} \cdot \frac{v_i - v_{i-1}}{\frac{\Delta x_{i-1}}{2} + \frac{\Delta x_i}{2}} \Bigg] \end{aligned} \tag{2.3}$$

where the other interfacial quantities are approximated by building weighted averages whose weights are the size of the adjacent finite volumes, so that $\Delta x_i/\Delta x_{i+1}$ and $\Delta x_{i-1}/\Delta x_i$ are em-

ployed at the interfaces $x_{1+\frac{1}{2}}$ and $x_{i-\frac{1}{2}}$ respectively. Therefore, we obtain

$$v_i' = rv_i(1-v_i) + \frac{D}{\Delta x_i}\left[\frac{(1-u_i)\Delta x_i + (1-u_{i+1})\Delta x_{i+1}}{\Delta x_i + \Delta x_{i+1}} \cdot \frac{v_{i+1}-v_i}{\frac{\Delta x_i}{2} + \frac{\Delta x_{i+1}}{2}} - \frac{(1-u_{i-1})\Delta x_{i-1} + (1-u_i)\Delta x_i}{\Delta x_{i-1} + \Delta x_i} \cdot \frac{v_i - v_{i-1}}{\frac{\Delta x_{i-1}}{2} + \frac{\Delta x_i}{2}}\right] \tag{2.4}$$

Finally, we consider the equation for the lactic acid concentration w and its finite volume integral version given by

$$\frac{1}{\Delta x_i}\int_{C_i} w_t\, dx = \frac{c}{\Delta x_i}\int_{C_i} v\, dx - \frac{c}{\Delta x_i}\int_{C_i} w\, dx + \frac{1}{\Delta x_i}\int_{C_i} \left(Aw_x\right)_x dx,$$

and proceeding as for (2.3) we obtain

$$w_i' = c(v_i - w_i) + \frac{1}{\Delta x_i}\left(\frac{A_i\Delta x_i + A_{i+1}\Delta x_{i+1}}{\Delta x_i + \Delta x_{i+1}} \cdot \frac{w_{i+1}-w_i}{\frac{\Delta x_i}{2} + \frac{\Delta x_{i+1}}{2}} - \frac{A_{i-1}\Delta x_{i-1} + A_i\Delta x_i}{\Delta x_{i-1} + \Delta x_i} \cdot \frac{w_i - w_{i-1}}{\frac{\Delta x_{i-1}}{2} + \frac{\Delta x_i}{2}}\right) \tag{2.5}$$

For the case of a uniform mesh with $\Delta x_i = \Delta x$ for all $i = 1, 2, \ldots, N$, the semi-discrete system is simplified as follows

$$u_i' = u_i(1-u_i) - du_iw_i, \tag{2.6}$$

$$v_i' = rv_i(1-v_i) + \frac{D}{\Delta x}\left[\frac{2-u_i-u_{i+1}}{2} \cdot \frac{v_{i+1}-v_i}{\Delta x} - \frac{2-u_{i-1}-u_i}{2} \cdot \frac{v_i - v_{i-1}}{\Delta x}\right], \tag{2.7}$$

$$w_i' = c(v_i - w_i) + \frac{1}{\Delta x}\left(\frac{A_i + A_{i+1}}{2} \cdot \frac{w_{i+1}-w_i}{\Delta x} - \frac{A_{i-1}+A_i}{2} \cdot \frac{w_i - w_{i-1}}{\Delta x}\right). \tag{2.8}$$

Remark 2.1.1. The use of the arithmetic average for dealing with diffusive equations is not standard in numerical analysis, and the *harmonic mean* is instead preferable for practical reasons. Hence, for instance, we can consider the following alternative version of the equation (2.8) for the diffusion function A of the lactic acid concentration:

$$w_i' = c(v_i - w_i) + \frac{1}{\Delta x}\left(\frac{2A_iA_{i+1}}{A_i + A_{i+1}} \cdot \frac{w_{i+1}-w_i}{\Delta x} - \frac{2A_{i-1}A_i}{A_{i-1}+A_i} \cdot \frac{w_i - w_{i-1}}{\Delta x}\right). \tag{2.9}$$

Nonetheless, it is important to observe that choosing harmonic mean leads to numerical issues when dealing with degenerate diffusion functions [20], so that the use of harmonic mean for diffusive equations with singularities can be pursued with advanced techniques and artifacts. For

example, in the case of equation (2.7) for tumour cells density, as soon as the (nonlinear) diffusion function $(1-u)$ becomes null somewhere. Then, the diffusion matrix which defines the numerical scheme becomes singular and, unfortunately, this is precisely the case of our simulations. Thus, we can not straightforwardly apply the harmonic average and we finally recurred to the arithmetic mean, although this issue will be better discussed in the future.

Remark 2.1.2. We point out that the equation (2.8) can be rewritten as follows

$$\begin{aligned} w_i' = c(v_i - w_i) + \frac{1}{2\Delta x^2}\big[&A_i(w_{i+1} - 2w_i + w_{i-1}) \\ &+A_{i+1}(w_{i+1} - w_i) - A_{i-1}(w_i - w_{i-1})\big] \end{aligned}$$

which actually corresponds to the analytical splitting of the derivative $(Aw_x)_x$ in $A_x w_x + Aw_{xx}$, as observed in Remark 2.0.1, and analogous considerations can be done for the nonlinear diffusion term in the equation (2.10).

For the time discretization of the ordinary differential system obtained by grouping (2.6), (2.7) and (2.8) we employ a semi-implicit strategy by considering a time step $\Delta t_n = |t^{n+1} - t^n|$ for $n = 0, 1, \dots$. In particular, the reaction terms are treated explicitly, whilst the differential terms on the right-hand side can be approximated implicitly, so that we obtain the following system

$$\begin{cases} u_i^{n+1} = u_i^n + \Delta t\Big(u_i^n(1-u_i^n) - d u_i^n w_i^n\Big) \\ v_i^{n+1} = v_i^n + r\Delta t\, v_i^n(1-v_i^n) \\ \qquad + D\dfrac{\Delta t}{\Delta x}\Big(\dfrac{2 - u_i^{n+1} - u_{i+1}^{n+1}}{2}\cdot\dfrac{v_{i+1}^{n+1} - v_i^{n+1}}{\Delta x} \\ \qquad - \dfrac{2 - u_{i-1}^{n+1} - u_i^{n+1}}{2}\cdot\dfrac{v_i^{n+1} - v_{i-1}^{n+1}}{\Delta x}\Big) \\ w_i^{n+1} = w_i^n + c\,\Delta t(v_i^n - w_i^n) \\ \qquad + \dfrac{\Delta t}{\Delta x}\Big(\dfrac{A_i + A_{i+1}}{2}\cdot\dfrac{w_{i+1}^{n+1} - w_i^{n+1}}{\Delta x} \\ \qquad - \dfrac{A_{i-1} + A_i}{2}\cdot\dfrac{w_i^{n+1} - w_{i-1}^{n+1}}{\Delta x}\Big) \end{cases} \tag{2.10}$$

The boundary conditions are the Neumann-type $v_1^n = v_2^n$, $w_1^n = w_2^n$ and $v_N^n = v_{N-1}^n$, $w_N^n = w_{N-1}^n$, for $n = 1, 2, \dots$.
This implicit-explicit (IMEX) mixed approach allows to make less expensive choices for the time step, compared to fully explicit algorithms which would be heavily conditioned by stability restrictions and consequently slower in computational time [24].

Remark 2.1.3. In practical applications, we need to impose boundary conditions also for u, namely $u_1^n = u_2^n$ and $u_{N-1}^n = u_N^n$, even if the equation for the healthy tissue is indeed purely ordinary one. In order to be consistent with the biological context, a diffusion term should be considered also for the normal cells population, but the diffusivity of u would be extremely slower than those for v and w, hence it can be omitted in the Gatenby-Gawlinski model (1.1). Nevertheless, this simplification has to be taken into account when imposing numerical boundary conditions for all the three equations to efficiently solve the fully discrete system (2.10).

2.1.1 Short appendix: why have we used finite volumes?

There are essentially two methods for the discretization of derivatives, namely finite differences and finite volumes [24]. In the one dimensional case, these two methods typically lead to the same results, but the procedure through which they are obtained are significantly different. In order to explain this point, we analyse the two approaches applied to the system (2.1) and in particular to the equation for w by focusing on the functional $(Aw_x)_x$ with A replaced by its piecewise constant projection on the spatial mesh (see Figure 1).
Firstly, we rewrite this term by splitting the derivatives as done in Remark 2.1.2

$$(Aw_x)_x = A_x w_x + A w_{xx}.$$

Thus, the finite volume integral formulation of the right-hand side is

$$\frac{1}{\Delta x}\int_{x_{i-\frac{1}{2}}}^{x_{i+\frac{1}{2}}} A_x w_x \, dx + \frac{A_i}{\Delta x}\int_{x_{i-\frac{1}{2}}}^{x_{i+\frac{1}{2}}} w_{xx} \, dx \tag{2.11}$$

where we have considered a uniform spatial mesh. We notice that we took out A_i from the second integral because it is constant inside each finite volume (see Figure 1). We discretize the second integral as follows

$$\frac{A_i}{\Delta x}\left(\frac{w_{i+1}-w_i}{\Delta x} - \frac{w_i - w_{i-1}}{\Delta x}\right) = \frac{A_i}{\Delta x^2}\big(w_{i+1} - 2w_i + w_{i-1}\big) \tag{2.12}$$

where the derivatives are approximated at the interfaces $i-\frac{1}{2}$ and $i+\frac{1}{2}$ respectively. Then, we discretize the first integral in (2.11) as follows, for instance

$$\frac{1}{2}\frac{A_i - A_{i-1}}{\Delta x}.\frac{w_i - w_{i-1}}{\Delta x} + \frac{1}{2}\frac{A_{i+1} - A_i}{\Delta x}.\frac{w_{i+1} - w_i}{\Delta x} \tag{2.13}$$

where the products of derivatives are approximated with the average values at the interfaces $i-\frac{1}{2}$ and $i+\frac{1}{2}$ respectively and the Δx in the denominator is simplified with the one resulting from the length of the integral interval.
Finally, we can come back to recover the original discretization of $(Aw_x)_x$ as done in (2.10).

Now let us apply the finite differences for discretizing Aw_{xx}, so that we obtain

$$A_i \frac{w_{i+1} - 2w_i + w_{i-1}}{\Delta x^2}.$$

which is the same as done in (2.12).
The difference occurs for the product $A_x w_x$, which is typically discretized by centred finite differences as follows

$$\frac{A_{i+1} - A_{i-1}}{\Delta x}.\frac{w_{i+1} - w_{i-1}}{2\Delta x}$$

and, therefore, it seems not to be possible to recover from the sum of these two parts any (consistent) finite difference discretization of the compact form $(Aw_x)_x$, differently from finite volumes approach.

2.2 Space-averaged propagation speed approximation

Once the numerical framework has been established, the natural step to proceed with experiments and simulations consists in defining a wave speed estimation for the numerical solution. Therefore, with the aim of providing a numerical approximation for the wave speed at time t^n, we employ the space-averaged estimate proposed in [19] and successfully applied to the case of a reactive version of the Goldstein- Kac model for correlated reaction-diffusion systems in [17, 18, 22]. We briefly derive the main analytical concepts behind its formulation: let ϕ be a differentiable function describing the travelling front profile, then we can write

$$\begin{aligned}\int_{\mathbb{R}} \big[\phi(\xi+h)-\phi(\xi)\big]\,d\xi = h\int_{\mathbb{R}}\int_0^1 \frac{\partial\phi}{\partial\xi}(\xi+\theta h)\,d\theta d\xi = h\int_0^1\int_{\mathbb{R}}\frac{\partial\phi}{\partial\mu}(\mu)\,d\mu\,d\theta \\ = h\int_0^1 \big[\phi(+\infty)-\phi(-\infty)\big]\,d\theta = h\big(\phi_+-\phi_-\big)\end{aligned}$$

where $h>0$ is an increment, ϕ_+ and ϕ_- are two different asymptotic states for the function ϕ (heteroclinic travelling front). Setting $h=-s\Delta t$, we deduce the following integral equation for the wave speed

$$s = \frac{1}{\big(\phi_+-\phi_-\big)\Delta t}\int_{\mathbb{R}}\big[\phi(\xi)-\phi(\xi-s\Delta t)\big]\,d\xi. \tag{2.14}$$

We recall that travelling front are computed by imposing the change of variable $\xi = x-st$ in the system (2.1). For instance, if we focus on the invasion front with speed $s>0$ of the tumour cells density, hence $\phi(\xi)$ corresponds to $v(x,t)$ in the original variables and the discrete version of the space averaged wave speed estimation (2.14) over a uniform spatial mesh at time t^n is given by the LeVeque-Yee formula ([19])

$$s^n = \frac{\Delta x}{\Delta t}.\frac{1}{\big(v_+-v_-\big)}\sum_{i=1}^{N}\big(v_i^n-v_i^{n+1}\big), \tag{2.15}$$

with v_+ and v_- the stationary states of v in the system (2.1).
It is important to underline the strength of estimate (2.15) lying on its independence from the dynamics of the solution provided by the differential model (2.1), thus being always numerically computable.

2.3 Numerical simulations with homogeneous diffusion A

In order to validate the numerical algorithm, several simulations have been performed using the scheme (2.10), with a uniform spatial mesh.

In this section, we are interested in recovering computational results described in the literature, therefore the experiments are carried out with the parameters available in [7], as listed in Table 2.1, and then with the parameters in [21], as listed in Table 2.2. We assume T as the final time and L the semi-length of the space interval $[-L,L]$, while the spatio-temporal mesh is built by fixing $\Delta x = 0.005$ and $\Delta t = 0.01$. We point out that the choice of the spatial mesh indeed depends on the tissues structure and geometry since the space-step Δx should be small enough to capture the inhomogeneities of the lactic acid diffusion function (refer to Section 2.1. This numerical issue becomes even more crucial in multidimensional simulations, for which unstructured nonuniform

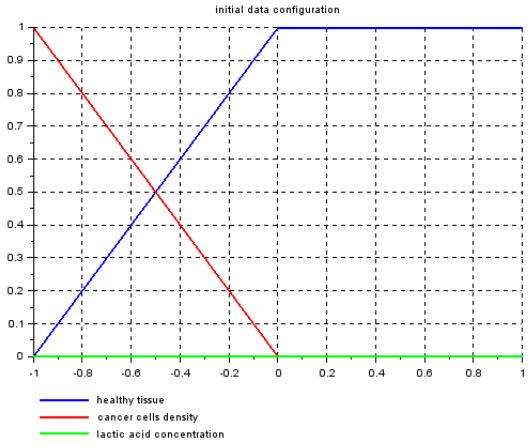

Figure 2.2: Initial profiles for the numerical simulations

meshes are usually adopted to account for different geometrical characteristics (see Figure 1.1) without penalising the computational time.
On the other hand, the choice of the time step Δt depends not only on biological and physical considerations, but also on the numerical stability which is established by the CFL condition [24].

The diffusion function A for the lactic acid concentration is assumed to be uniform with $A > 0$ constant. This assumption means that the tissues are completely homogeneous without structural or functional differentiation, which represents a restrictive hypothesis typically far *in vivo* and *in vitro* situation.
However, such case is considered mainly for numerical issues, in order to validate the scheme (2.10) in view of more complex applications.

d	r	D	c	A	L	T
$\{0.5, 1.5, 2.5, 3, 12.5\}$	1	$4 \cdot 10^{-5}$	70	1	1	20

Table 2.1: Numerical values for the simulation parameters

For the choice of the initial profiles, a piecewise linear decreasing density is taken into account for the cancer cells extending out from its core, where $v = 1$, and getting towards zero; for the healthy cells density, the starting profile is simply obtained through a reflection, by imposing a complementary behaviour with respect to the cancer cells density; finally, the extracellular lactic acid concentration is initially equal to zero. The corresponding graphs are shown in Figure 2.2.

The results reported in Figure 2.4 demonstrate two different types of behaviours, which are regulated by the parameter d measuring the destructive influence of the environment acidity on the healthy tissue, and so taken as an indicator of the *tumour aggressiveness*. From a qualitative point of view, all solutions evolve as forward propagation fronts moving from left to right with positive wave speed. The plot displayed in Figure 2.4 (a) corresponds to a phenomenological regime known as *heterogeneous invasion*, which turns out to happen when $d < 1$. It is characterized by the coexistence of tumour and healthy tissue behind the wavefront, because a group of normal cells survives to the low aggressiveness of the tumour. On the other hand, when $d \gg 1$, a different

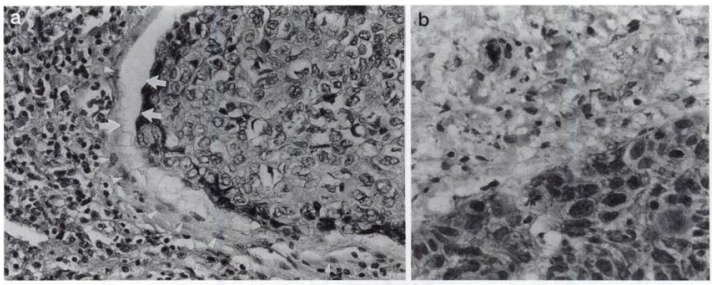

Figure 2.3: Microscope images of tumour-host interstitial gap. Source: [10]

evolution shape takes place, the so-called *homogeneous invasion* shown in Figure 2.4 (d), which is the most aggressive configuration. Indeed, the healthy tissue is being completely destroyed behind the advancing tumour cells wavefront because of the intensity of acidity induced into the environment. A narrow overlapping zone actually persists for increasing values of $d > 1$, which produces *hybrid congurations* as shown in Figure 2.4 (b) and Figure 2.4 (c).

We point out the presence of the so-called *tumour-host hypocellular interstitial gap* (Figure 2.3) in the homogeneous invasion which is a separation zone practically depleted of cells between the healthy and cancer populations (see Figure 2.4 (d)). Such modelling prediction has been experimentally verified in both unfixed in vitro experiments and in flash-frozen tissues, by providing stronger evidence to this phenomenon [10].

From a mathematical point of view, the strong dissimilarity in terms of steepness of the wave profiles for u and v observed in Figure 2.4 is justified by the fact that somehow u inherits the parabolic regularity of the lactic acid concentration w through the reaction term (see the fist equation of the system (2.1), whereas the diffusion constant D of the neoplastic tissue is typically very small (see Table 2.1). In fact, when passing from the system (1.1) to its non-dimensionalized version (2.1), that parameter is deduced as $D = D_2/D_3$ and it is physically relevant to assume the value of D_3 larger than D_2 [10].

For theoretical issues, we also consider the case with $A \ll 1$ and the formation of the gap emerges for values greater than $d = 12.5$, because the acid diffusion is slower and hence the tumour is less invasive (see in Figure 2.5).

Another effect on the shape of the wave profile can be appreciated dealing with the adimensional parameter r, which is expected to be greater than 1 since deduced as $r = \rho_2/\rho_1$ from physical considerations (refer to Section 1.1). Numerical simulations of such kind are significant, since an increasing of the tumour cells reproduction rate r results in a different spatial invasion, because the value of r actually modifies the wave propagation speed (see Figure 2.6).
Indeed, the second equation of system (2.1) with a logistic reaction term belongs to the class of the Fisher-KPP equations [9], for which there exist travelling wave solutions if and only if their wave speed is greater than $2\sqrt{rD}$ with r and D the corresponding reaction and diffusion rate, respectively (refer to Section 1.1). Therefore, the propagation speed of the tumour front increases together with the value of r and moreover this modification affects also the lactic acid and healthy tissue concentration. We point out that, in order to appreciate the faster propagation dynamics, we have widened to the right the spatial interval of the numerical simulations (see Figure 2.6).
Finally, it can be observed that the wave profile of the tumour front is steeper when r is larger.

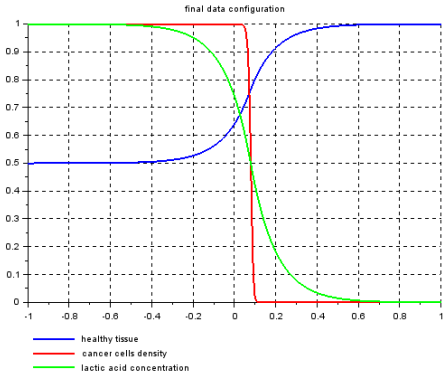

(a) *heterogeneous invasion*, $d = 0.5$

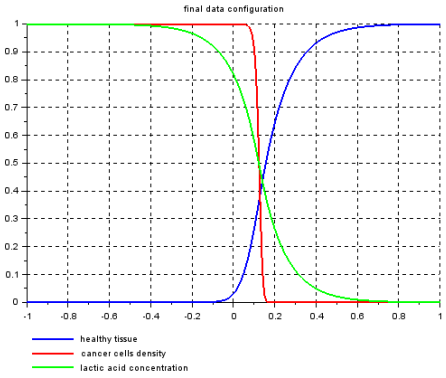

(b) *hybrid configuration*, $d = 1.5$

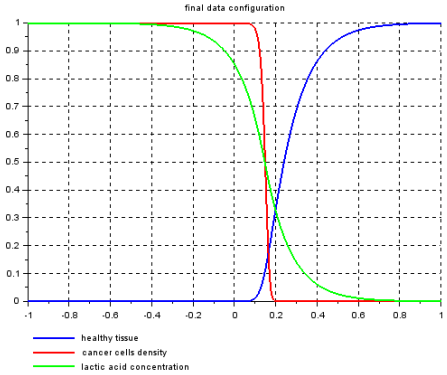

(c) *hybrid configuration*, $d = 2.5$

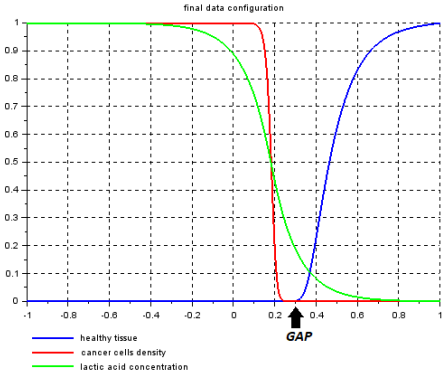

(d) *homogeneous invasion*, $d = 12.5$

Figure 2.4: Different configurations of the numerical solution: comparison between heterogeneous evolution (a) and existence of the spatial interstitial gap within the homogeneous invasion (d)

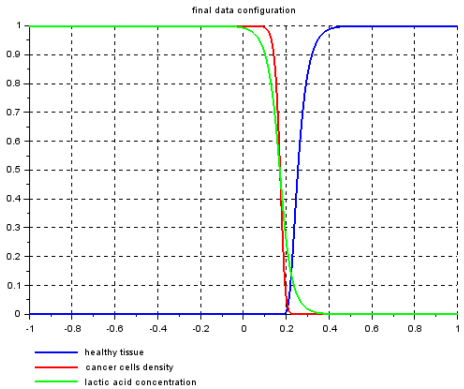

Figure 2.5: Numerical solution still exhibiting a heterogeneous invasion for $d = 12.5$ and $A = 0.1$

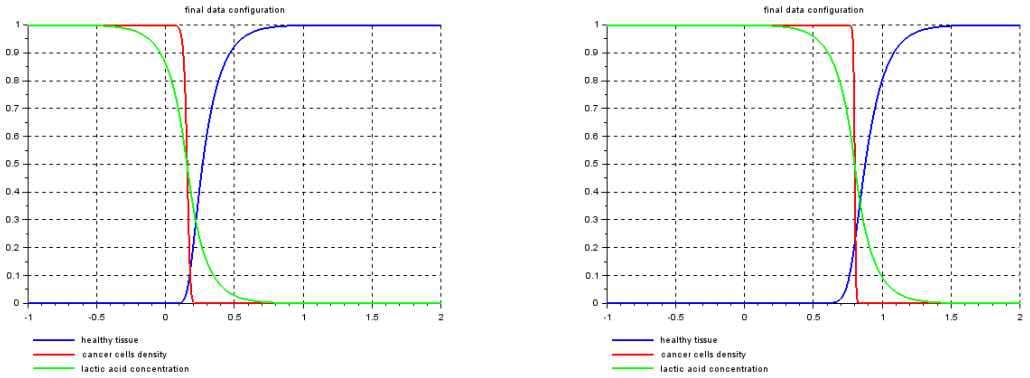

(a) *moderate growth* $r = 1$ (b) *uncontrolled growth* $r = 10$

Figure 2.6: Qualitative analysis of tumour propagation fronts and spatial invasion as function of the adimensional growth rate (for $d = 3$)

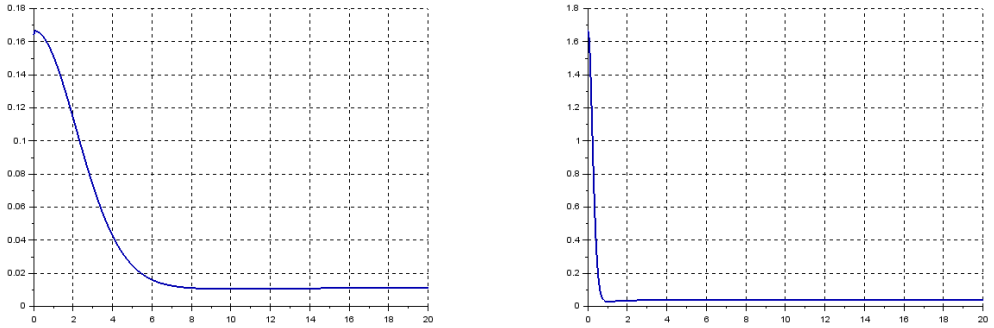

(a) *moderate growth,* $r = 1$, (b) *uncontrolled growth,* $r = 10$

Figure 2.7: Wave speed approximation for different values of the adimensional growth rate r (for $d = 3$)

Another substantial difference between the two simulation settings in Figure 2.6 is observed when evaluating the wave speed approximation for tumour front, referring to the LeVeque-Yee formula (2.14). We construct the graphs in Figure 2.7 by fixing the time scale on the x-axis, while the values of the approximate wave speed s are reported on the on the y-axis.

It is evident that the more r is large, the more the wave speed is high and in both cases it is possible to recognize the convergence towards an asymptotic threshold: the asymptotic wave speed is estimated $s^* = 0.0111$ for $r = 1$ and $s^* = 0.0387$ for $r = 10$. Furthermore, the transient time required before achieving the asymptotic propagation speed is smaller for larger r values and a higher velocity is measured at the beginning: these are common features of dynamical systems involving travelling front solutions [22].
More precisely, the wave speed asymptotic value is estimated as 0.01 for $r = 1$ and 0.038 for $r = 10$, thus previous consideration about the crucial role of r in determining the wave speed are confirmed. The trend of the wave speed approximation for increasing r values is plotted in Figure

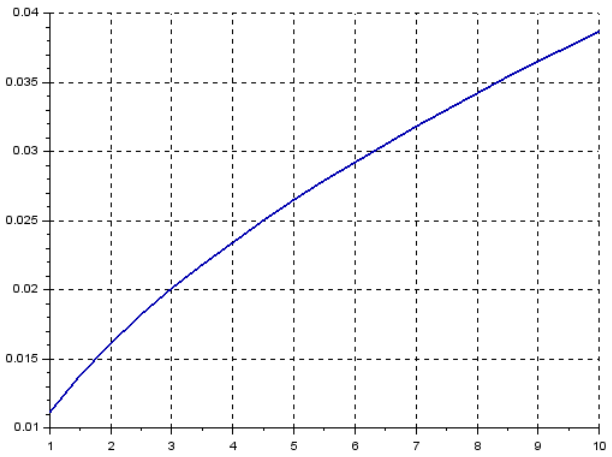

Figure 2.8: Numerical trend of the asymptotic wave speed (taken at time $T = 20$) for increasing values of the adimensional growth rate r (for $d = 3$).

2.8, where the graph has been constructed by interpolating the asymptotic wave speed value for $r = 1$ to $r = 10$ with evaluation step $\Delta r = 0.5$.

Then, we consider other numerical simulations using the parameters listed in Table 2.2 and we are interested in tracking the formation of the interstitial gap, whose appearance is expected for $d > 2$ [7].

In particular, the reason for a different choice of parameters is to investigate the effects of reducing the production of lactic acid by the cancer cells (whose rate is represented by c). Taking a smaller value for c consequently implies to increase the length of the spatial interval $[-L, L]$ in order to better observe the asymptotic behaviour of the solution far from the origin, because the stronger effects of diffusion with respect to reaction terms in the third equation of system (2.1).

d	r	D	c	A	L	T
$\{1.5, 2.5, 4\}$	1	$4 \cdot 10^{-5}$	2	1	5	20

Table 2.2: Numerical values for the simulation parameters

The graphs displayed in Figure 2.9 actually confirm such prediction, although some discrepancies are revealed with respect to the results in [7] especially concerning the smoothness of the wave profile for the healthy cells density, thus determining a smaller size for the gap separating the host and tumour populations.

As done for the experimental data in Table 2.1, we consider the case with $A \ll 1$, since diminishing the value of diffusion coefficient for the acid affects the gap width as shown by the comparison illustrated in Figure 2.10.

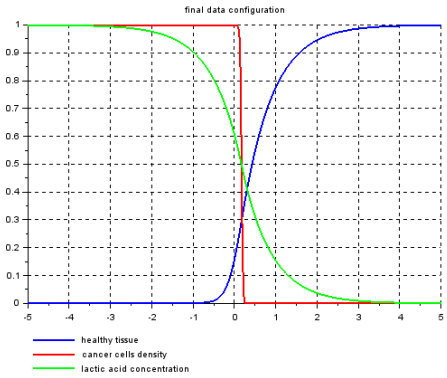

(a) *hybrid configuration*, $d = 1.5$

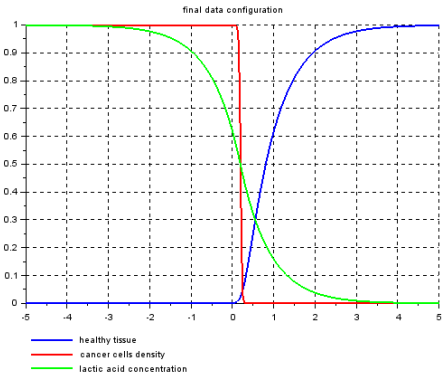

(b) *threshold regime*, $d = 2.5$

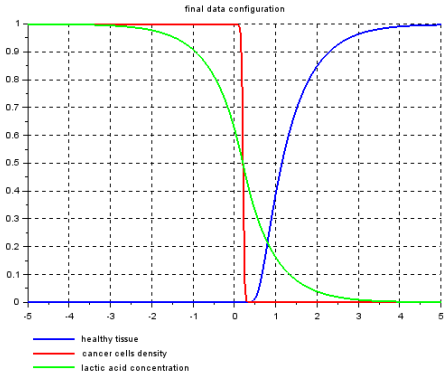

(c) *homogeneous invasion*, $d = 4$

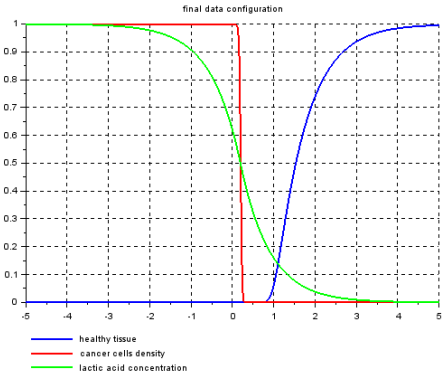

(d) *homogeneous regime*, $d = 7$

Figure 2.9: Numerical simulation of the spatial interstitial gap formation from heterogeneous evolution (a) to homogeneous invasion (c)-(d)

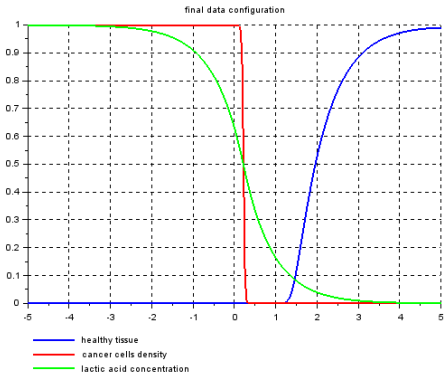

(a) *homogeneous invasion* ($d = 12.5$) *for* $A = 1$

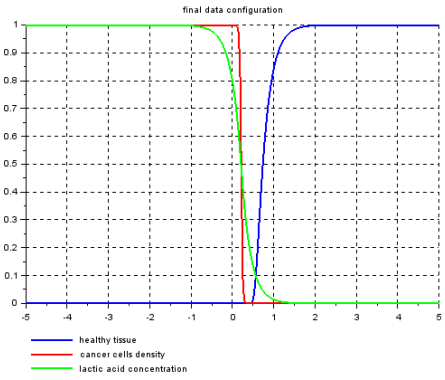

(b) *homogeneous invasion* ($d = 12.5$) *for* $A = 0.1$

Figure 2.10: Comparison between different regimes of the lactic acid diffusion coefficient with respect to the gap formation.

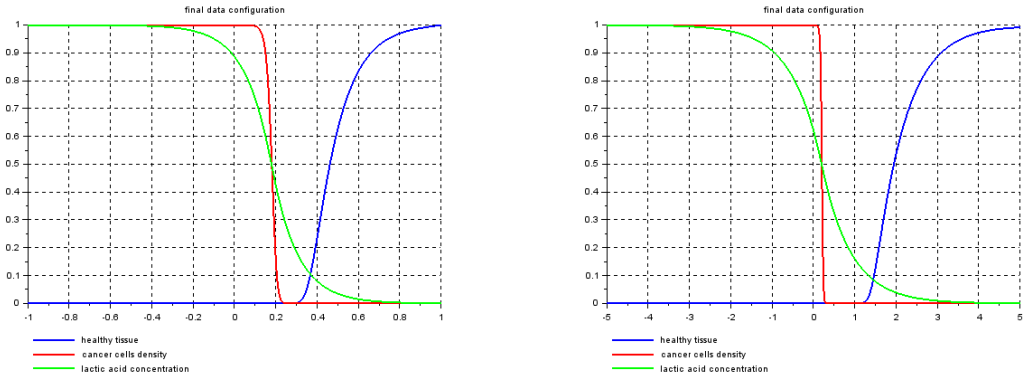

(a) *homogeneous invasion for* $c = 70$ *and* $d = 12.5$ (b) *homogeneous invasion for* $c = 2$ *and* $d = 12.5$

Figure 2.11: Comparison between homogeneous configuration obtained with the same value for d and different one for the production rate of lactic acid c

2.3.1 Modifying the parameter c

The rescaled parameter c appears in the reaction term $c(v-w)$ of the third equation of system (2.1)) and represents the production of lactic acid by the cancer cells. Thus, it is predictable that changes in the value of c affect considerably the final configuration of the numerical solution. Figure 2.11 (a) and (b) display two simulations obtained for $d = 12.5$ and the initial profile in Figure 2.2, using the parameters of Table 2.1 and Table 2.2, respectively, with homogeneous diffusion $A = 1$.

It is evident that the width of the spatial interstitial gap is much larger in the case $c = 2$ and this fact could appear paradoxical, since diminishing the lactic acid production is expected to negatively affect the cancer spread.
However, looking at the non-dimensionalized Gatenby-Gawlinsky model (2.1), we observe that the value of c determines a linear increase of the lactic acid concentration but also an exponential decrease, since the solution of a homogeneous ODE of the form

$$\frac{dw}{dt} = -cw$$

is actually $w(t) = e^{-ct}$. Consequently, if c is smaller, the tumour produces acid at slow rate but the physiological reabsorption is slow too; conversely, if c is larger, the cancer cells spread a higher quantity of acid, which is nonetheless is absorbed at a much faster rate. Hence, the results in Figure 2.11 are intrinsic to our model.
Finally, in Figure 2.12, we compare the two wave speed profiles related to the simulations in Figure 2.11, obtained using the LeVeque-Yee formula (2.14). It can be seen that c affects the propagation speed and its asymptotic value, which is estimated as $s^* = 0.0124$ for (a) and $s^* = 0.0156$ for (b), thus a smaller rate of acid production results in a faster velocity of the fronts.

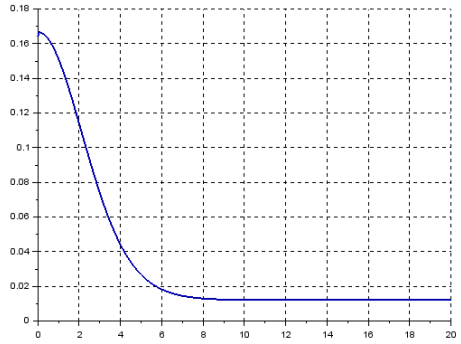

(a) *homogeneous invasion* ($d = 12.5$) *for* $c = 70$

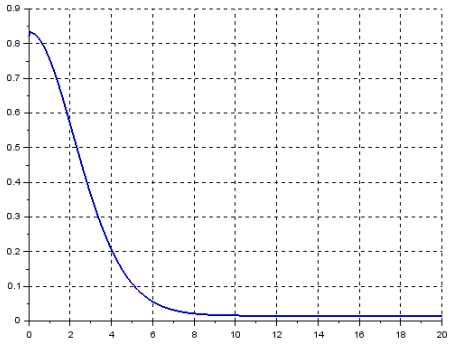

(b) *homogeneous invasion* ($d = 12.5$) *for* $c = 2$

Figure 2.12: Wave speed trends for the same value for d and different production rate of lactic acid c

2.4 Numerical simulations with heterogeneous piecewise constant diffusion A

In this section, we provide numerical simulations for the system (2.1) by applying the scheme (2.10), in presence of a heterogeneous diffusion coefficient $A(x)$. We simplify the framework by taking a piecewise constant function.
There are biological and physical reasons behind this particular choice: indeed, we suppose that A represents the diffusion of the lactic passing from a specific tissue or organ to another one, hence the diffusivity changes with the different nature and geometry of the environment. We aim at investigating the effects of this transition on the motility of lactic acid, the consequences for the consumption of healthy tissue and, finally, the modification occurring to the tumour propagation fronts.

We assume the parameters d, r, D and c as described in the previous sections, T as the final time and L the length of the spatial interval $[0, L]$, with the spatio-temporal mesh built by fixing $\Delta x = 0.005$ and $\Delta t = 0.01$. As already discussed, the value of Δx depends on the particular organ or tissue considered, whilst Δt has to be chosen also according to the CFL condition [24]. We deal with different initial profiles either piecewise constant or piecewise linear and different values of A, so that we distinguish two main cases with relative subcases.
The first type of initial data is composed by a decreasing piecewise constant density for the cancer cells extending out from its core, where $v = 1$, and having a jump at $x = \frac{L}{4}$; for the healthy cells density, the starting graph is simply obtained through a reflection, by imposing a complementary behaviour with respect to v; finally, the extracellular lactic acid concentration is initially equal to zero. The corresponding graph are shown in Figure 2.13 (b), referring to the spatial interval $[0, 1]$ whilst the second type is similar to that used in the previous Subsection as shown in Figure 2.13 (a).

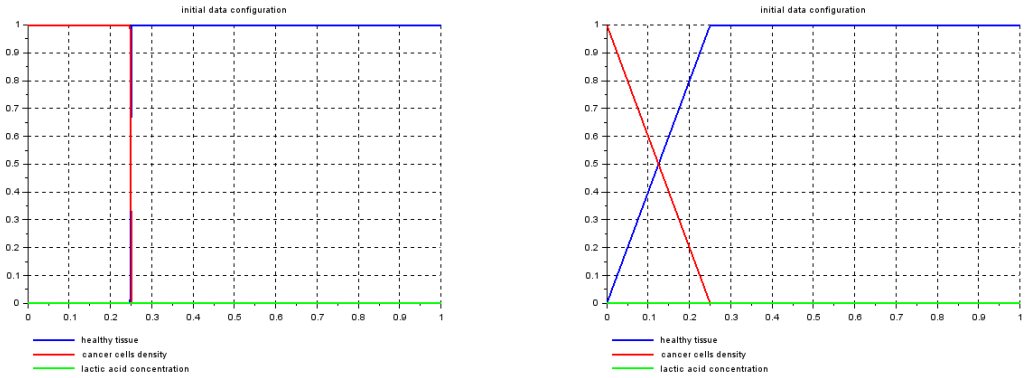

(a) *piecewise constant* (b) *piecewise linear*

Figure 2.13: Initial profiles for the numerical simulations

2.4.1 A with single jump

As diffusion function A, we choose

$$A(x) = \begin{cases} a_1 & \text{if } x \in [0, \frac{5}{8}L] \\ a_2 & \text{if } x \in [\frac{5}{8}L, L] \end{cases}$$

as illustrated for example in Figure 2.14.

We initially refer to the experimental data reported in Table 2.1 with the exception of A which is not anymore homogeneous and we select a piecewise constant initial profile as shown in Figure 2.13 (a).

The results obtained with A strictly increasing $a_1 < a_2$ are displayed in Figure 2.15, specifically for $a_1 = 0.1$ and $a_2 = 1$. We notice the formation of the spatial interstitial gap when $d \gg 1$, and in particular for $d = 35$.

If we decrease the value of $|a_1 - a_2|$, this modification of the diffusion inhomogeneity significantly affects the formation of the gap, which occurs for smaller values of d (see Figure 2.16).

Remark 2.4.1. At this stage, we point out another advantage of using the finite volume method, together with those already discussed in Subsection 2.1.1. Indeed, when considering a heterogeneous function A with discontinuities, the mathematical problem associated with system (2.1) loses its regularity, since the characteristics of parabolicity are weaker, and this phenomenon is quite clear from Figure 2.15. From an analytical point of view, this means that the functional $A_x w_x$ may not be well defined at $x = \frac{5}{8}L$, which is the point of irregularity.
The integral formulation of the finite volume approach allows to correctly deal with this issue.

The results obtained with A strictly decreasing ($a_1 > a_2$) are displayed in Figure 2.17, specifically for $a_1 = 1$ and $a_2 = 0.1$. We notice again the formation of the spatial interstitial gap when $d \gg 1$, but in this case for $d = 12.5$ the gap is largely present.

It is also interesting to remark that the final profile on the healthy tissue density for hybrid and heterogeneous regimes clearly manifests a discontinuity in its derivative, which is inherited from the lactic acid configuration through the nonlinear reaction term in the first equation of system

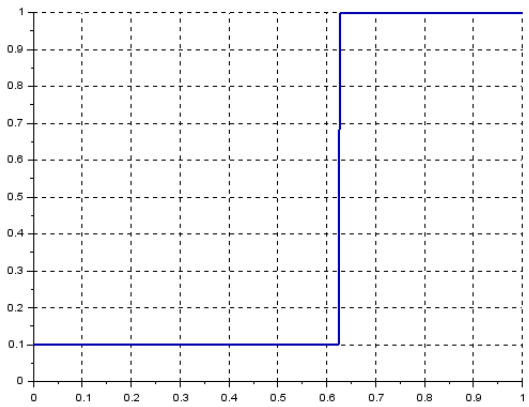

Figure 2.14: Profile of the lactic acid diffusion function with $a_1 = 0.1$ and $a_2 = 1$ in the spatial interval $[0, 1]$

(2.1). The magenta vertical (dashed) line on the graphs of Figure 2.17 indicates the abscissa of discontinuity for the diffusion function A, which passes exactly through the point where the lactic acid and the healthy tissue concentrations have a discontinuity in their derivative (*corner points*).

Moreover, if we decrease the value of $|a_1 - a_2|$, this does not affect the formation and the width of the gap, but the final profile of the lactic acid concentration is smoother and the corner point is not anymore visible (see Figure 2.18).

Now we refer to the experimental data reported in Table 2.2 with the exception of A which is not anymore homogeneous and we select a piecewise constant initial profile as shown in Figure 2.13 (a) on the spatial interval $[0, 5]$. As for the case of homogeneous diffusion in Section 2.3, we increase the length of the spatial interval in order to better observe the asymptotic behaviour of the propagating fronts when the production rate of H^+ ions is smaller [21].
Firstly, we suppose A strictly increasing ($a_1 < a_2$) and we obtain the results shown in Figure 2.19, where $a_1 = 0.1$ and $a_2 = 1$ have been chosen.

Then, we suppose A strictly decreasing ($a_1 > a_2$) and we obtain the results shown in Figure 2.20, where $a_1 = 1$ and $a_2 = 0.1$ have been chosen.

At the end of this Section, we make some comparisons and comments.
First of all, the presence of corner points in the solution profiles for u and w, which is observed when A becomes discontinuous, obviously disappears in the case of homogeneous diffusion (see Figure 2.4 and Figure 2.9).
Furthermore, the profile of solution u becomes smoother as d becomes larger enough for the interstitial gap to emerge, as shown in Figure 2.17, because then the discontinuity point of A falls into the region where the healthy tissue is null(see Figure 2.16).

Now we change the initial profile and we use the one displayed in Figure 2.13 (b). Performing numerical simulations with the same data used above, we can see substantial differences only for small values of d.

The results obtained for $d = 0.5$ and the other parameters of Table 2.1 are reported in Figure 2.21 with a comparison between the case of A strictly increasing $a_1 < a_2$ and strictly decreasing

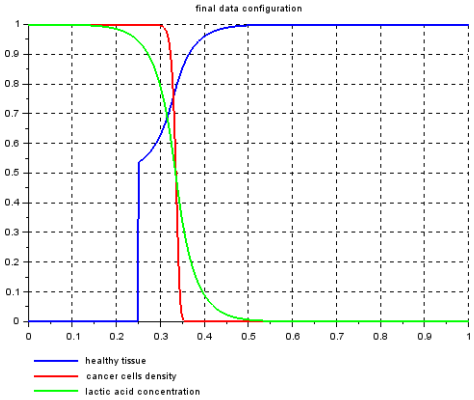

(a) *heterogeneous invasion*, $d = 0.5$

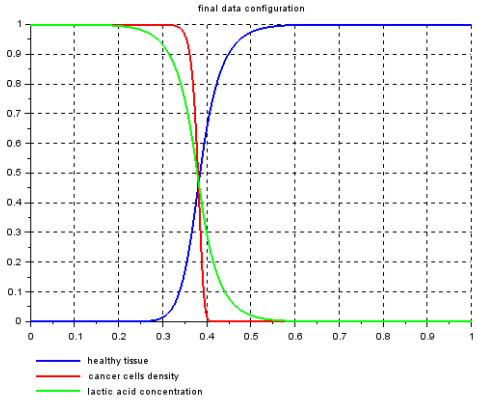

(b) *hybrid configuration*, $d = 1.5$

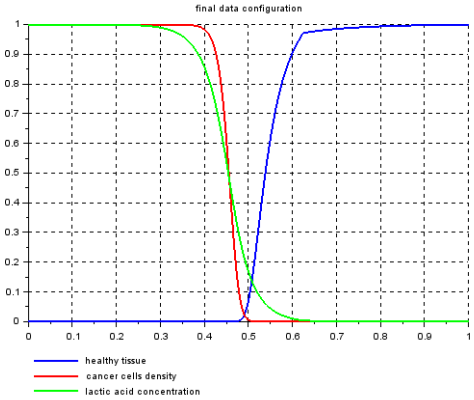

(c) *hybrid configuration*, $d = 12.5$

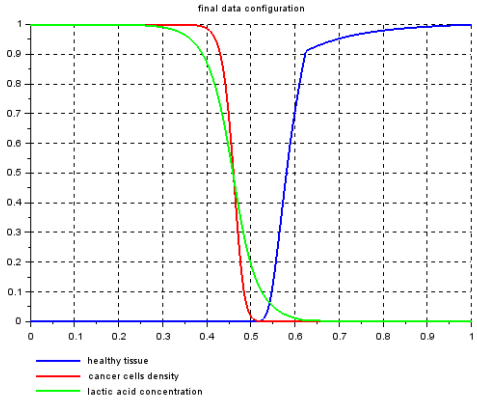

(d) *homogeneous invasion*, $d = 35$

Figure 2.15: Different configurations of the numerical solution in presence of heterogeneous diffusion ($a_1 < a_2$): comparison between heterogeneous evolution (a) and existence of the spatial interstitial gap within the homogeneous invasion (d)

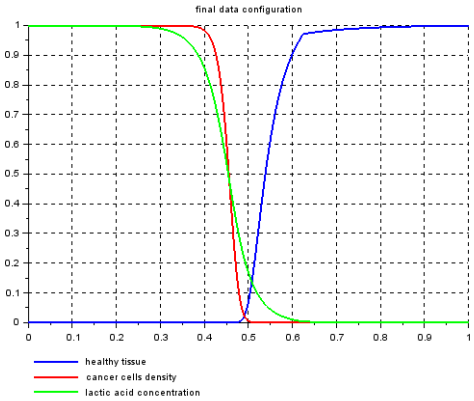

(a) *hybrid configuration* ($d = 12.5$) *for* $a_1 = 0.1$ *and* $a_2 = 1$

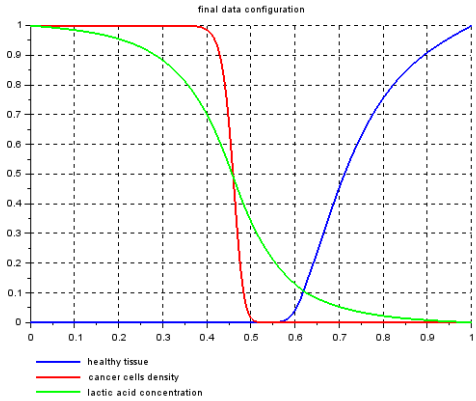

(b) *homogeneous invasion* ($d = 12.5$) *for* $a_1 = 0.8$ *and* $a_2 = 1$

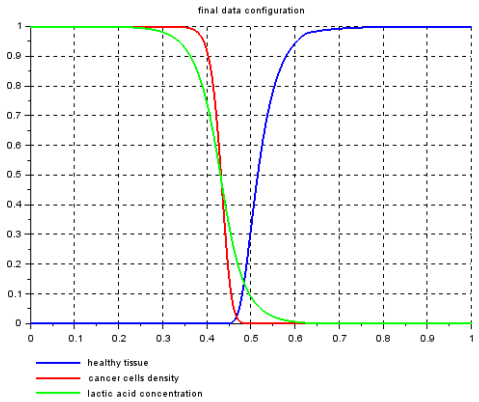

(c) *hybrid configuration,* $d = 12.5$ *for* $a_1 = 0.1$ *and* $a_2 = 0.3$

Figure 2.16: Homogeneous invasion with different values of the jump $|a_1 - a_2|$

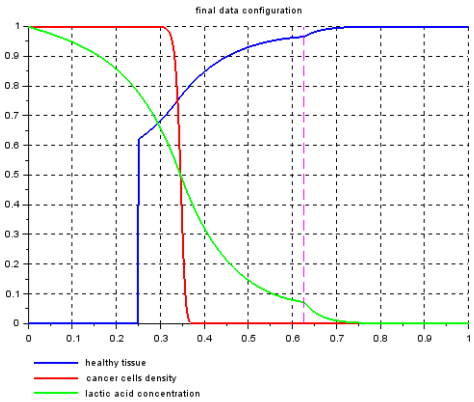

(a) *heterogeneous invasion*, $d = 0.5$

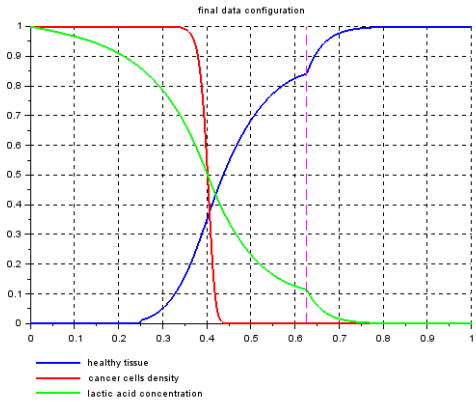

(b) *hybrid configuration*, $d = 1.5$

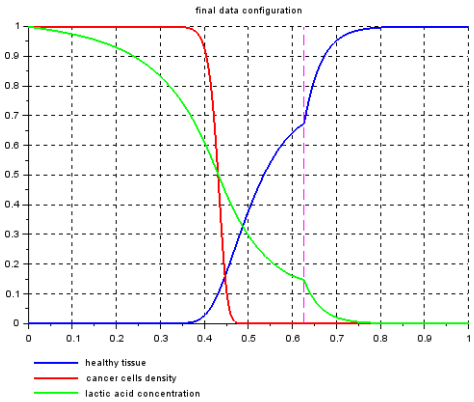

(c) *hybrid configuration*, $d = 2.5$

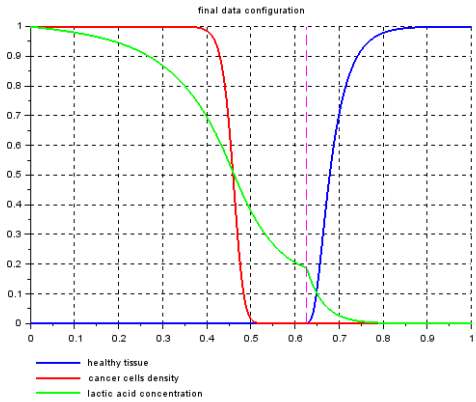

(d) *homogeneous invasion*, $d = 12.5$

Figure 2.17: Different configurations of the numerical solution in presence of heterogeneous diffusion ($a_1 > a_2$): comparison between heterogeneous evolution (a) and existence of the spatial interstitial gap within the homogeneous invasion (d)

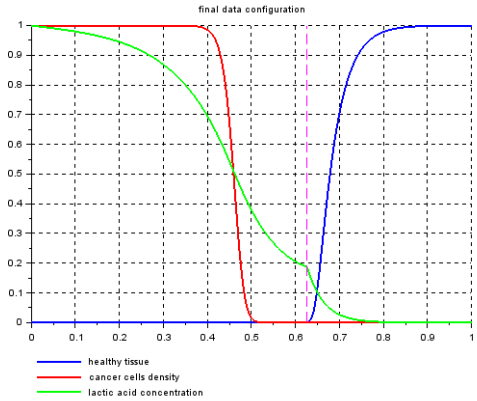

(a) *homogeneous invasion* ($d = 12.5$) *for* $a_1 = 1$ *and* $a_2 = 0.1$

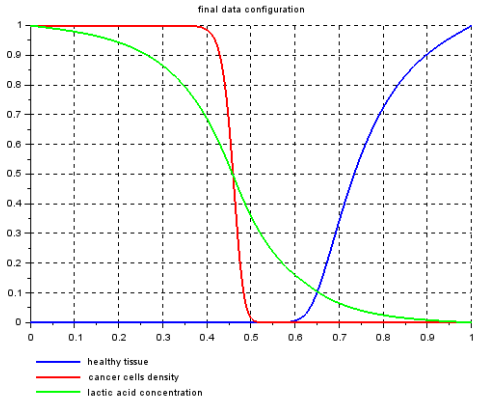

(b) *homogeneous invasion* ($d = 12.5$) *for* $a_1 = 1$ *and* $a_2 = 0.8$

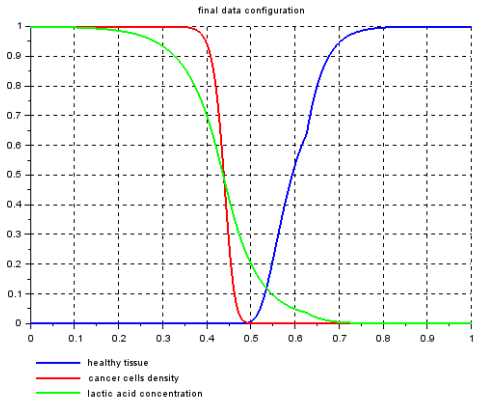

(c) *homogeneous invasion* ($d = 12.5$) *for* $a_1 = 0.3$ *and* $a_2 = 0.1$

Figure 2.18: Homogeneous invasion with different values of the jump $|a_1 - a_2|$

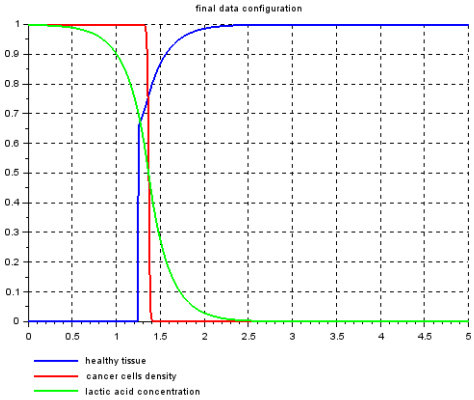

(a) *heterogeneous invasion*, $d = 0.5$

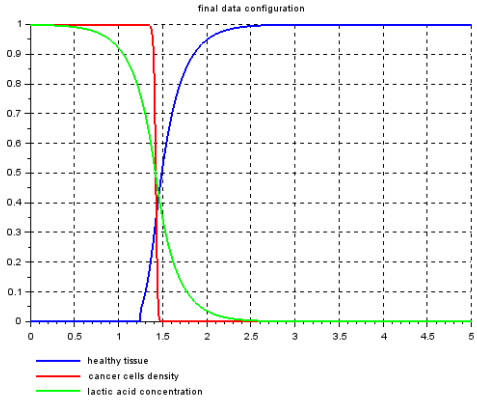

(b) *hybrid configuration*, $d = 1.5$

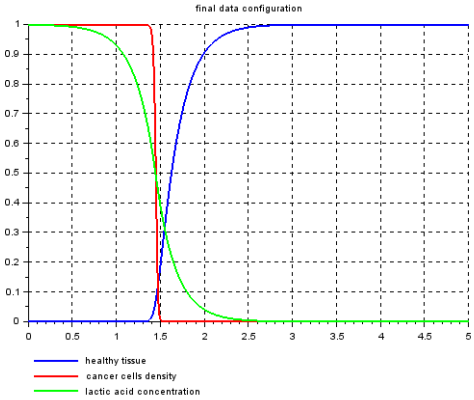

(c) *hybrid configuration*, $d = 2.5$

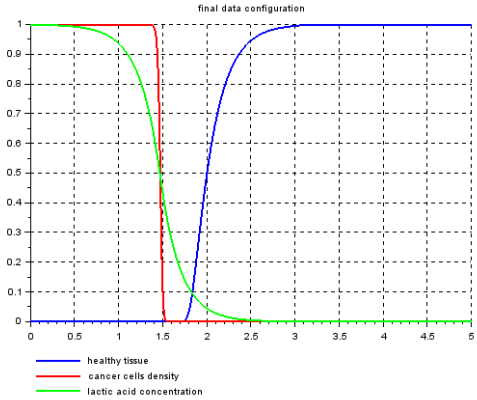

(d) *homogeneous invasion*, $d = 12.5$

Figure 2.19: Different configurations of the numerical solution in presence of heterogeneous diffusion ($a_1 < a_2$): comparison between heterogeneous evolution (a) and existence of the spatial interstitial gap within the homogeneous invasion (d)

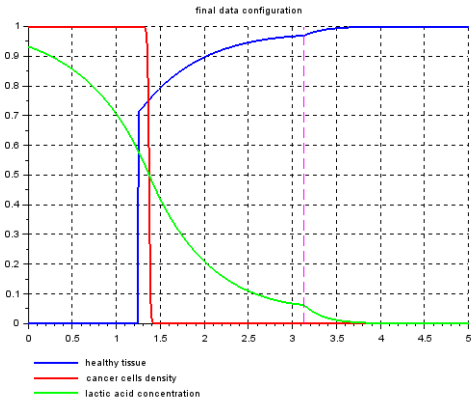

(a) *heterogeneous invasion*, $d = 0.5$

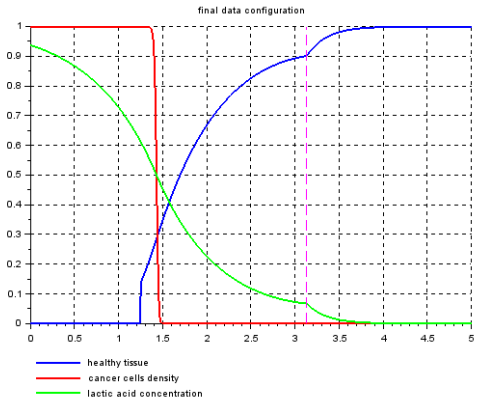

(b) *hybrid configuration*, $d = 1.5$

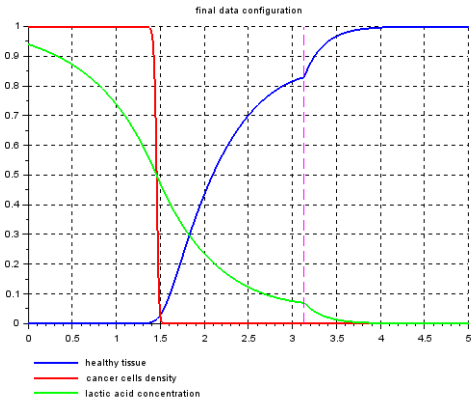

(c) *hybrid configuration*, $d = 2.5$

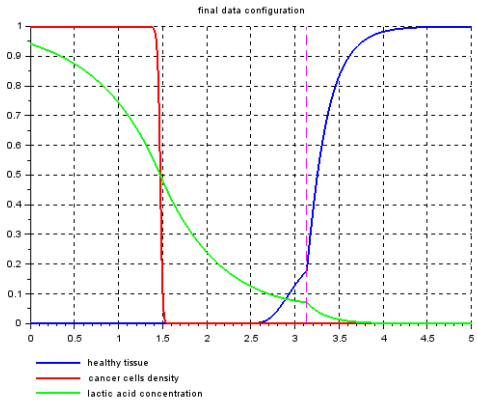

(d) *homogeneous invasion*, $d = 12.5$

Figure 2.20: Different configurations of the numerical solution in presence of heterogeneous diffusion ($a_1 > a_2$): comparison between heterogeneous evolution (a) and existence of the spatial interstitial gap within the homogeneous invasion (d)

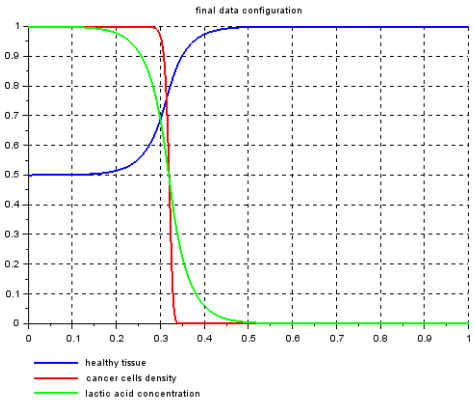

(a) *heterogeneous invasion with A strictly increasing ($a_1 = 0.1$ and $a_2 = 1$)*

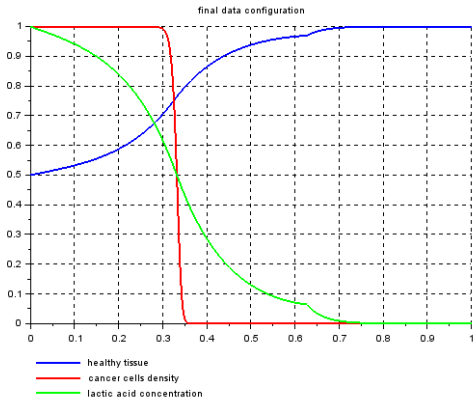

(b) *heterogeneous invasion with A strictly decreasing ($a_1 = 1$ and $a_2 = 0.1$)*

Figure 2.21: Configurations of the numerical solution starting from initial data in figure 2.13 (b) in presence of heterogeneous piecewise constant diffusion function A for $d = 0.5$

$(a_1 > a_2)$.

This suggests that if the tumour is not very aggressive (i.e. d is small), then the healthy tissue is not completely destroyed.

There is a specific experimental purpose for the choice of two different initial profiles. Indeed, the Riemann-type initial data in Figure 2.13 (a) reproduces many *in vitro* experiments where a group of healthy cells is removed to inoculate a small colony of cancer ones, hence the initial profile has a strong discontinuity which depends on sudden modifications of the environment.
On the other hand, the initial data in Figure 2.13 (b) refers to *in vivo* situations, where the earlier development of cancer cells within a healthy tissue happens gradually without immediately destroying the host environment.

In conclusion of this section, in Figure 2.22 we consider the data on Table 2.2 and we compare A strictly increasing $a_1 < a_2$ with A strictly decreasing $a_1 > a_2$.

Remark 2.4.2. The numerical simulations presented in this section provide a support for strategies to efficiently struggle against cancer spread in both experimental and clinical applications. One may interfere with the tissue inhomogeneity to slow down the tumour front or rather act pharmacologically only on regions where the cancer cells spread faster. Moreover, the fact that some specific acid diffusion profiles lead to inefficient solutions could explain why some tissue seems to be naturally tumour-free. For instance, soft tissue sarcomas of muscles, nerves and blood vessels are very rare [14], maybe because of the fibrous tissues structure which obstructs the destructive acid infiltration.

2.4.2 Modifying the parameter r

In this short section, we provide some examples about the behaviour of wavefront solutions to the system (2.1) when the parameter r changes.
We assume a piecewise constant diffusion A with single jump, as illustrated in Figure 2.14 and the piecewise linear initial profile in Figure 2.13 (b).

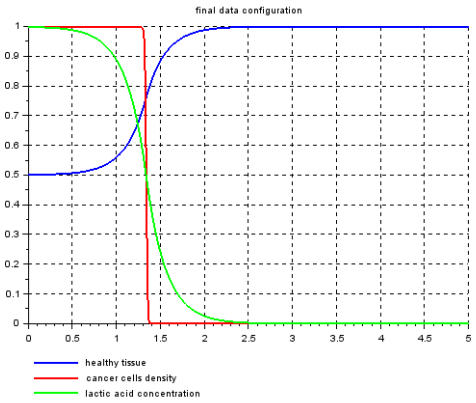

(a) *heterogeneous invasion and A strictly increasing* $a_1 < a_2$ *(*$a_1 = 0.1$ *and* $a_2 = 1$*)*

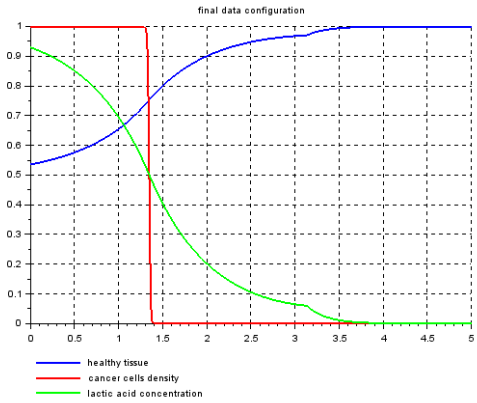

(b) *heterogeneous invasion and A strictly decreasing* $a_1 > a_2$ *(*$a_1 = 1$ *and* $a_2 = 0.1$*)*

Figure 2.22: Configurations of the numerical solution starting from initial data in figure 2.13 (b) in presence of heterogeneous piecewise constant diffusion function A for $d = 0.5$

The results of the comparison between small and bigger values of r are shown in Figure 2.23,, referring to Table 2.1 for the other numerical parameters and choosing $d = 3$. The inhomogeneous function A is supposed to be strictly increasing or strictly decreasing with values $a_1 = 0.1$ and $a_2 = 1$ and $a_1 = 1$ and $a_2 = 0.1$ respectively. The wave speed approximation for the tumour front, computed by means of the LeVeque-Yee formula (2.14), is also plotted along with time in Figure 2.24.
We observe that if r is larger, then the tumour cells invade the healthy tissue faster and this leads to the shift of the wave front toward the right. Moreover, a reduction of the thickness of the spatial interstitial gap is noticeable for larger r values.

As already noticed for the simulations with homogeneous diffusion A, the more r is large, the more the wave speed is high: : for example, the wave speed asymptotic value is estimated as 0.001 for $r = 1$ and 0.0325 for $r = 10$ in Figure 2.24 (a) and (b) and in both cases it is possible to appreciate the convergence towards the asymptotic threshold and this approach is faster in the case of larger r, thus the previous considerations about the crucial role of r in determining the wave speed are numerically confirmed.
Moreover, comparing there results with those obtained in Figure 2.7 for homogeneous A, we notice that the behaviour of the wave speed is graphically similar, but the asymptotic value of velocity changes. This suggests that the profile of A is determinant for the wave speed trend in the long run.

As a matter of fact there are two main properties characterizing the tumour dynamics, namely its aggressiveness and its invasiveness, which are represented in system (2.1) by the parameters d and D respectively. For clinical application, the duality between highly aggressive but scarcely invasive and rapidly extended but less aggressive tumours one constitutes a crucial issue [27].
The previous simulations suggest that fast growing tumours (i.e. large values of the growth rate r) result also in enhanced invasiveness, hence these other properties are not independent. This fact is extremely interesting for applied scientists and clinical researchers since finding optimal strategies to control both these tumour parameters is still an open question [8].

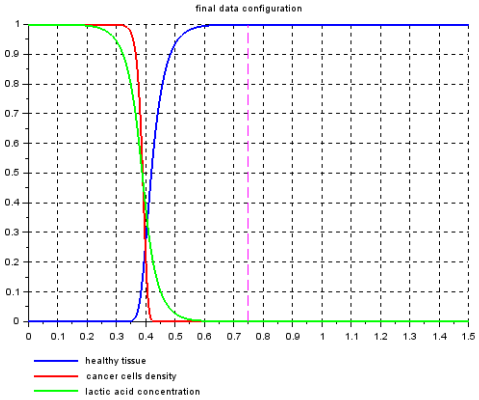

(a) *moderated growth* $r = 1$ *and* A *strictly increasing*

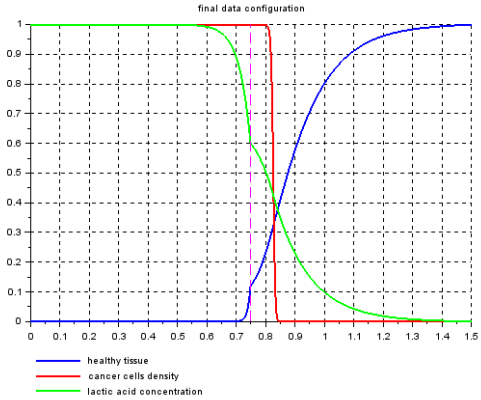

(b) *uncontrolled growth* $r = 10$ *and* A *strictly increasing*

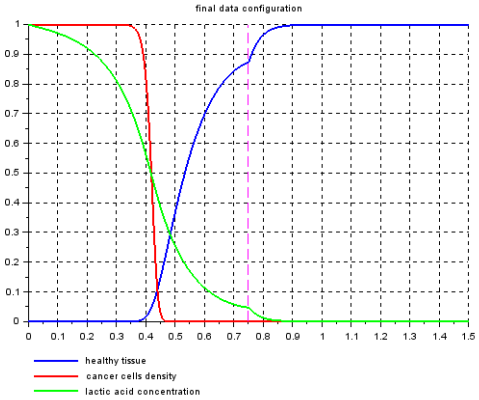

(c) *moderate growth,* $r = 1$ *and* A *strictly decreasing*

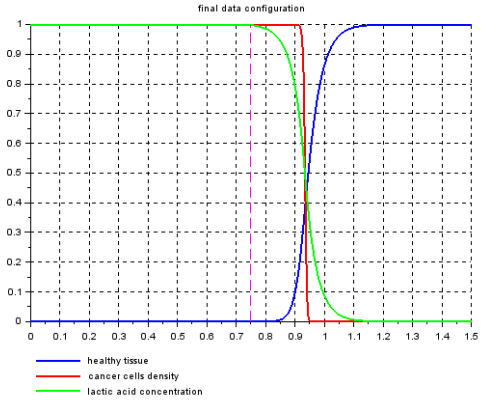

(d) *uncontrolled growth* $r = 10$ *and* A *strictly decreasing*

Figure 2.23: Qualitative analysis of tumour front steepness and spatial invasion as function of the adimensional growth rate in case of strictly increasing or decreasing diffusion function A (for $d = 3$)

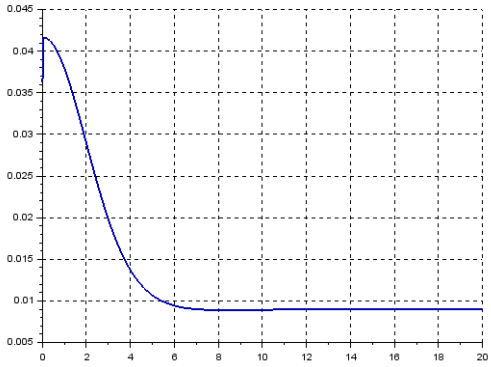

(a) *moderated growth* $r = 1$ *and* A *strictly increasing*

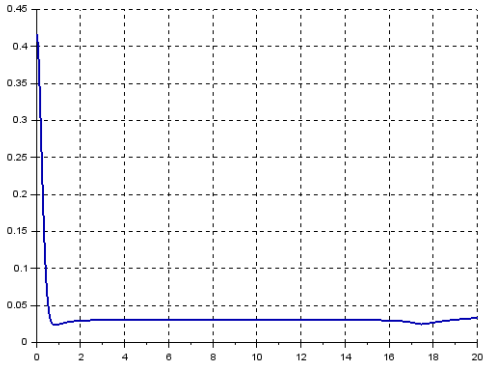

(b) *uncontrolled growth* $r = 10$ *and* A *strictly increasing*

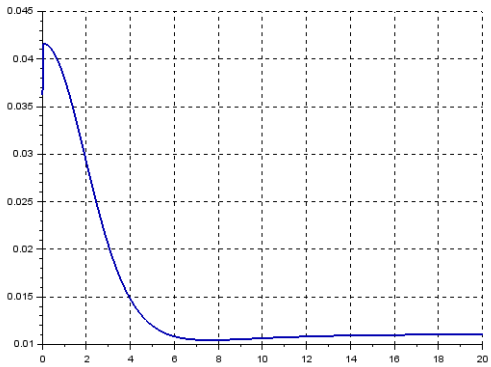

(c) *moderate growth* $r = 1$ *and* A *strictly decreasing*

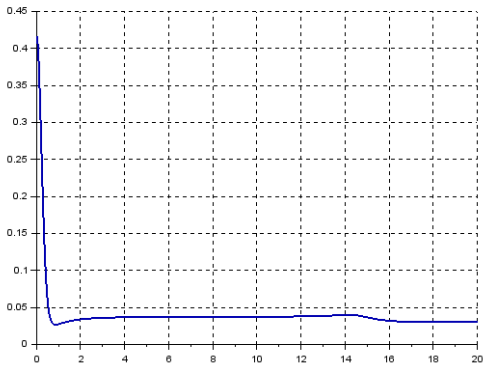

(d) *uncontrolled growth* $r = 10$ *and* A *strictly decreasing*

Figure 2.24: Wave speed approximation trend of the tumour front for different values of the adimensional growth rate r

Another substantial difference between Table 2.1 and Table 2.2 is inherent to the value of c, the parameter which measures the lactic acid production through the glycolitic metabolic process adopted by the tumour. Therefore, a further critical question could be: does the modification of lactic acid production affect the invasiveness and/or aggressiveness of the cancer cells? And if yes, in which specific way?

2.5 Numerical simulations with periodic diffusion A

In this section, we provide numerical simulations for system (2.1)using the scheme (2.10), in presence of a heterogeneous function A, which is supposed to be periodic.
This choice is related to the structure of most part of tissues, which are porous and heterogeneously permeable and hence responsible of a non-uniform invasion by the lactic acid. Such a function A may thus represent the effect of increased diffusivity for the H^+ ions due to easy passage through tissues for half its period, and the effect of reduction due to obstacles along the way [5].
It is worthwhile to underline that the choice of Δx has to be made carefully, in order to avoid trivial interpolations of the periodic diffusion function A if the space-step is too close to (a multiple of) its period.

We choose the initial profiles in Figure 2.13 (b) on the spatial interval $[0, 1]$ and we refer to Table 2.1 for the numerical parameters (as the simulations referring to Table 2.2 are qualitatively similar) . We analyse different configurations for the diffusion function A by changing the amplitude and frequency of its oscillations, according to the following expression

$$\begin{aligned} A(x) &= \frac{1}{2}[a_0(1-\sin(\omega x)) + \alpha(1+\sin(\omega x))] \\ &= \frac{1}{2}(a_0+\alpha) + \frac{1}{2}(\alpha - a_0)\sin(\omega x) \end{aligned} \tag{2.16}$$

where α is the fixed amplitude of each oscillation and ω is the frequency (so that $\frac{1}{\omega}$ is the period). In order to be physically consistent with the non-dimensionalized model (2.1), it is assumed that $0 < a_0 \leq A(x) \leq \alpha$ for all x in the domain, thus a_0 defining the uniformly positivity constant of A.

2.5.1 Modifying the frequency

A modification of the parameter ω in (2.16) implies a change in the frequency of oscillations: we suppose $\omega \gg 1$ and we initially choose $a_0 = 0.1$ and $\alpha = 1$.
Numerical simulations with $\omega = 50$ on the spatial interval $[0, 1]$ with respect to the parameters of Table 2.1 are displayed in Figure 2.25. The initial data are those illustrated in Figure 2.13 (b).

We propose three relevant considerations. First of all, despite the perturbations observed in Figure 2.25 for the profiles u and w (with those for u inherited from w through the reaction term $-duw$), the solutions still exhibit a front-type behaviour which is then very robust (such stability is actually preserved for smaller values of the frequency).
Secondly, the value of ω affects the formation of the interstitial gap, which becomes visible for $d = 60$.
Indeed, analogous simulations are reported in Figure 2.26, where we increase the frequency value to $\omega = 100$ and the appearance of the interstitial gap is again for $d = 50$.

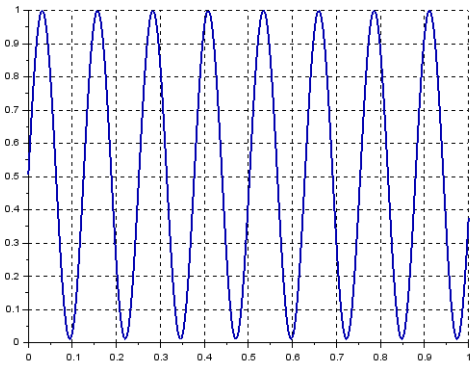

(a) *Profile of A*

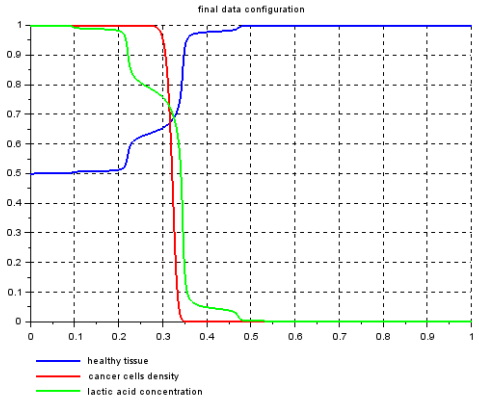

(b) *heterogeneous invasion,* $d = 0.5$

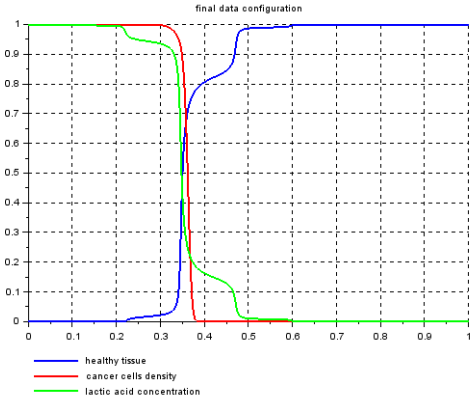

(c) *hybrid configuration,* $d = 1.5$

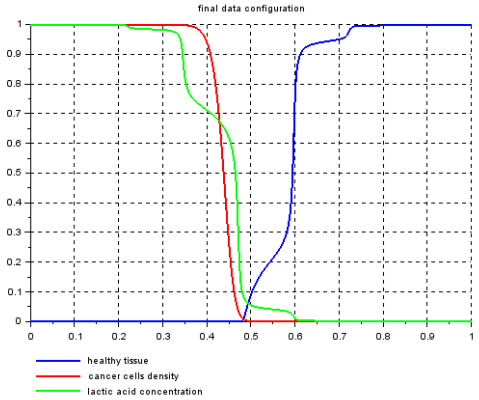

(d) *hybrid configuration,* $d = 30$

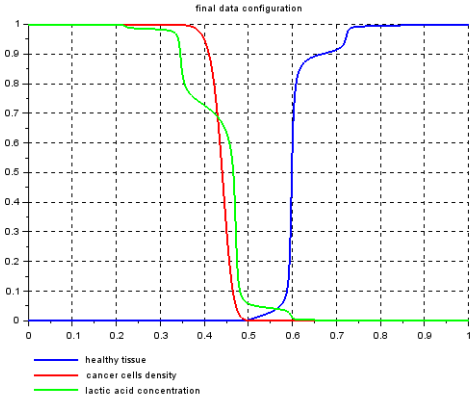

(e) *hybrid configuration,* $d = 50$

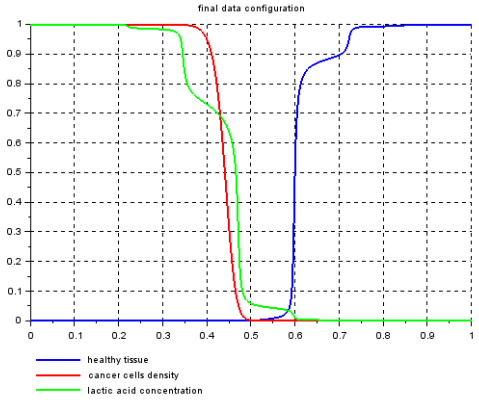

(f) *homogeneous invasion,* $d = 60$

Figure 2.25: Different configurations of the numerical solution in presence of periodic diffusion A with frequency $\omega = 50$ and existence of the spatial interstitial gap within the homogeneous invasion (f)

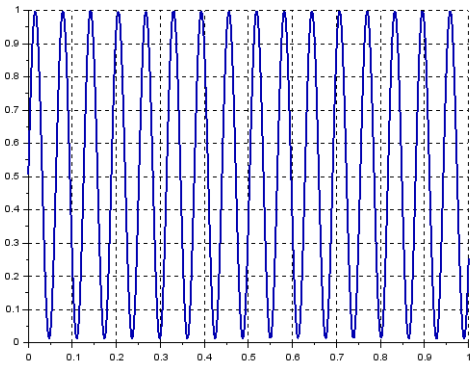

(a) *Profile of A*

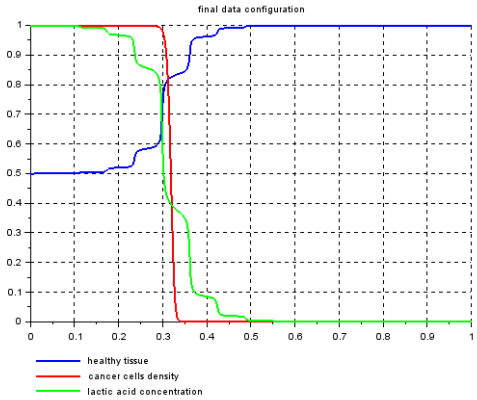

(b) *heterogeneous invasion,* $d = 0.5$

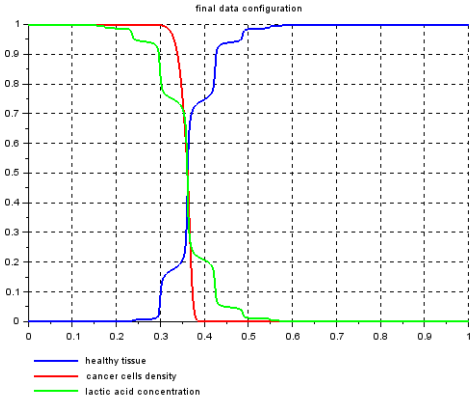

(c) *hybrid configuration,* $d = 1.5$

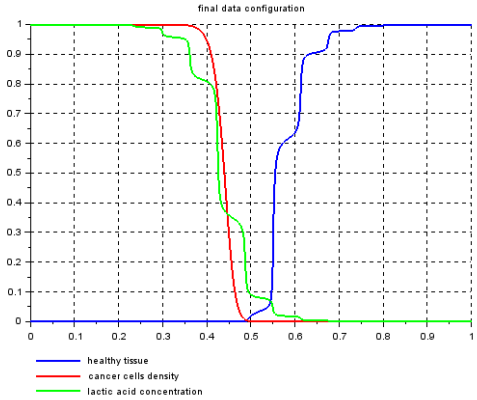

(d) *heterogeneous invasion,* $d = 30$

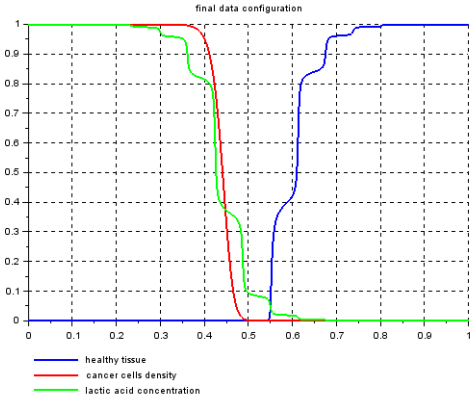

(e) *hybrid configuration,* $d = 50$

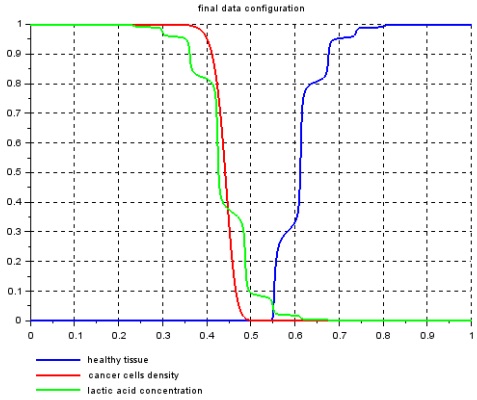

(f) *heterogeneous invasion,* $d = 60$

Figure 2.26: Different configurations of the numerical solution in presence of periodic diffusion A with frequency $\omega = 100$ and existence of the spatial interstitial gap within the homogeneous invasion (e)-(f)

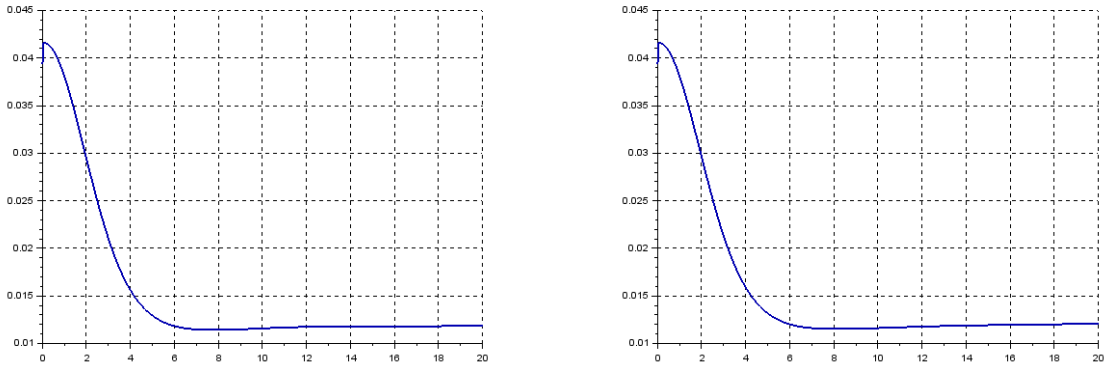

(a) $\omega = 50$ (b) $\omega = 100$

Figure 2.27: Wave speed approximation for different values of the frequency ω (for $d = 20$)

Moreover, the perturbations are more intense for higher values of ω, whilst they are obviously damped for larger values of d since the healthy tissue becomes null.

Finally, looking at the wave speed approximation given by the LeVeque-Yee formula (2.14) for different frequencies of the diffusion function A (see Figure 2.27), we can infer that the value of ω does not affect the propagation velocity (the solutions for $\omega = 50$ and $\omega = 100$ converge to the same asymptotic value $s^* = 0.012$).
This suggests to look for homogenization (see Section 2.5.4.

Before concluding this Section, we look at the spatial derivative of the numerical solutions for $\omega = 100$, which are represented in Figure 2.28. It can be noticed that, despite the perturbations induced by the oscillatory diffusion function A, the front-type solution profiles continue to be monotonic (increasing for u or decreasing for v and w) since their derivatives do not change sign. Therefore, the profiles are not oscillatory.

2.5.2 Modifying the amplitude and the intensity

The amplitude and intensity of the diffusion function A also modifies the behaviour of the numerical solution, especially when the value of ω is very large.
For the following simulations, we use the formula (2.16) with different values of α and a_0.

Firstly, we choose $\alpha = 0.6$ and $a_0 = 0.4$, so that the amplitude is $|\alpha - a_0| = 0.2$, while the other parameters are those in Table 2.1, with $\omega = 50$. The numerical solutions displayed in Figure 2.29 are smoother with respect to Figure 2.25 and this characteristics do not depend on the values of α and a_0, but on their difference in absolute value, as shown in Figure 2.30 Figure 2.31 where $\alpha = 1$ and $a_0 = 0.8$ and $\alpha = 0.3$ and $a_0 = 0.1$ are chosen respectively.

In Figure 2.32 and Figure 2.33 we choose a very small intensity for A, which is $|\alpha - a_0| = 0.05$ and we compare the case $\alpha = 1$ and $a_0 = 0.95$ with $\alpha = 0.06$ and $a_0 = 0.01$. It is observable that the more the acid concentration is weak, the more the interstitial gap appears for large value of d (see Figure 2.33 (e), where the gap is not yet present for $d = 200$).

An interesting fact is the front profile of numerical solution remains even if we increase the value of ω. For example the results for $\omega = 200$ and $|\alpha - a_0| = 0.2$ and for $\omega = 200$ and

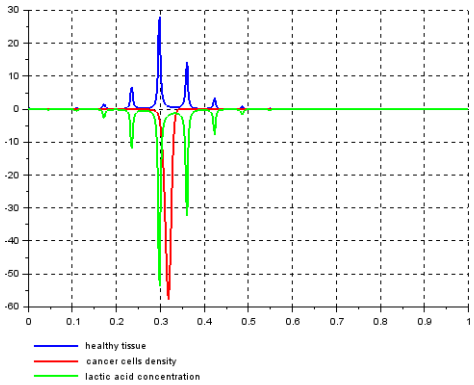

(a) *heterogeneous invasion,* $d = 0.5$

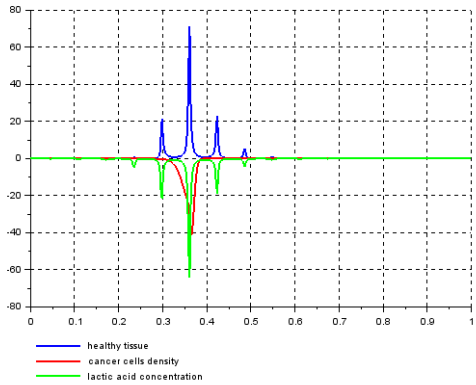

(b) *hybrid configuration,* $d = 1.5$

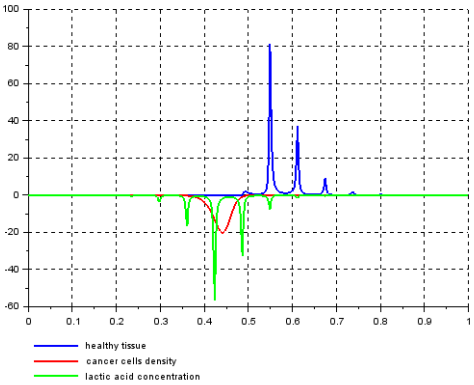

(c) *hybrid configuration,* $d = 30$

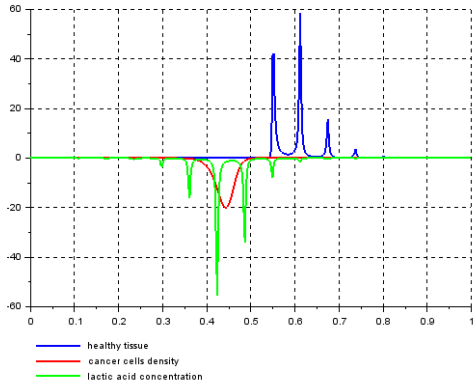

(d) *homogeneous invasion,* $d = 50$

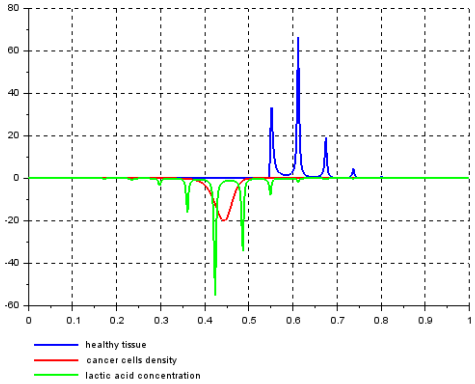

(e) *homogeneous invasion,* $d = 60$

Figure 2.28: First order derivative of the numerical solution reported in Figure 2.26

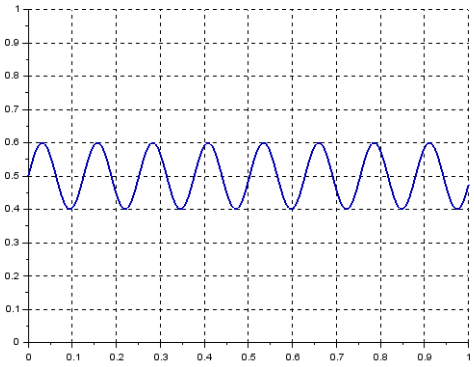

(a) *Profile of A for* $\alpha = 0.6$ *and* $a_0 = 0.4$

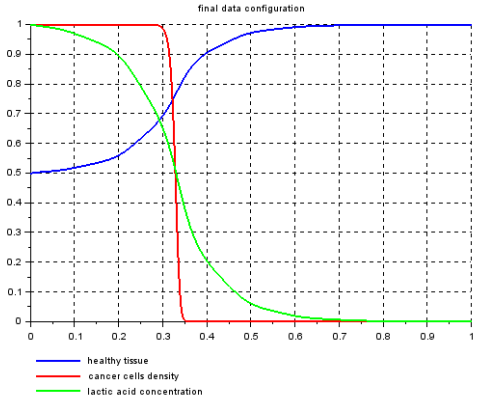

(b) *heterogeneous invasion,* $d = 0.5$

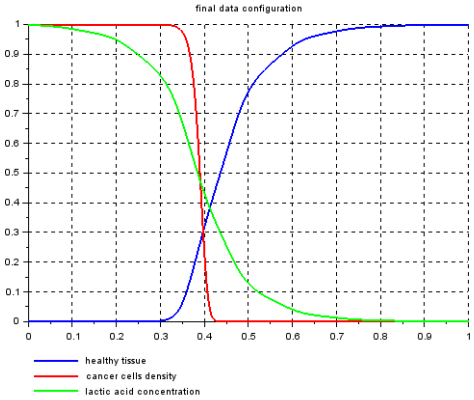

(c) *hybrid configuration,* $d = 2.5$

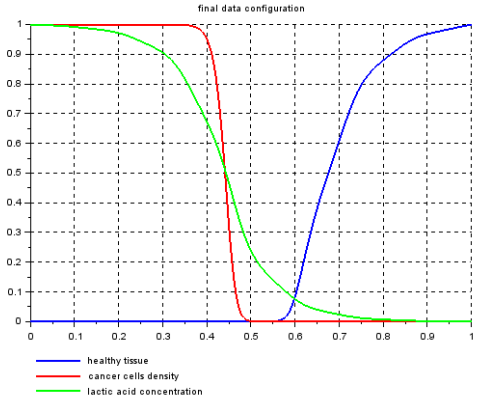

(d) *homogeneous invasion,* $d = 20$

Figure 2.29: Different configurations of the numerical solution in presence of periodic diffusion with frequency $\omega = 50$ and amplitude $|a_0 - \alpha| = 0.2$

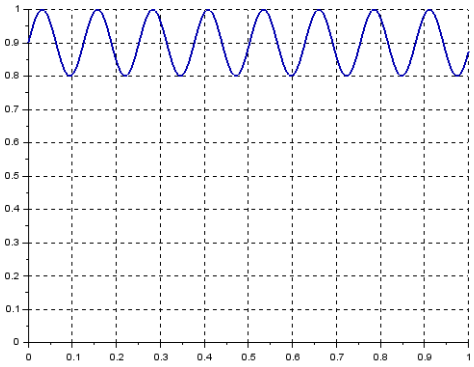

(a) *Profile of A for* $\alpha = 1$ *and* $a_0 = 0.8$

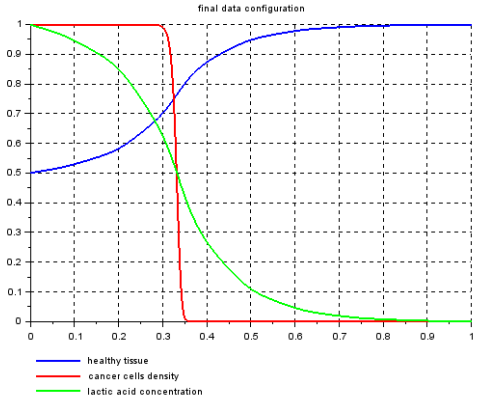

(b) *heterogeneous invasion,* $d = 0.5$

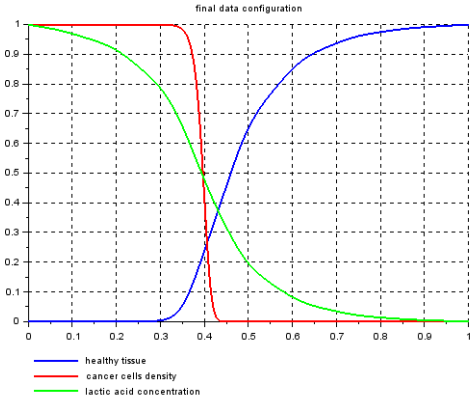

(c) *hybrid configuration,* $d = 2.5$

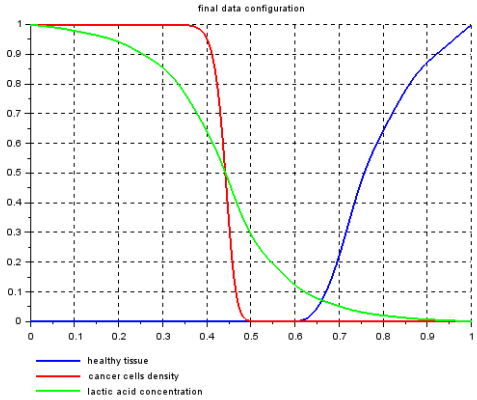

(d) *homogeneous invasion,* $d = 20$

Figure 2.30: Different configurations of the numerical solution in presence of periodic diffusion A with frequency $\omega = 50$ and amplitude $|\alpha - a_0| = 0.2$

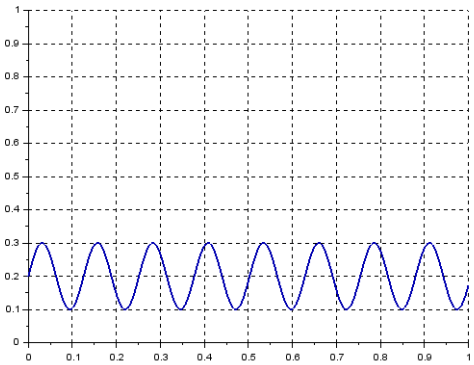

(a) *Profile of A for* $\alpha = 0.3$ *and* $a_0 = 0.1$

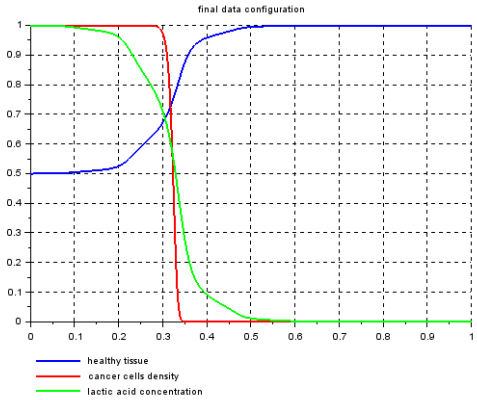

(b) *heterogeneous invasion,* $d = 0.5$

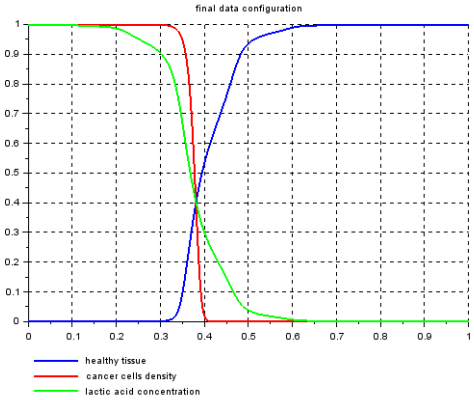

(c) *hybrid configuration,* $d = 2.5$

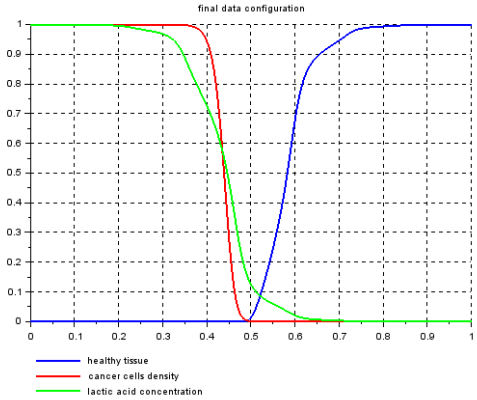

(d) *hybrid configuration,* $d = 20$

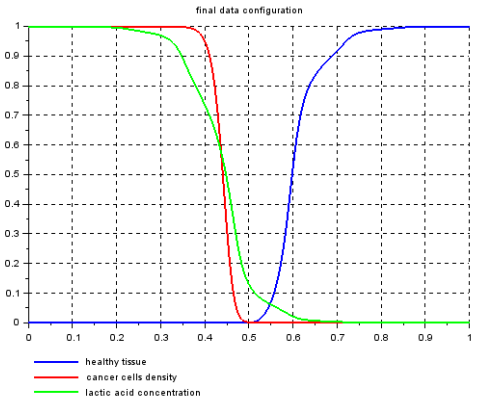

(e) *homogeneous invasion,* $d = 30$

Figure 2.31: Different configurations of the numerical solution in presence of periodic diffusion A with frequency $\omega = 50$ and amplitude $|\alpha - a_0| = 0.2$

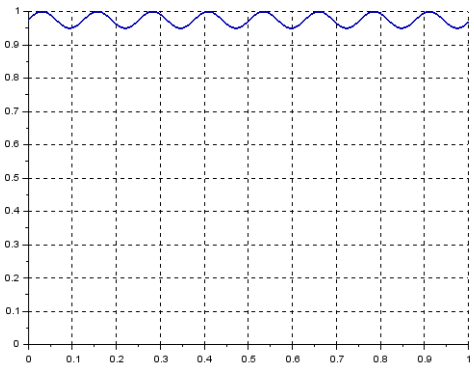

(a) *Profile of A for* $\alpha = 1$ *and* $a_0 = 0.95$

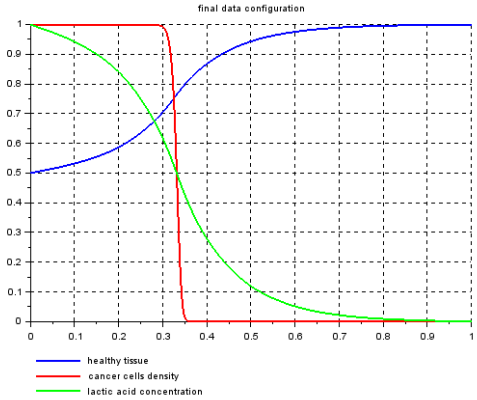

(b) *heterogeneous invasion,* $d = 0.5$

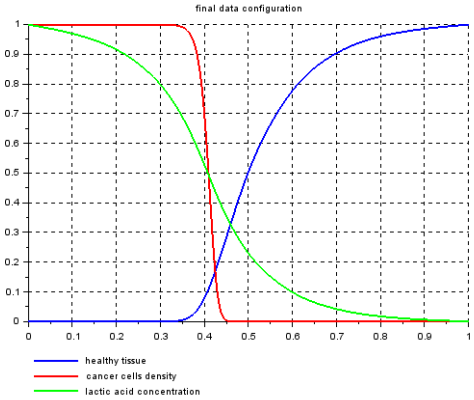

(c) *hybrid configuration,* $d = 2.5$

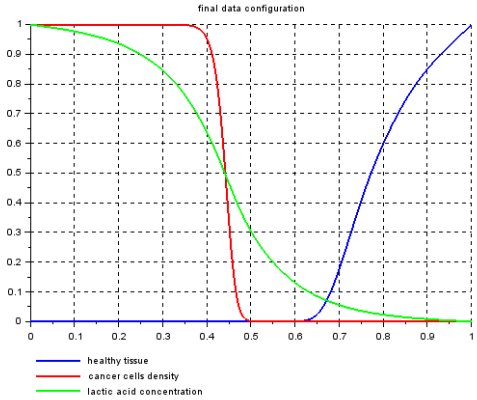

(d) *homogeneous invasion,* $d = 20$

Figure 2.32: Different configurations of the numerical solution in presence of periodic diffusion A with frequency $\omega = 50$ and amplitude $|\alpha - a_0| = 0.05$

(a) *Profile of A for* $\alpha = 0.06$ *and* $a_0 = 0.01$

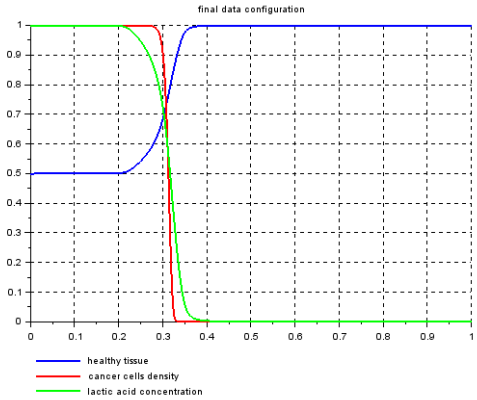

(b) *heterogeneous invasion,* $d = 0.5$

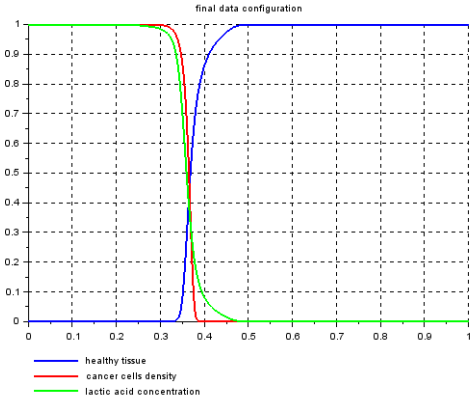

(c) *hybrid configuration,* $d = 2.5$

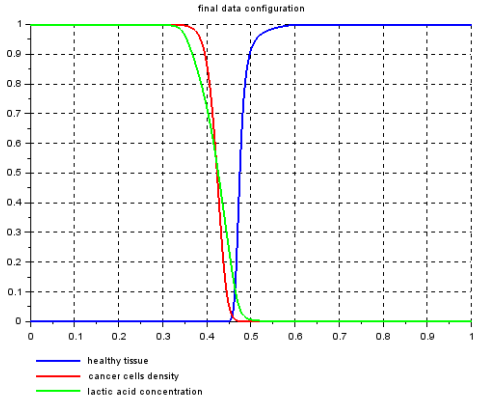

(d) *hybrid configuration,* $d = 20$

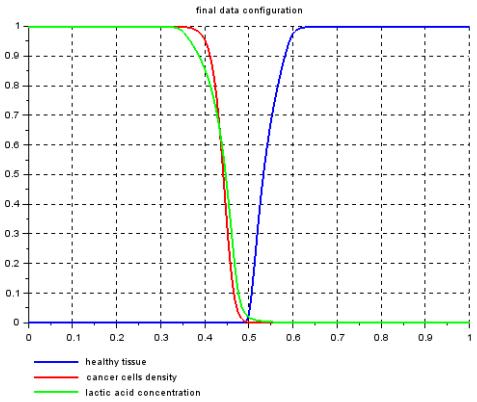

(e) *hybrid configuration,* $d = 200$

Figure 2.33: Different configurations of the numerical solution in presence of periodic diffusion A with frequency $\omega = 50$ and amplitude $|\alpha - a_0| = 0.05$

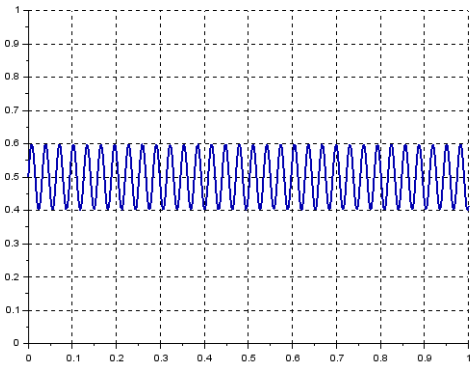

(a) *Profile of A for* $\alpha = 0.6$ *and* $a_0 = 0.4$

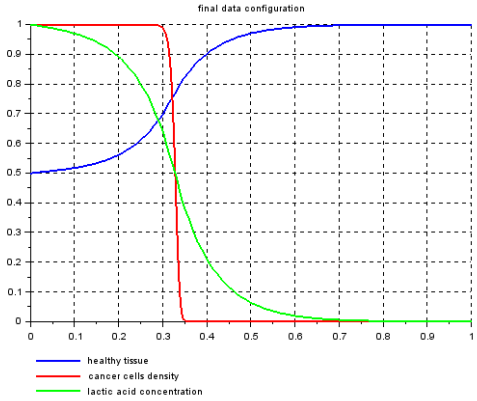

(b) *heterogeneous invasion,* $d = 0.5$

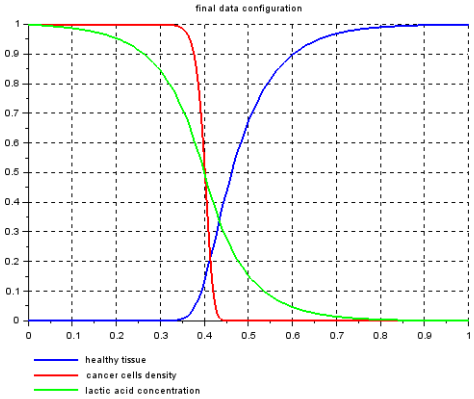

(c) *hybrid configuration,* $d = 2.5$

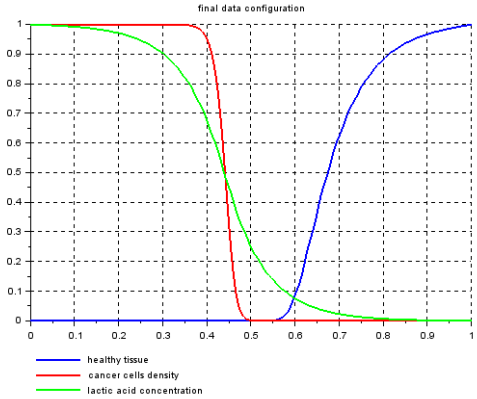

(d) *homogeneous invasion,* $d = 20$

Figure 2.34: Different configurations of the numerical solution in presence of periodic diffusion A with frequency $\omega = 200$ and amplitude $|\alpha - a_0| = 0.2$

$|\alpha - a_0| = 0.05$ are shown in Figure 2.34 and Figure 2.35 respectively, and, although the period is very small, fluctuations on the solutions are not present.

Interesting observations can be made also concerning the wave speed approximation. In the previous Section, we have proved with numerical simulations that the value of ω does not affect the propagation velocity. Furthermore, looking at Figure 2.36 and Figure 2.37 for $d = 20$, where $\omega = 50$ and $|\alpha - a_0| = 0.05$, $\omega = 50$ and $|\alpha - a_0| = 0.2$ have been chosen respectively, from a first sight the two graphs could appear similar, but the asymptotic velocities are slightly different. Indeed, the values of a_0 and α affect the asymptotic speed, which is estimated $s^* = 0.0125$ for Figure 2.36 (a) and $0.0106 \leq s^* \leq 0.0113$ for Figure 2.36 (b), and $s^* = 0.0125$ for Figure 2.37 (a) and $0.0116 \leq s^* \leq 0.011$ for Figure 2.37 (b). The final time is $T = 40$ in order to really appreciate the asymptotic behaviour.ì

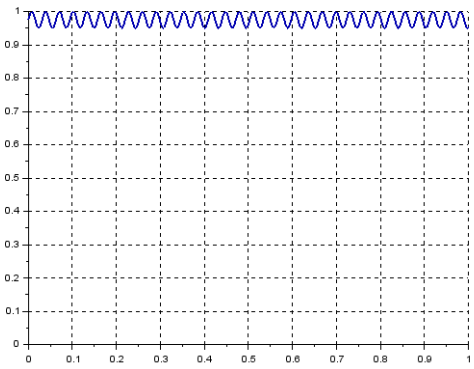

(a) *Profile of* A *for* $\alpha = 1$ *and* $a_0 = 0.95$

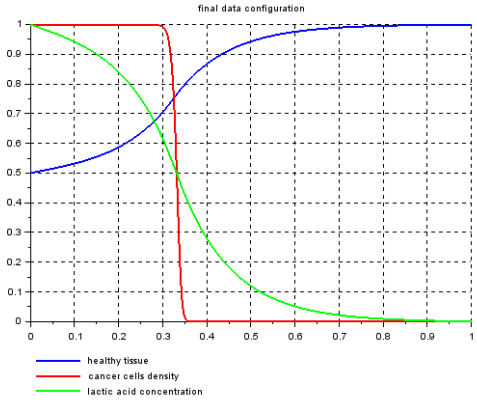

(b) *heterogeneous invasion,* $d = 0.5$

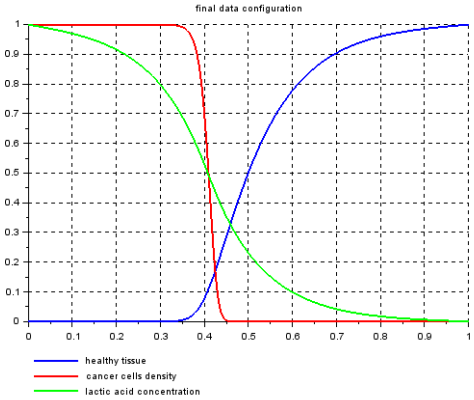

(c) *hybrid configuration,* $d = 2.5$

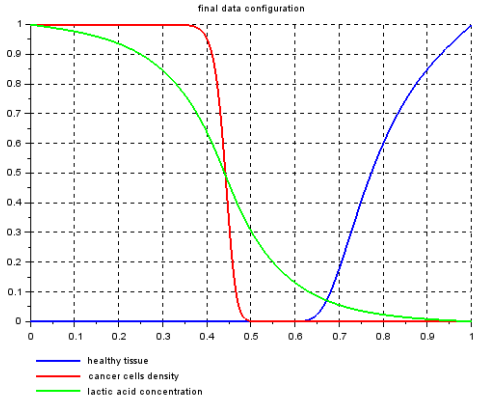

(d) *homogeneous invasion,* $d = 20$

Figure 2.35: Different configurations of the numerical solution in presence of periodic diffusion A with frequency $\omega = 200$ and amplitude $|\alpha - a_0| = 0.05$

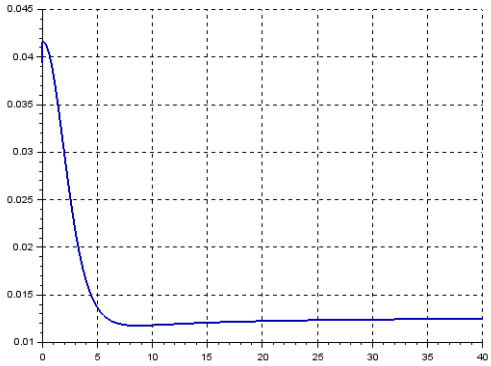

(a) $\alpha = 1$ *and* $a_0 = 0.95$

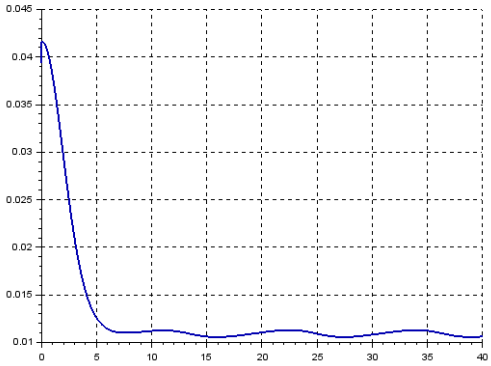

(b) $\alpha = 0.06$ *and* $a_0 = 0.01$

Figure 2.36: Wave speed approximation of the tumour front v for different values of the oscillation amplitude (for $\omega = 50$)

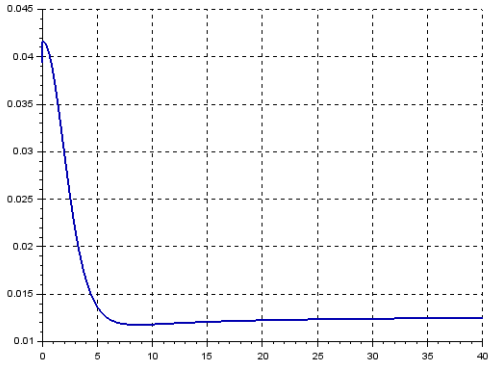

(a) $\alpha = 1$ *and* $a_0 = 0.8$

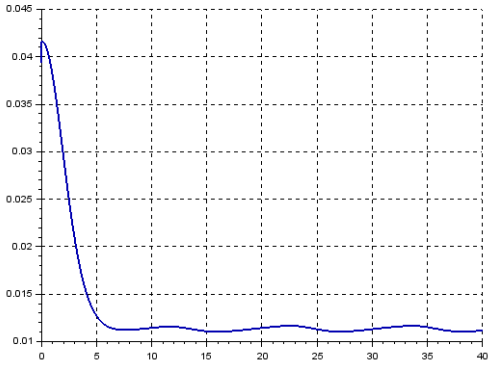

(b) $\alpha = 0.21$ *and* $a_0 = 0.01$

Figure 2.37: Wave speed approximation of the tumour front v for different values of the oscillation amplitude (for $\omega = 50$)

2.5.3 Modifying the parameter r

In order to investigate the variations of the wave speed propagation, we compare the approximation provided by the LeVeque-Yee formula (2.14) for the case in Figure 2.25 ($\omega = 50$ and $r = 1$) with that in Figure 2.38, which is constructed using the same parameters, frequency and amplitude but with a larger value $r = 10$. We have widen to the right the spatial interval in order to see the swipe of fronts.

The results of the wave speed approximation are displayed in Figure 2.39 and Figure 2.40, where we have used the final time $T = 40$ to better appreciate the asymptotic behaviour.

Two main considerations can be made. Firstly, it is evident that both d and r affect the propagation speed, and in particular the fronts propagate faster for larger values of d and r (see Figure 2.40). Secondly, we can observe that if d is small (for instance, $d = 0.5$ or $d = 1.5$), namely if the final configuration is heterogeneous or hybrid, then the wave speed does not approach an asymptotic threshold, but it seems almost periodic; moreover, the closer the final configuration is to a homogeneous regime, the more this phenomenon attenuates. This behaviour could be explained by the fact that, for the same frequency and amplitude, if the diffusion has greater intensity, then the acid particles are so fast than their velocity is not affected by the tissue inhomogeneity; on the contrary, if the acid diffusion is weak, then particles are possibly entrapped in pores and their speed trend is oscillatory.

2.5.4 Homogenization: is that possible in the long run?

The aim of this Section is to find a (homogeneous) diffusion function A which may approximate a periodic diffusive trend in the long run. We take a solution to system (2.1) with periodic function A and we look for a constant $\widetilde{A}$, called *effective* A, such that the new solution computed for this homogeneous diffusion possibly exhibits the same asymptotic wave speed as the original one.

Since we are dealing with periodic diffusion functions, the harmonic mean seems a reasonable choice to predict an approximate value instead of taking other types of averages such as the geometric or weighted mean. The harmonic mean m_h for any positive function A is defined as follows

$$\frac{1}{m_h} = \frac{1}{T}\int_0^T \frac{1}{A(x)}\,dx \tag{2.17}$$

where T is the period.
We compare the wave speed trends for different periodic diffusions A with the corresponding ones obtained by assuming $\widetilde{A} = m_h$.

First, we analyse the case of piecewise constant periodic A. We take the function $b : \mathbb{R} \longmapsto \mathbb{R}$ defined as

$$b(y) = \begin{cases} \alpha & \text{if } y \in (0, \beta) \\ a_0 & \text{if } y \in (\beta, 1) \end{cases} \tag{2.18}$$

where $0 < \beta < 1$ is the discontinuity point. Then, we extend the function (2.18) by periodicity and rescale it to the interval $[0, 1]$ by using the following formula

$$A(x) = b\left(\frac{x}{\epsilon}\right) \tag{2.19}$$

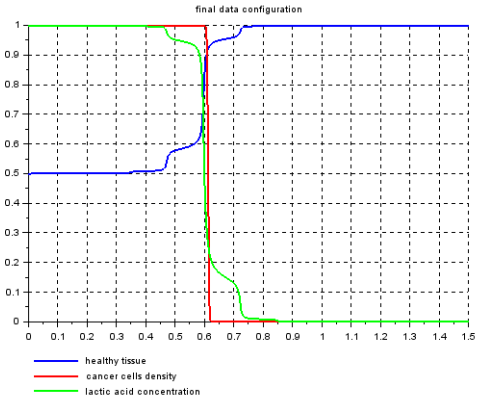

(a) *uncontrolled growth,* $d = 0.5$

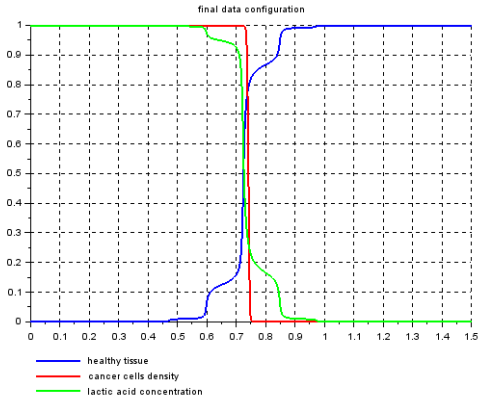

(b) *uncontrolled growth,* $d = 1.5$

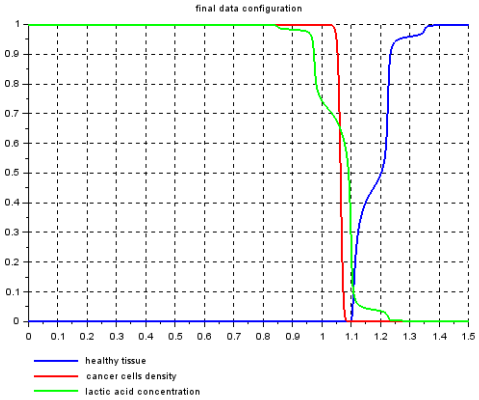

(c) *uncontrolled growth,* $d = 30$

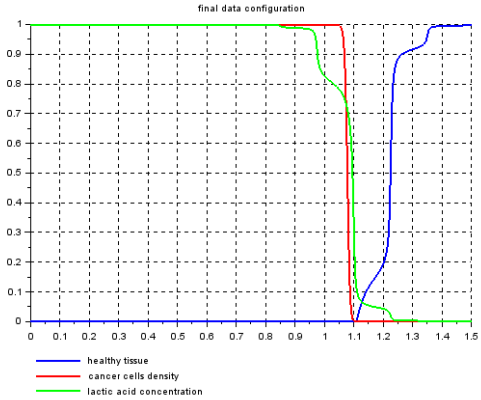

(d) *uncontrolled growth,* $d = 50$

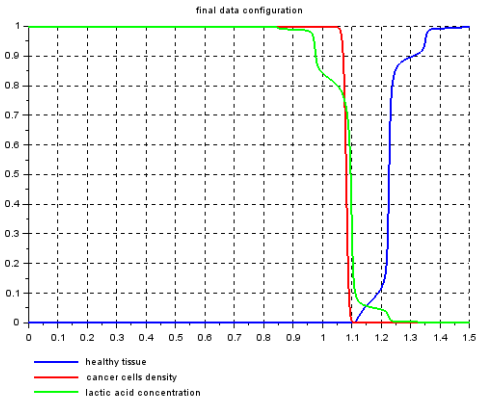

(e) *uncontrolled growth,* $d = 60$

Figure 2.38: Different configurations of the numerical solution in presence of periodic diffusion A with frequency $\omega = 50$ with $r = 10$

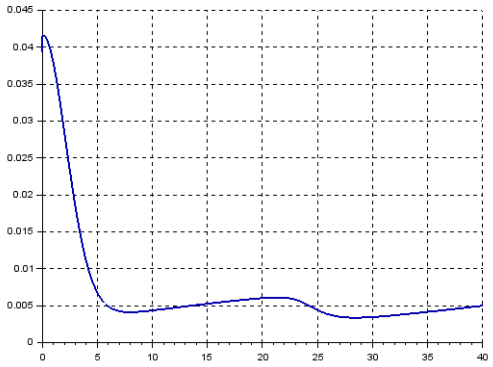

(a) *moderate growth,* $r = 1$ *and* $d = 0.5$

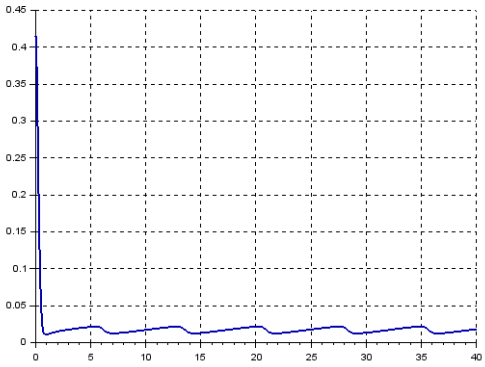

(b) *uncontrolled growth,* $r = 10$ *and* $d = 0.5$

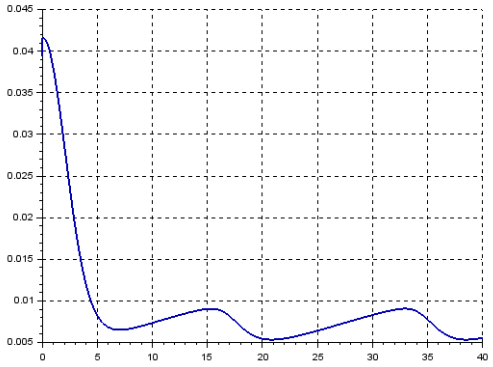

(c) *moderate growth,* $r = 1$ *and* $d = 1.5$

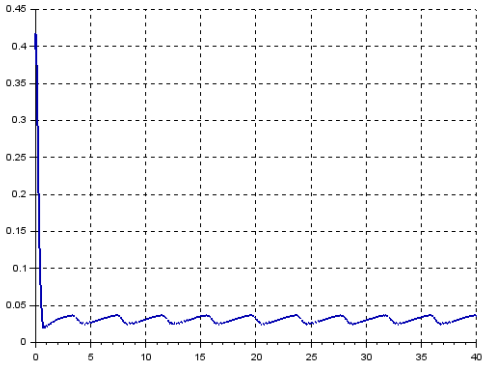

(d) *uncontrolled growth,* $r = 10$ *and* $d = 1.5$

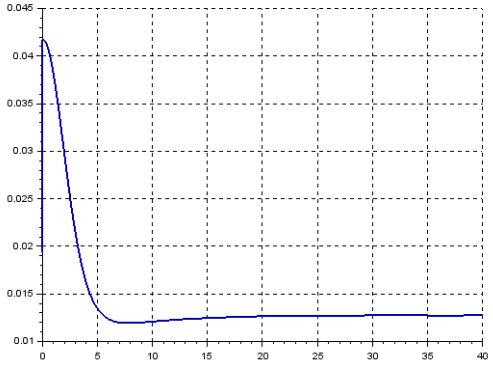

(e) *moderate growth,* $r = 1$ *and* $d = 30$

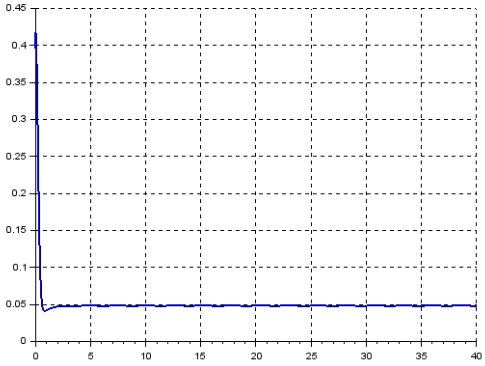

(f) *uncontrolled growth,* $r = 10$ *and* $d = 30$

Figure 2.39: Wave speed approximation of the tumour front v for different values of r and d

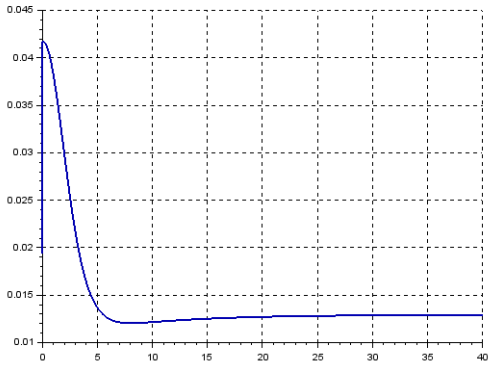

(a) *moderate growth,* $r = 1$ *and* $d = 50$

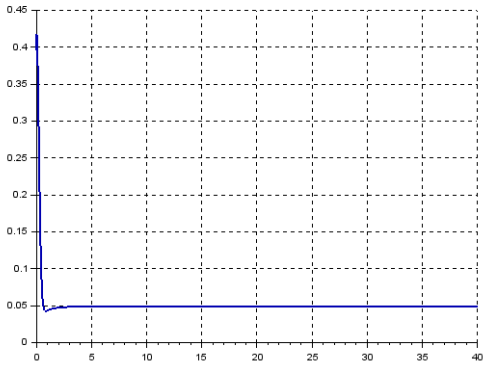

(b) *uncontrolled growth,* $r = 10$ *and* $d = 50$

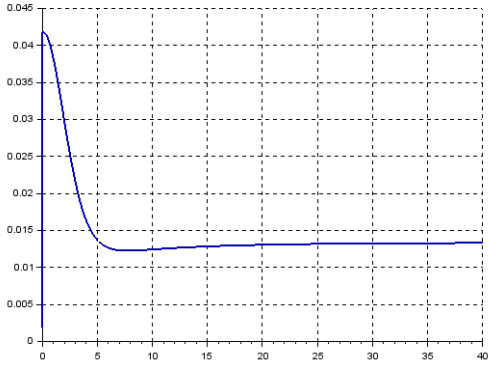

(c) *moderate growth,* $r = 1$ *and* $d = 60$

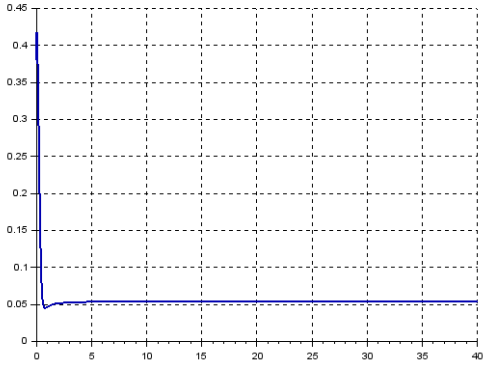

(d) *uncontrolled growth,* $r = 10$ *and* $d = 60$

Figure 2.40: Wave speed approximation of the tumour front v for different values of r and d

where ϵ is the number of oscillations inside the interval.
In this case, we can compute explicitly the harmonic mean and we have

$$m_h = \left(\int_0^1 \frac{1}{b(y)}\, dy \right)^{-1} = \left(\int_0^\beta \frac{1}{\alpha}\, dy + \int_\beta^1 \frac{1}{a_0}\, dy \right)^{-1}$$
$$= \left(\frac{\beta}{\alpha} + \frac{1-\beta}{a_0} \right)^{-1} = \frac{\alpha a_0}{a_0\beta + (1-\beta)\alpha}$$

We report the numerical wave speed approximations, obtained by using the LeVeque-Yee formula (2.14), with different values of α, β and $\omega = 2\epsilon$ in order to verify if $\widetilde{A} = m_h$ provides an effective equivalent for the periodic diffusion function A.

In Figure 2.41, we show the results obtained with $\alpha = 1$, $a_0 = 0.01$ and $\omega = 100$, together with the profile of A. We notice that for the cases $d = 0.5$ and $d = 1.5$ the wave speed does not converge asymptotically to any value, but rather oscillates between a minimun and a maximum, while $\widetilde{A}$ seems to tend to the mean value between these two.

Interesting considerations can be made for the results in Figure 2.42 and Figure 2.43, where we reduce the amplitude of oscillations taking $\alpha = 1$, $a_0 = 0.95$ and $\omega = 50$ in the first case and $\alpha = 0.6$, $a_0 = 0.4$ and $\omega = 50$ in the second one: homogenisation occurs for every value of d used in the simulations.

In Figure 2.44, we use the same parameters as for Figure 2.41 but with uncontrolled growth rate $r = 10$. The results obtained are similar to the previous simulations and there is no homogenisation for small values of d.

Now we consider a sinusoidal diffusion function A.
We point out that in general it is difficult to calculate analytically the formula for m_h, thus we construct a numerical approximation of the harmonic mean of A by using a quadrature formula [24].
In Figure 2.45, we consider the periodic diffusion function A in (2.16) with the same parameters as Figure 2.41. We notice that, as for relative case with piecewise constant periodic A, homogenisation occurs only for $d \gg 1$.

Then, in Figure 2.46, Figure 2.47 and Figure 2.48, we use the same parameters as Figure 2.42, 2.43 and 2.44 respectively and we make similar conclusions, since homogenisation occurs for all d in the first and second case and for $d \gg 1$ in the third one.

Looking at the previous simulations, it is evident that a good agreement with $\widetilde{A}$ equal to the harmonic mean of the periodic function A always occurs for homogeneous configurations (i.e. when d is such that a spatial interstitial gap appears). This fact can be justified by observing that the interstitial gap is actually an area where both u and v become null, therefore in this case the equation for v in system (2.1) is a Fisher-KPP equation. It can be proven that homogenization for Fisher-KPP equations is possible [6], thus we can expect a similar phenomenon to occur also for the model (2.1) when we consider a homogeneous configuration.

Table 2.3 resumes all the parameters used in the Figures of this section, with the relative outcome in terms of homogenisation.

It is evident that there are two special cases for which the two profiles for A have different behaviours referring to homogenization: these are the ones for $a_0 = 0.01$, $\alpha = 1$, $\omega = 100$ and $r = 1, 10$ (see Figure 2.41 and 2.45 (c) and Figure 2.44 and 2.48(c)). The reasons seems to be found in the final configurations: while in the piecewise constant case there is not a purely homogeneous invasion, in the sinusoidal case the formation of the interstitial gap has already started.

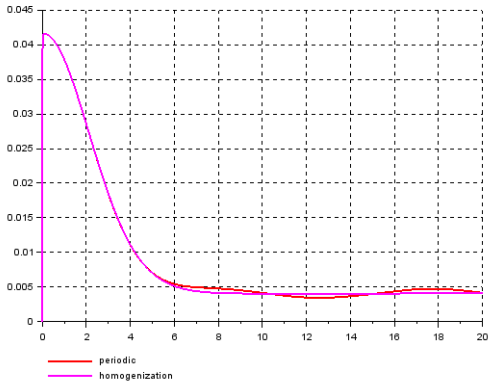

(a) $d = 0.5$

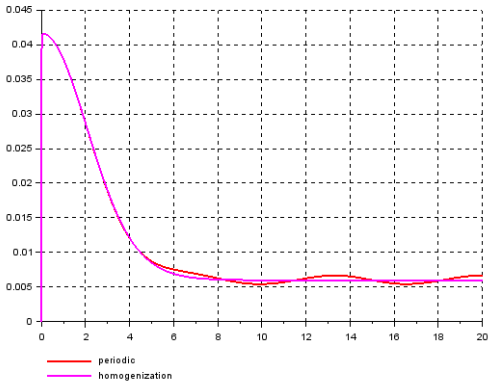

(b) $d = 1.5$

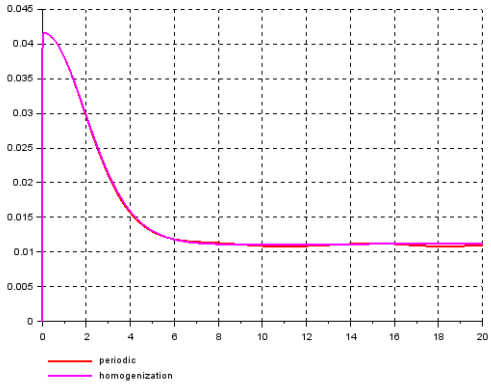

(c) $d = 30$

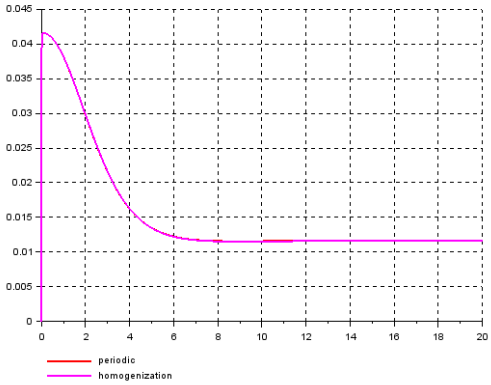

(d) $d = 60$

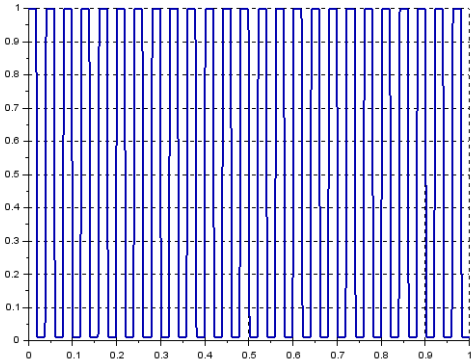

(e) *Profile of A*

Figure 2.41: Comparison between wave speed trends for piecewise constant periodic diffusion A (red line) and for the average diffusion $\widetilde{A}$ (magenta line) obtained by the harmonic mean

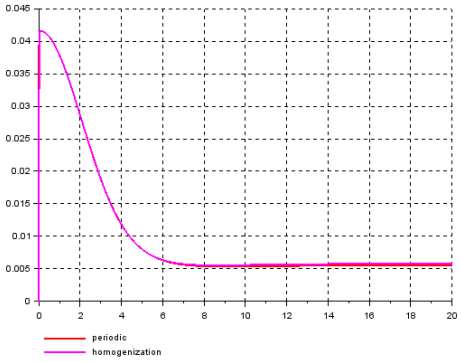

(a) $d = 0.5$

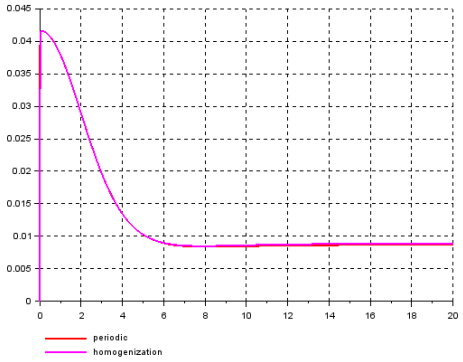

(b) $d = 1.5$

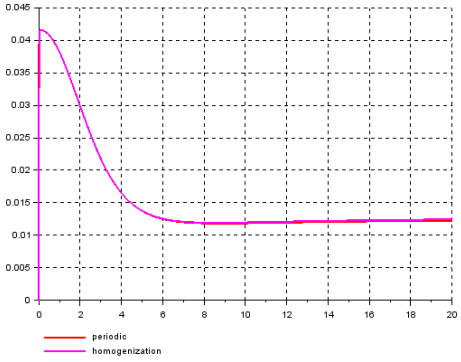

(c) $d = 30$

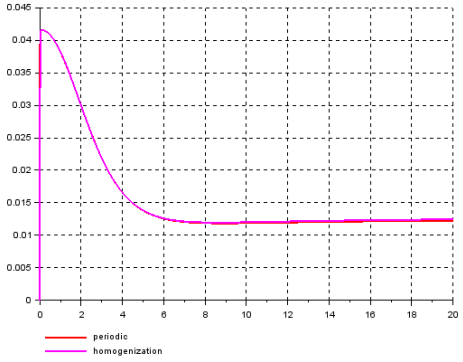

(d) $d = 60$

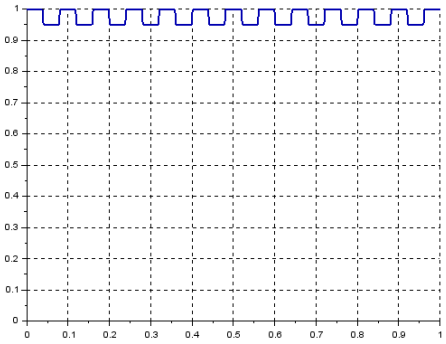

(e) *Profile of A*

Figure 2.42: Comparison between wave speed trends for piecewise constant periodic diffusion A (red line) and for the average diffusion $\widetilde{A}$ (magenta line) obtained by the harmonic mean

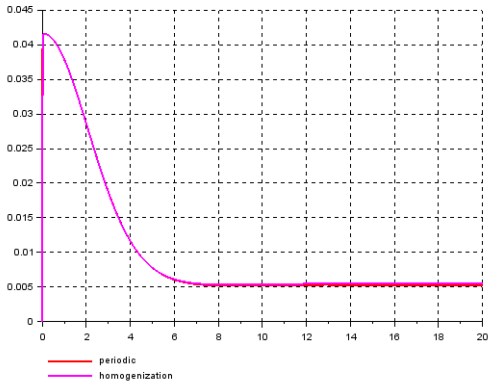

(a) $d = 0.5$

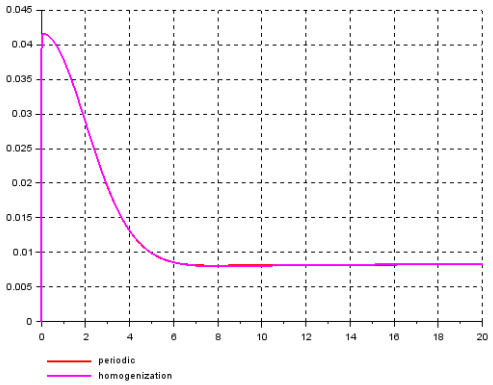

(b) $d = 1.5$

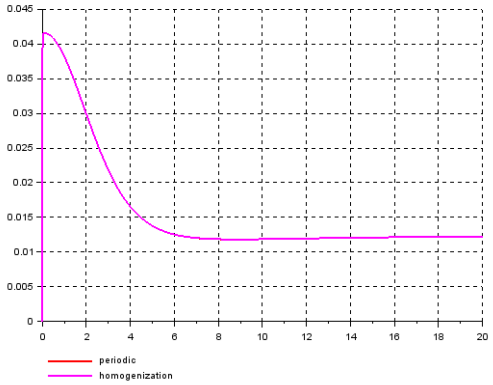

(c) $d = 30$

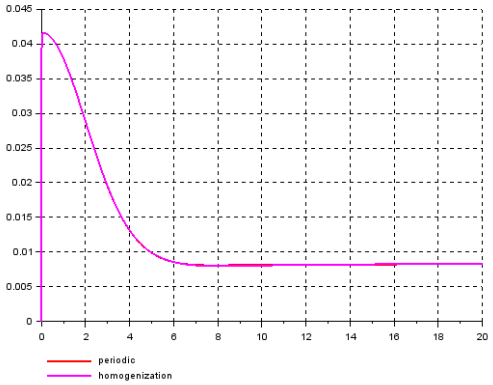

(d) $d = 60$

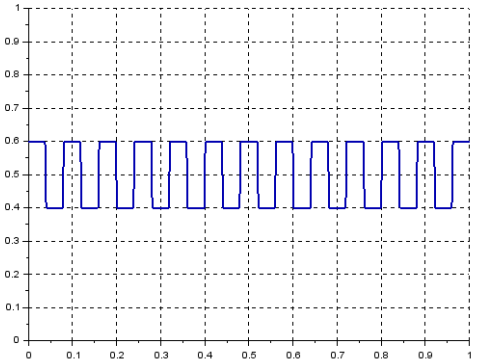

(e) *Profile of A*

Figure 2.43: Comparison between wave speed trends for piecewise constant periodic diffusion A (red line) and for the average diffusion $\widetilde{A}$ (magenta line) obtained by the harmonic mean

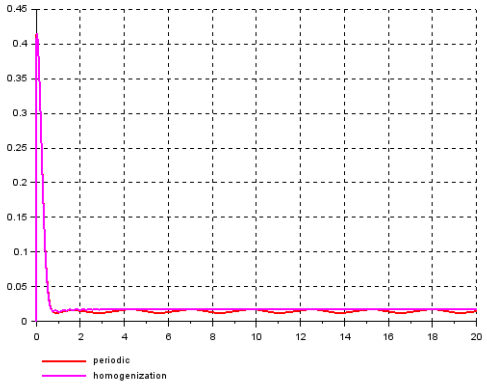

(a) $d = 0.5$, *uncontrolled growth*

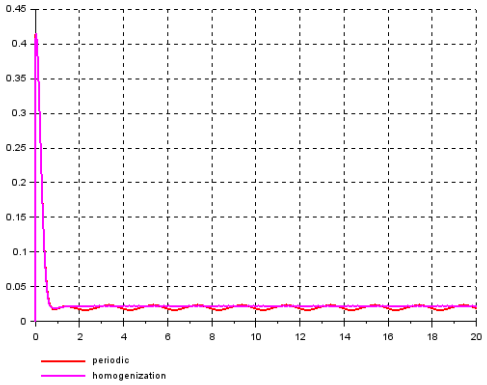

(b) $d = 1.5$, *uncontrolled growth*

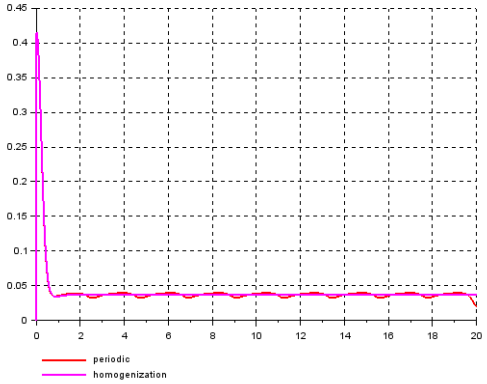

(c) $d = 30$, *uncontrolled growth*

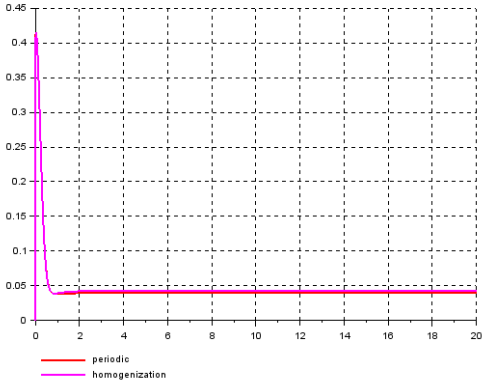

(d) $d = 60$, *uncontrolled growth*

Figure 2.44: Comparison between wave speed trends for piecewise constant periodic diffusion A (red line) and for the average diffusion $\widetilde{A}$ (magenta line) obtained by the harmonic mean

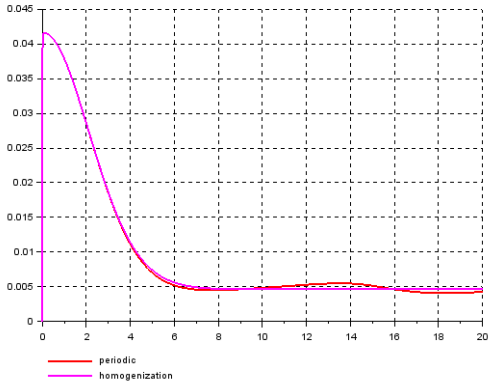

(a) $d = 0.5$

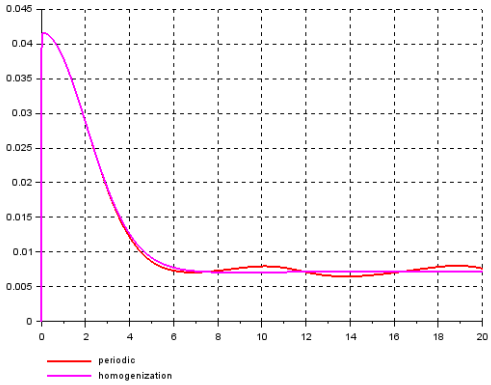

(b) $d = 1.5$

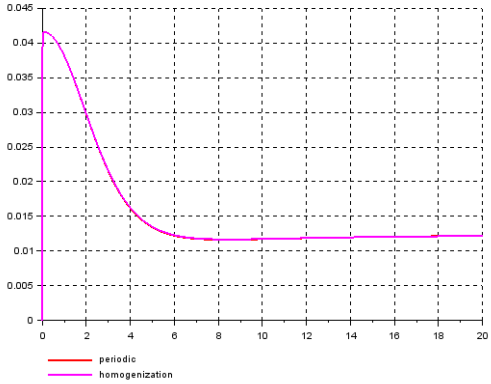

(c) $d = 30$

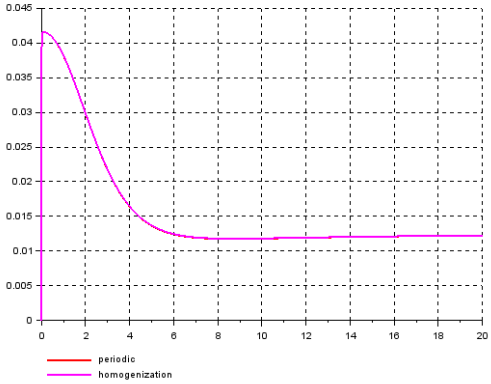

(d) $d = 60$

Figure 2.45: Comparison between wave speed trends for piecewise constant periodic diffusion A (red line) and for the average diffusion $\widetilde{A}$ (magenta line) obtained by the harmonic mean

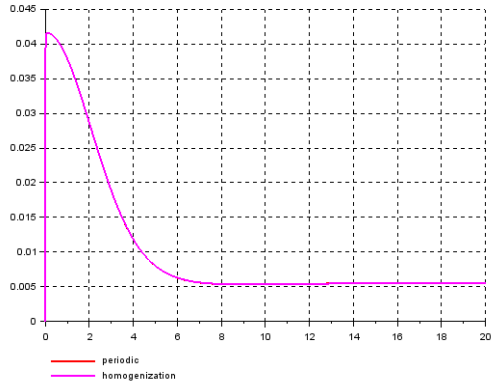

(a) $d = 0.5$

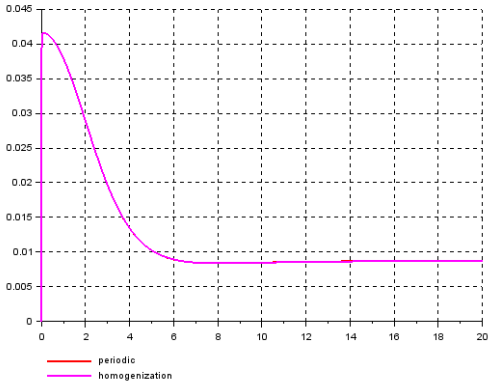

(b) $d = 1.5$

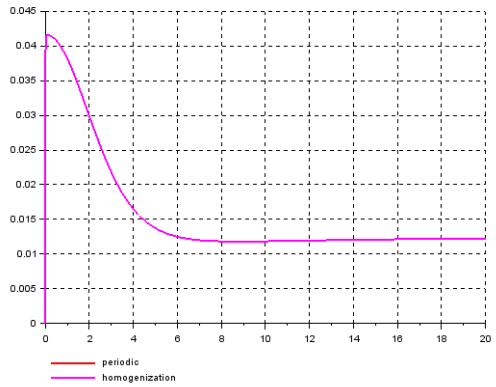

(c) $d = 30$

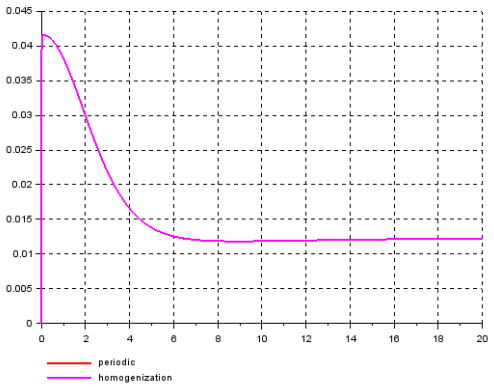

(d) $d = 60$

Figure 2.46: Comparison between wave speed trends for piecewise constant periodic diffusion A (red line) and for the average diffusion $\widetilde{A}$ (magenta line) obtained by the harmonic mean

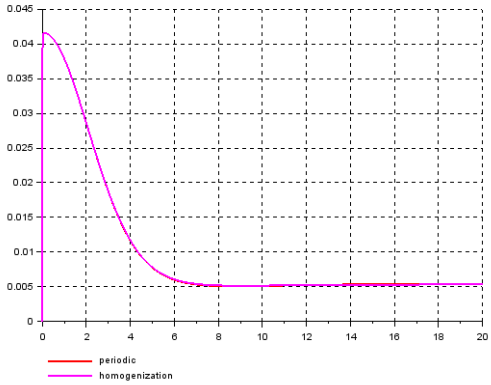

(a) $d = 0.5$

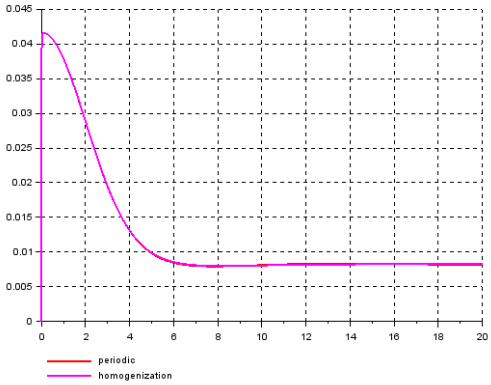

(b) $d = 1.5$

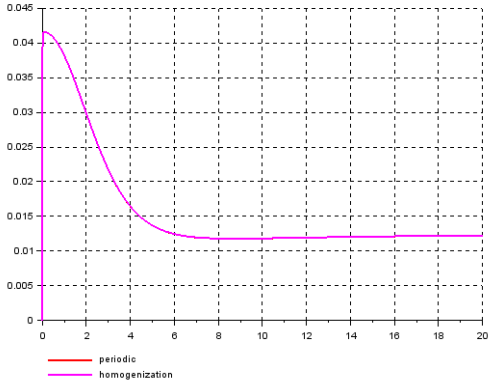

(c) $d = 30$

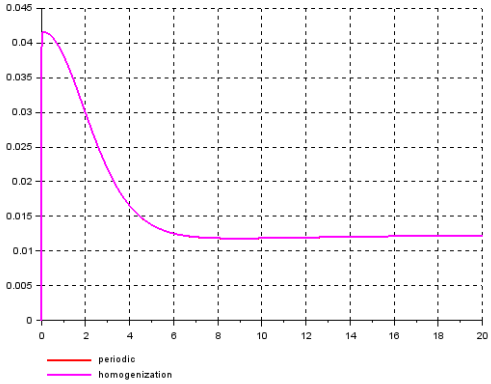

(d) $d = 60$

Figure 2.47: Comparison between wave speed trends for piecewise constant periodic diffusion A (red line) and for the average diffusion $\widetilde{A}$ (magenta line) obtained by the harmonic mean

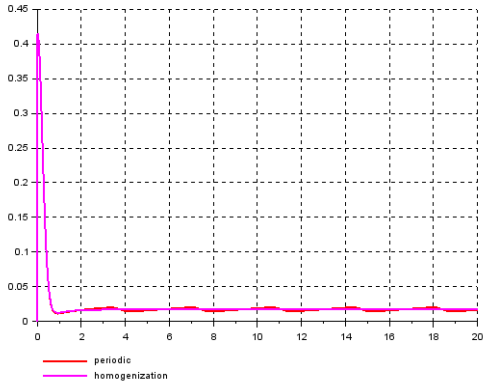

(a) $d = 0.5$

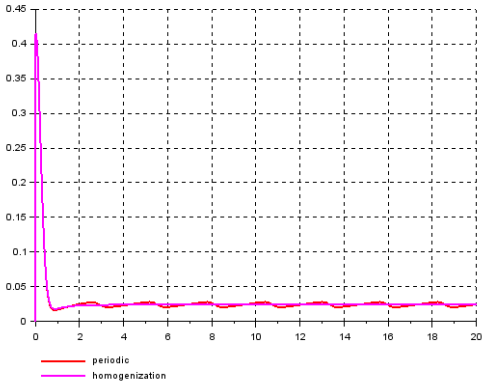

(b) $d = 1.5$

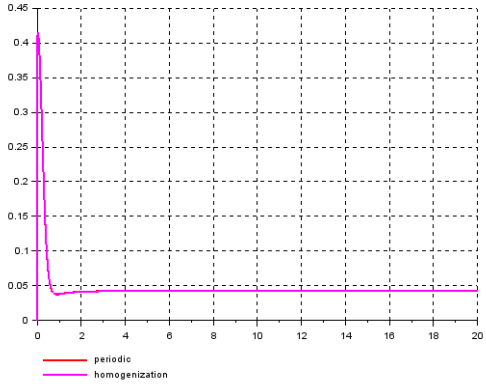

(c) $d = 30$

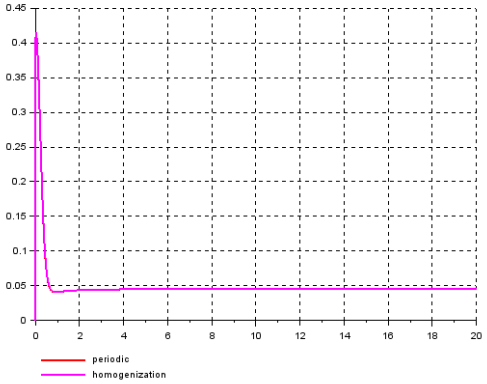

(d) $d = 60$

Figure 2.48: Comparison between wave speed trends for piecewise constant periodic diffusion A (red line) and for the average diffusion $\widetilde{A}$ (magenta line) obtained by the harmonic mean

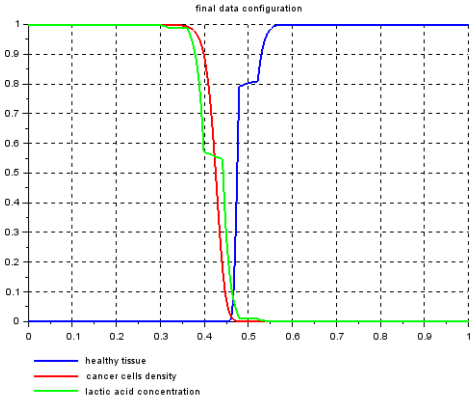

(a) *final configuration,* $d = 30$*,* $r = 1$*, piecewise*

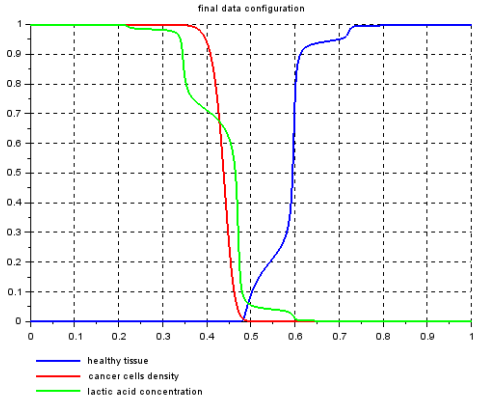

(b) *final configuration,* $d = 30$*,* $r = 1$*, sinusoidal*

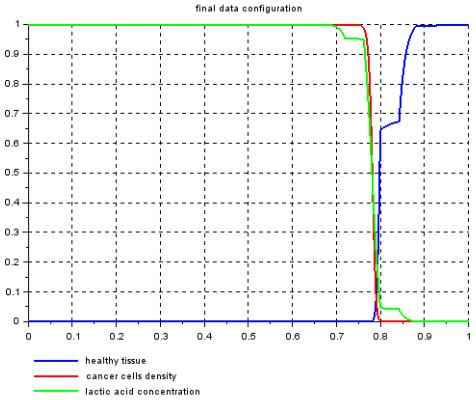

(c) *final configuration,* $d = 30$*,* $r = 10$*, piecewise*

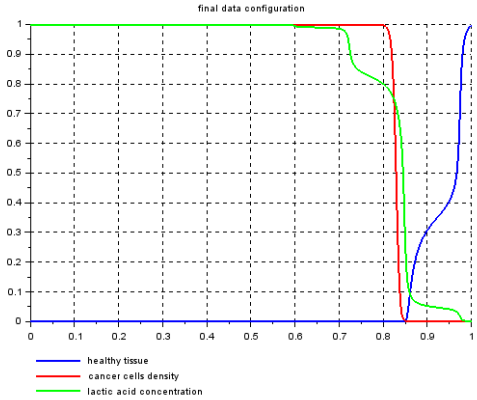

(d) *final configuration,* $d = 30$*,* $r = 10$*, sinusoidal*

Figure 2.49: Comparison between final configurations for piecewise constant and sinusoidal periodic diffusion A in the case of different behaviour relatively to homogenisation

figure	d	r	ω	a_0	α	piecewise constant	sinusoidal
2.41, 2.45 (a)	0.5	1	100	0.01	1	NO	NO
2.41, 2.45 (b)	1.5	1	100	0.01	1	NO	NO
2.41, 2.45 (c)	30	1	100	0.01	1	NO	HOM
2.41, 2.45 (d)	60	1	100	0.01	1	HOM	HOM
2.42, 2.46 (a)	0.5	1	50	0.95	1	HOM	HOM
2.42, 2.46 (b)	1.5	1	50	0.95	1	HOM	HOM
2.42, 2.46 (c)	30	1	50	0.95	1	HOM	HOM
2.42, 2.46 (d)	60	1	50	0.95	1	HOM	HOM
2.43, 2.47 (a)	0.5	1	50	0.4	0.6	HOM	HOM
2.43, 2.47 (b)	1.5	1	50	0.4	0.6	HOM	HOM
2.43, 2.47 (c)	30	1	50	0.4	0.6	HOM	HOM
2.43, 2.47 (d)	60	1	50	0.4	0.6	HOM	HOM
2.44, 2.48 (a)	0.5	10	100	0.01	1	NO	NO
2.44, 2.48 (b)	1.5	10	100	0.01	1	NO	NO
2.44, 2.48 (c)	30	10	100	0.01	1	NO	HOM
2.44, 2.48 (d)	60	10	100	0.01	1	HOM	HOM

Table 2.3: Numerical parameters for the simulations. The values for $D = 4 \cdot 10^{-5}$ and $c = 70$ are fixed and the spatial interval is $[0, 1]$

2.6 Convergence and consistency of the numerical scheme

2.6.1 Consistency order for regular solutions

We analyse the consistency of the numerical scheme (2.10) in the case of uniform mesh, by assuming Δx constant.
We consider the equations for u and for w, but we omit the computation for v, since its equation is structurally similar to the one for w (although nonlinear) and it would give rise to further complications.
We recall that the integral cell-average of the solution u on the spatial mesh is given by

$$\widetilde{u}_j(t) = \frac{1}{\Delta x} \int_{C_j} u(t, x)\, dx = u(t, x_j) + O(\Delta x^2) \tag{2.20}$$

where C_j is the jth (finite volume) mesh cell. In particular, the numerical solution u_j^n is supposed to be an approximation of $\widetilde{u}_j(t^n)$ for all j, namely

$$u_j^n \simeq \widetilde{u}_j(t^n).$$

The ordinary differential equation for the healthy tissue concentration u is discretized as in (2.10) and we recall the forward discretization of the first derivative in time, together with $u_j^n \simeq u(t_n, x_j)$, hence we have

$$\frac{u_j^{n+1} - u_j^n}{\Delta t} \simeq \frac{u(t_{n+1}, x_j) - u(t_n, x_j)}{\Delta t} \tag{2.21}$$

By using the Taylor formula of order 2 centred in t_n and assuming u regular enough, we obtain

$$u(t_{n+1}, x_j) = u(t_n, x_j) + \partial_t u(t_n, x_j)\Delta t + \frac{\partial_{tt} u(t_n, x_j)}{2}\Delta t^2 + O(\Delta t^3) \tag{2.22}$$

and substituting (2.22) to (2.21) we conclude that

$$\frac{u(t_{n+1}, x_j) - u(t_n, x_j)}{\Delta t} = \partial_t u(t_n, x_j) + \frac{\partial_{tt} u(t_n, x_j)}{2}\Delta t + O(\Delta t^2)$$

therefore the numerical approximation for the first equation of system (2.10) has order 1 consistency (in time).

Then, we consider the equation for w with (homogeneous) diffusion coefficient $A = 1$, which is discretized as follows

$$\frac{w_j^{n+1} - w_j^n}{\Delta t} = c\big(v_j^n - w_j^n\big) + \frac{w_{j+1}^n - 2w_j^n + w_{j-1}^n}{\Delta x^2} \tag{2.23}$$

where the last term is the standard discretization of the second order spatial derivative. By using the Taylor formula of order 4 centred in x_j and assuming w regular enough, we obtain

$$\begin{aligned} w(t_n, x_{j+1}) = w(t_n, x_j) &+ \partial_x w(t_n, x_j)\Delta x + \partial_{xx} w(t_n, x_j)\frac{\Delta x^2}{2} \\ &+ \partial_{xxx} w(t_n, x_j)\frac{\Delta x^3}{3!} + \partial_{xxxx} w(t_n, x_j)\frac{\Delta x^4}{4!} + O(\Delta x^5); \end{aligned} \tag{2.24}$$

$$\begin{aligned} w(t_n, x_{j-1}) = w(t_n, x_j) &- \partial_x w(t_n, x_j)\Delta x + \partial_{xx} w(t_n, x_j)\frac{\Delta x^2}{2} \\ &- \partial_{xxx} w(t_n, x_j)\frac{\Delta x^3}{3!} + \partial_{xxxx} w(t_n, x_j)\frac{\Delta x^4}{4!} + O(\Delta x^5); \end{aligned} \tag{2.25}$$

and substituting (2.24) and (2.25) to (2.23) we conclude that

$$\frac{w_{j+1}^n - 2w_j^n + w_{j-1}^n}{\Delta x^2} = \partial_{xx} w(t_n, x_j) + \partial_{xxxx} w(t_x, x_j)\frac{2\Delta x^2}{4!} + O(\Delta x^3)$$

therefore the numerical approximation for lactic acid concentration with homogeneous diffusion A has order 1 consistency in time and order 2 in space.

Now we consider the equation for w with heterogeneous diffusion function A, which is discretized in (2.10) and we aim at recovering the split form $(Aw_x)_x = A_x w_x + A w_{xx}$.
We assume A regular enough and its Taylor expansion of order 1 centred in x_j, thus we have

$$A(x_{j+1}) = A(x_j) + \partial_x A(x_j)\Delta x + O(\Delta x^2); \tag{2.26}$$

$$A(x_{j-1}) = A(x_j) - \partial_x A(x_j)\Delta x + O(\Delta x^2); \tag{2.27}$$

so that

$$\frac{A(x_j) + A(x_{j+1})}{2} = A(x_j) + \frac{\partial_x A(x_j)\Delta x}{2} + O(\Delta x^2); \tag{2.28}$$

$$\frac{A(x_j) + A(x_{j-1})}{2} = A(x_j) - \frac{\partial_x A(x_j)\Delta x}{2} + O(\Delta x^2) \tag{2.29}$$

Using (2.24) and (2.25), the first order spatial derivatives of w can be rewritten as follows

$$\begin{aligned}\frac{w(t_n,x_{j+1})-w(t_n,x_j)}{\Delta x} &= \partial_x w(t_n,x_j)+\partial_{xx}w(t_n,x_j)\frac{\Delta x}{2}\\ &+\partial_{xxx}w(t_n,x_j)\frac{\Delta x^2}{3!}+\partial_{xxxx}w(t_n,x_j)\frac{\Delta x^3}{4!}\\ &+O(\Delta x^4);\end{aligned} \tag{2.30}$$

$$\begin{aligned}\frac{w(t_n,x_j)-w(t_n,x_{j-1})}{\Delta x} &= \partial_x w(t_n,x_j)-\partial_{xx}w(t_n,x_j)\frac{\Delta x}{2}\\ &+\partial_{xxx}w(t_n,x_j)\frac{\Delta x^2}{3!}-\partial_{xxxx}w(t_n,x_j)\frac{\Delta x^3}{4!}\\ &+O(\Delta x^4);\end{aligned} \tag{2.31}$$

We collect the terms with common factor leader $A(x_j)$ and, using (2.29), (2.30) and (2.31) we have

$$A(x_j)\partial_{xx}w(t_n,x_j)+\partial_{xxxx}w(t_n,x_j)\Delta x^2\frac{A(x_j)}{4!}+O(\Delta x^3) \tag{2.32}$$

Thus, since A is bounded by its definition (it is normalized in $[0,1]$), then we conclude that the discretization of the term Aw_{xx} has order 2 consistency.
The remaining quantities are

$$\begin{aligned}&\frac{1}{2}\partial_x A(x_j)\Big(\partial_x w(t_n,x_j)+\partial_{xx}w(t_n,x_j)\frac{\Delta x}{2}\\ &+\partial_{xxx}w(t_n,x_j)\frac{\Delta x^2}{3!}+\partial_{xxxx}w(t_n,x_j)\frac{\Delta x^3}{4!}+O(\Delta x^4)\Big)\\ &+\frac{1}{2}\partial_x A(x_j)\Big(\partial_x w(t_n,x_j)+\partial_{xx}w(t_n,x_j)\frac{\Delta x}{2}\\ &-\partial_{xxx}w(t_n,x_j)\frac{\Delta x^2}{3!}+\partial_{xxxx}w(t_n,x_j)\frac{\Delta x^3}{4!}+O(\Delta x^4)\Big)\\ &=\partial_x A(x_j)\partial_x w(t_n,x_j)+\partial_x A(x_j)\partial_{xx}w(x_j)\Delta x+O(\Delta x^2)\end{aligned} \tag{2.33}$$

Thus, the discretization of the term $A_x w_x$ has order 1 consistency and therefore the numerical approximation for lactic acid concentration with heterogeneous diffusion function A has order 1 consistency both in time and in space.

2.6.2 Numerical order of convergence

We attempt at estimating the order of convergence by using the empirical method illustrated below.

Let us consider system (2.1) with the parameters of Table 2.1 and the smallest spatial step Δx which is tolerated by our computing architecture. We compute the numerical solution with this value and we assume that it represents the exact solution for our system. Let us call it $z^* = (u^*, v^*, w^*)$.
Then, we calculate the numerical solution with different Δx_k in order to evaluate the error

$$E_k = \left(\sum_{h=1}^{N_k} |z_h^* - z_h^k|^2 \, \Delta x_k\right)^{\frac{1}{2}} \tag{2.34}$$

where N_k is the number of points of the spatial mesh constructed with Δx_k and z^k is the numerical solution obtained with this spatial step. We have adopted the discrete L^2-norm for the numerical error.
The convergence order p is estimated for different Δx_i and Δx_j as follows

$$p = \log_{\frac{\Delta x_i}{\Delta x_j}} \left(\frac{E_i}{E_j} \right). \tag{2.35}$$

Firstly, we consider a homogeneous diffusion $A = 1$ and $d = 12.5$ and the piecewise linear initial profile in Figure 2.2. We choose $N^* = 1600$ as the number of points of the finest mesh for z^* and we compare with the solutions for $N_1 = 800$, $N_2 = 400$, $N_3 = 200$, $N_4 = 100$ and $N_5 = 50$. The experimental results are the following:

$$p_1 = \log_{\frac{\Delta x_2}{\Delta x_1}} \left(\frac{E_2}{E_1} \right) = 0.765$$

$$p_2 = \log_{\frac{\Delta x_3}{\Delta x_2}} \left(\frac{E_3}{E_2} \right) = 2.26$$

$$p_3 = \log_{\frac{\Delta x_4}{\Delta x_3}} \left(\frac{E_4}{E_3} \right) = 1.52$$

$$p_4 = \log_{\frac{\Delta x_5}{\Delta x_4}} \left(\frac{E_5}{E_4} \right) = 1.23$$

Then, we consider a piecewise constant increasing diffusion function A with $a_1 = 0.1$ and $a_2 = 1$, and the same data as above. The experimental results are the following:

$$p_1 = \log_{\frac{\Delta x_2}{\Delta x_1}} \left(\frac{E_2}{E_1} \right) = 0.696$$

$$p_2 = \log_{\frac{\Delta x_3}{\Delta x_2}} \left(\frac{E_3}{E_2} \right) = 2.27$$

$$p_3 = \log_{\frac{\Delta x_4}{\Delta x_3}} \left(\frac{E_4}{E_3} \right) = 1.48$$

$$p_4 = \log_{\frac{\Delta x_5}{\Delta x_4}} \left(\frac{E_5}{E_4} \right) = 1.3$$

From preliminary considerations on the values obtained above, it seems that using a dense mesh is not always the best option to achieve optimal convergence rates, although further investigations are mandatory on these topics.

2.7 Final remarks and perspectives

In this section, we provide numerical simulations of travelling wave solution to system (2.1) in order to compare the results with the approximate width of the interstitial gap given by (1.31) for the three different cases analysed in Section 1.3.

Let us start with $0 < d < 1$. In Figure 2.50 we compare the numerical approximation (2.10) with the analytical approximation one provided in Section 1.3. The simulation parameters are those of Table 2.2 with $d = 0.5$ and the auxiliary parameter θ is assumed to be $\theta = 2 \cdot 10^{-5}$.

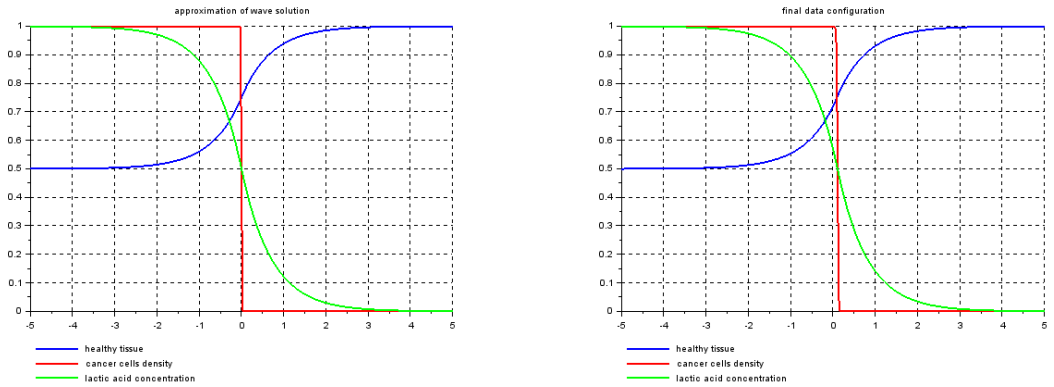

(a) *analytical approximation of slow waves* ($d = 0.5$) (b) *numerical approximation of slow waves* ($d = 0.5$)

Figure 2.50: Comparison between analytical and numerical approximations of the travelling wave solution to system (2.1) for $0 < d < 1$

Then, we take $1 < d < 2$. In Figure 2.51 we compare the numerical and analytical approximation for the parameters in Table 2.2 with $d = 1.5$. The parameters θ and α are assumed to be $\theta = 3.4641 \cdot 10^{-5}$ and $\alpha = \frac{1}{4}$. Even if the two simulations are overall very similar, between z_- and 0 the two solutions for the healthy tissue have a different shape: on the left, the blue line shows a corner point in z_- (there is a sharp change of u from 0 to positive values), whilst this is not present in the plot on the right.

Finally, we take $d > 2$. In Figure 2.52 we compare the numerical and analytical approximations for the parameters in Table 2.2 with $d = 4$. The parameters θ and α are assumed to be $\theta = 4 \cdot 10^{-5}$ and $\alpha = \frac{1}{4}$. Even if the two simulation are overall very similar, the width of the interstitial gap is much larger in the plot on the left. The reason for this difference is in the shape of the healthy tissue on the neighbourhood of z_+. Hence, the numerical approximation for $d > 2$ is in agreement with the theoretical results outside the neighbourhood of z_+, but it also inherits the qualities of the numerical scheme analysed in the previous section, and in particular a smoothing effect close to singular points.

In conclusion, it is worthwhile to point out that the obtained results can be crucial for diagnostic and therapeutic applications, in particular for cancer forecasting and prevention.
However, some open problems deserve future studies. First of all, the issue of homogenization must be analysed in terms of analytical convergence, especially taking into consideration the large sensitivity of the model with respect to the parameter d. Furthermore, we emphasize that the use of a non-uniform mesh could better model the homogeneity of human tissues, thus our numerical

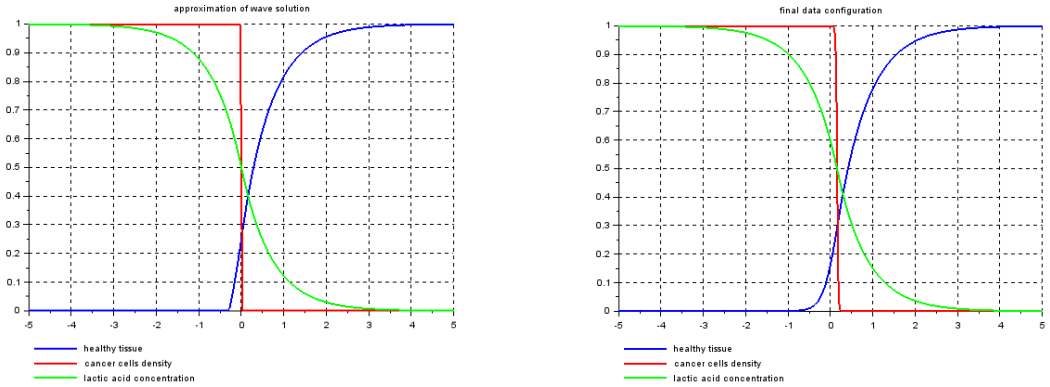

(a) *analytical approximation of slow waves* ($d = 1.5$) (b) *numerical approximation of slow waves* ($d = 1.5$)

Figure 2.51: Comparison between analytical and numerical approximation of the travelling wave solution to system (2.1) for $1 < d < 2$. The estimate of z_- is $z_- = -0.287$.

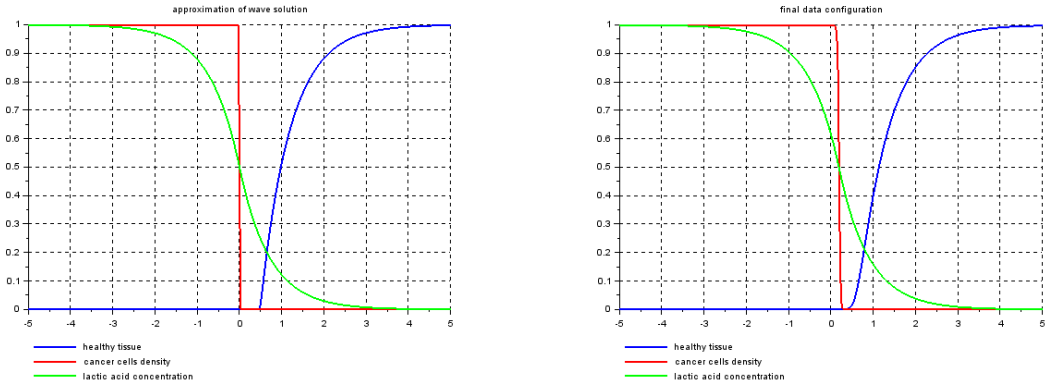

(a) *analytical approximation of slow waves* ($d = 4$) (b) *numerical approximation of slow waves* ($d = 4$)

Figure 2.52: Comparison between analytical and numerical approximation of the travelling wave solution to system (2.1) for $d > 2$. The estimate of z_+ is $z_+ = 0.49$.

algorithm will be modified in order to be more consistent with the biological context. Finally, an analytical approximation for inhomogeneous diffusion function A could lead to new results and comparison with the numerical simulations which may be important for validating more our work.

Bibliography

[1] Archetti, M., *Evolutionary dynamics of the Warburg effect: glycolysis as a collective action problem among cancer cells*, J. Theor. Biol. 341, 1-8, 2014

[2] Astanin, S., Preziosi, L.,*Mathematical modeling of the Warburg effect in tumour cords*, J. Theor. Biol. 258, 578-590, 2009

[3] Bender, C.M., Orszag, S.A., *Advanced Mathematical Methods for Scientists and Engineers*, McGraw-Hill, New York, pp 266-267, 1978

[4] Bertolini, F., Mancuso, P., Gobbi, A., Pruneri, G., *The thin red line: angiogenesis in normal and malignant hematopoiesis*, Exp. Hematol. 28, 993–1000, 2000

[5] Chaplain, M.A.J., *The mathematical modelling of tumour angiogenesis and invasion*, Acta Biotheor. 43, 387–402, 1995

[6] El Smaily, M., *Pulsating traveling fronts: Asymptotics and homogenization regimes*, Euro. Jnl of Applied Mathematics, vol. 19, pp 393–434, 2008

[7] Fasano, A., Herrero, M.A., Rodrigo, M.R., *Slow and fast invasion waves in a model of acid-mediated tumour growth*, Math. Biosci., 45-56, 2009

[8] Fasano, A., Bertuzzi, A., Gandolfi, A., *Mathematical modelling of tumour growth and treatment*, Complex Systems in Biomedicine, Springer Milan; pp 71–108, 2006

[9] Fisher, R.A., *The advance of advantageous genes*, Ann. of Eugenics 7, 335-369, 1937

[10] Gatenby, R.A., Gawlinski, E.T., *A reaction-diffusion model of cancer invasion*, Cancer Res. 56, 5745-5753, 1996

[11] Gatenby, R.A., Gawlinski, E.T., *The glycolytic phenotype in carcinogenesis and tumour invasion: insights through mathematical models*, Cancer Res. 63, 3847-54, 2003

[12] Gatenby, R.A., Maini, P.K., Gawlinski, E.T.: Analysis of tumor as an inverse problem provides a novel theoretical framework for understanding tumor biology and therapy, Appl. Math. Lett. 15, 339-345, 2002

[13] Hadeler, K.P., Rothe, F., *Travelling fronts in nonlinear diffusion equations*, J. Math. Biology, 2, 251-263, 1975

[14] Hudzik, B., Miszalski-Jamka, K., Glowacki, J., Lekston, A., Gierlotka, M., Zembala, M., Polonski, L., Gasior, M., *Malignant tumors of the heart*, Cancer Epidemiol., 39(5), 665–72, 2015

[15] Kevorkian, J., Cole, J.D., *Multiple Scales and Singular Perturbation Methods*, volume 114 of Applied Mathematical Sciences. Springer-Verlag New York, 1995

[16] Kolliker, A.V., *Manual of Human Histology*, London, Adlard, 1853

[17] Lattanzio, C., Mascia, C., Plaza, R.G., Simeoni, C., *Analytical and numerical investigation of traveling waves for the Allen-Cahn model with relaxation*, Math. Models Methods Appl. Sci. 26, 931-985, 2016

[18] Lattanzio, C., Mascia, C., Plaza, R.G., Simeoni, C., *Kinetic schemes for assessing stability of traveling fronts for the Allen-Cahn equation with relaxation*, Appl. Numer. Math. 141, 234-247, 2019

[19] LeVeque, R.J., Yee, H.C., *A study of numerical methods for hyperbolic conservation laws with stiff source terms*, J. Comput. Phys. 86, 187-210, 1990

[20] Maddix, D., Sampaio, L., Gerritsen, M., *Numerical artifacts in the generalized porous medium equation: Why harmonic averaging itself is not to blame*, J. Comput. Phys., 361, pp. 280–298, 2018

[21] McGillen, J.B., Gaffney, E.A., Martin, N.K., Maini, P.K., *A general reaction-diffusion model of acidity in cancer invasion*, J. Math. Biol. 68(5), 1199-1224, 2014

[22] Moschetta, P., Simeoni, C., *Numerical investigation of the Gatenby-Gawlinski model for acid-mediated tumour invasion*, Rendiconti di Matematica e delle sue Applicazioni, 2019.

[23] Porporato, P.E., Dhup, S., Dadhich, R.K., Copetti, T., Sonveaux, P., *Anticancer targets in the glycolytic metabolism of tumors: a comprehensive review*, Front Pharmacol. 2, 49, 2011

[24] Quarteroni, A., *Numerical models for differential problems*, Springer, Milano, 2014

[25] Sattinger, D.H., *Topics in Stability and Bifurcation Theory*, SV. 5.8, 1973

[26] Sattler, U.G., Meyer, S.S., Quennet, V., Hoerner, C., Knoerzer, H., Fabian, C., Yaromina, A., Zips, D., Walenta, S., Baumann, M., Mueller-Klieser, W., *Glycolytic metabolism and tumour response to fractionated irradiation*, Radiother Oncol., 94(1), 102-109, 2010

[27] Schrier, B.P., Hollander, M.P., Van Rhijn, B.W.G., Kiemeney, L.A.L.M., Witjes, J.A., *Prognosis of muscle-invasive bladder cancer: difference between primary and progressive tumors and implications for therapy*, Eur Urol, 45, 292–6, 2004

[28] Warburg, O., *The metabolism of tumours*, Arnold Constable, London, 1930

[29] Warburg, O., *On the origin of cancer cells*, Science 123, 309-314, 1956

[30] Weinberg, R.A., Hanahan, D., *The hallmarks of cancer*, Cell 100, 57–70, 2000

[31] Weinberg, R.A., Hanahan, D., *Hallmarks of cancer: the next generation*, Cell 144, 646, 2011

[32] Wesseling, P., *Principles of computational fluid dynamics*, Springer Berlin Heidelberg, 2001

[33] `https://it.wikipedia.org/wiki/Tessuto_epiteliale`

[34] `https://www.studenti.it/tessuto_connettivo.html`

[35] `https://istologiasapienza.weebly.com/tessuto-muscolare-striato.html`

[36] `http://people.unipi.it/static/istologia/tessuto20nervoso/tessuto_nervoso.htm`